Mineralogical and geochemical study of the metamorphic rocks from the W–Au deposit Blagojev Kamen, Serbia

Anzulović, Ana

UNIVERSITY OF ZAGREB

FACULTY OF MINING GEOLOGY AND PETROLEUM ENGINEERING

Graduate study of Geology

MINERALOGICAL AND GEOCHEMICAL STUDY OF THE METAMORPHIC ROCKS FROM THE W–Au DEPOSIT BLAGOJEV KAMEN, SERBIA

Master's Thesis

Ana Anzulović

G 398

Zagreb, 2022.

KLASA: 602-01/22-01/22
URBROJ: 251-70-15-22-2
U Zagrebu, 7. 2. 2022.

Ana Anzulović, studentica

RJEŠENJE O ODOBRENJU TEME

Na temelju vašeg zahtjeva primljenog pod KLASOM 602-01/22-01/22, URBROJ: 251-70-15-22-1 od 7. 2. 2022. priopćujemo vam temu diplomskog rada koja glasi:

MINERALOGICAL AND GEOCHEMICAL STUDY OF THE METAMORPHIC ROCKS FROM THE W–Au DEPOSIT BLAGOJEV KAMEN, SERBIA

Za mentoricu ovog diplomskog rada imenuje se u smislu Pravilnika o izradi i obrani diplomskog rada Prof. dr. sc. Sibila Borojević Šoštarić nastavnik Rudarsko-geološko-naftnog-fakulteta Sveučilišta u Zagrebu.

Mentorica:

(potpis)

Prof. dr. sc. Sibila Borojević Šoštarić

(titula, ime i prezime)

Predsjednik povjerenstva za završne i diplomske ispite:

(potpis)

Doc. dr. sc. Zoran Kovač

(titula, ime i prezime)

Prodekan za nastavu i studente:

(potpis)

Izv. prof. dr. sc. Borivoje Pašić

(titula, ime i prezime)

I would like to express my deepest gratitude to…

…my mentor Professor Sibila Borojević Šoštarić for giving me the opportunity to participate in iTarget project which made this paper possible and for offering knowledge, advice and encouragement, giving this paper a sense of direction and making the whole process run smoothly.

…Lucia Hergotić for her friendship and help during field work and after it.

…Tomislav Brenko M.Sc. for assistance with sampling, preparation of the samples and his helpful insights.

…my reviewers Associate Professor Marija Horvat and Professor Bruno Tomljenović for their invaluable feedback.

…my family, my parents, brother and sister for giving me support, understanding, love and encouragement with a perfect blend of insight and humour.

…my friends and my boyfriend for making this journey a memorable one.

Sveučilište u Zagrebu
Rudarsko geološko naftni
Fakultet

Diplomski rad

MINERALOŠKA I GEOKEMIJSKA STUDIJA METAMORFNIH STIJENA U OKOLICI VOLFRAMSKO–ZLATONOSNOG LEŽIŠTA BLAGOJEV KAMEN, SRBIJA

ANA ANZULOVIĆ

Diplomski rad izrađen: Sveučilište u Zagrebu
Rudarsko–geološko–naftni fakultet
Zavod za mineralogiju, petrologiju i mineralne sirovine
Pierottijeva 6, 10000 Zagreb

Četrnaest uzoraka metamorfnih stijena prikupljeno je u okolici Blagojevog Kamena u istočnoj Srbiji, s glavnim ciljem odredbe mineraloških i petroloških značajki stijena. Područje pripada Istočno Srpskim Karpato–balkanidima, dijelu orogenskog pojasa koji se prostire kroz Rumunjsku, Srbiju i Bugarsku, a okružuje Mezijsku platformu. Polarizacijskom mikroskopijom utvrđen je mineralni sastav metamorfnih stijena, a kombinacijom masene spektrometrije i atomske emisijske spektrometrije (ICP–MS i ICP–AES) određen je kemijski sastav stijena. Prema svojim petrografskim karakteristikama, stijene su određene kao hornfels i škriljavci.
Kordijerit–kvarc–epidote–klorit–aktinolitski hornfels nastao je kontaktnim metamorfizmom vezanim uz intruzije variscijskih granitoida koji su intrudirali u metamorfnu podlogu Kučaj terena u blizini mjesta uzorkovanja. Ostatak stijena pripada Barrow–vljevoj metamorfnoj sekvenci niskog i srednjeg stupnja, koje karakterizira zonalni raspored indeks–minerala: klorit, epidot, biotit, amfibol i granat. Uočeni metamorfni slijed Barrow–vljevog tipa uspoređen je s regionalnim Barrow–vljevim metamorfizmom na sjevernom dijelu mega jedinice Tisza–Dacia gdje graniči s Mezijskom platformom. Koristeći podatke o glavnim, sporednim i elementima u tragovima moguće je odrediti protolite i tektonski smještaj nastanka protolita. Albit–epidot–klorit–amfibolski škriljavac, epidot–klorit–feldspat–amfibolski škriljavac i klorit–epidot–albit–amfibolski škriljavac nastali su iz bazalta odnosno andezita ili subalkalnog bazalta, a granat–kvarc–klorit–amfibol–albitski škriljavac iz andezita. Albit–epidot–klorit–amfibolski škriljavac, epidot–klorit–feldspat–amfibolski škriljavac i klorit–epidot–albit–amfibolski škriljavac nastaju iz normalnih do blago obogaćenih bazalta srednjeoceanskih hrptova. Granat–kvarc–klorit–amfibol–albitski škriljavac nastaje iz protolita koji pokazuje svojstva bazalta vulkanskog luka i toleita unutar ploča do kalc–alkalnih bazalta.

Ključne riječi: metamorfne stijene, škriljavac, Barrow–ljev metamorfizam, Blagojev Kamen, Srbija, Karpato–Balkanidi, Tisza–Dacia

Diplomski rad sadrži 71 stranica, 12 tablica, 41 slika, i 105 referenci.

Jezik izvornika: engleski

Diplomski rad pohranjen: Rudarsko–geološko–naftni fakultet,
Pierottijeva 6, Zagreb

Voditeljica: Dr. sc. Sibila Borojević Šoštarić, redovita profesorica RGNF
Ocjenjivači: Dr. sc. Sibila Borojević Šoštarić, redovita profesorica RGNF
Dr. sc. Bruno Tomljenović, redoviti profesor RGNF
Dr. sc. Marija Horvat, naslovna izvanredna profesorica RGNF

Datum obrane: 11. 2. 2022.

University of Zagreb
Faculty of Mining, Geology
and Petroleum Engineering

Master's Thesis

MINERALOGICAL AND GEOCHEMICAL STUDY OF THE METAMORPHIC ROCKS FROM THE W–Au DEPOSIT BLAGOJEV KAMEN, SERBIA

ANA ANZULOVIĆ

Thesis completed in: University of Zagreb
Faculty of Mining, Geology and Petroleum Engineering
Department of Mineralogy, Petrology and Mineral Resources
Pierottijeva 6, 10 000 Zagreb

Fourteen samples of metamorphic rocks were collected in the vicinity of Blagojev Kamen in East Serbia with the main goal to determine mineralogical and petrological characteristics of the rocks. The area belongs to East Serbian Carpatho Balkanides, a part of the orogenic belt that stretches through Romania, Serbia and Bulgaria, and curves around the Moesian Platform. The mineral composition of metamorphic rocks was determined by polarisation microscopy and chemical composition by mass spectrometry and atomic emission spectrometry (ICP–MS and ICP–AES). According to their petrographic characteristics, rocks were determined as hornfels and schists.

The cordierite–quartz–epidote–chlorite–actinolite hornfels was formed by contact–metamorphism related to Variscan granitoids which intruded the metamorphic basement of Kučaj terrane near the sampling location. The rest of the rocks belong to low and medium grade Barrovian mineral assemblages, characterized by zonal distribution of the index–minerals: chlorite, epidote, biotite, amphibole and garnet. The observed Barrovian metamorphic sequence was compared to the regional Barrovian metamorphism of the northern part of Tisza–Dacia Mega Unit where it borders with Moesian Platform. Using the major, minor and trace elements data precursors and geotectonic environment of protolith formation were determined. Albite–epidote–chlorite–amphibole schist, epidote–chlorite–feldspar–amphibole schist and chlorite–epidote–albite–amphibole schist originate from basalt andesite or subalkaline basalt and garnet–quartz–chlorite–amphibole–albite schist originates from andesite. Albite–epidote–chlorite–amphibole schist, epidote–chlorite–feldspar–amphibole schist and chlorite–epidote–albite–amphibole schist show characteristics of normal to enriched MORB. Garnet–quartz–chlorite–amphibole–albite schist shows characteristics of volcanic arc basalts and within plate tholeiites to calc–alkaline basalts.

Keywords: metamorphic rocks, schists, Barrovian metamorphic sequence, Blagojev Kamen, Serbia, Carpatho–Balkanides, Tisza–Dacia
Thesis contains: 71 pages, 12 tables, 41 figures, and 105 references.
Original in: English
Thesis deposited in: Library of Faculty of Mining, Geology and Petroleum Engineering, Pierottijeva 6, Zagreb
Supervisor: Professor Sibila Borojević Šoštarić, PhD
Reviewers: Professor Sibila Borojević Šoštarić, PhD
Professor Bruno Tomljenović, PhD
Nominal Associate Professor Marija Horvat, PhD
Date of defence: February 11, 2022.

Table of Contents

Tables

Figures

Abbreviations

Act–Actinolite

Amp–Amphibole

ARC–arc tholeiite

Bt–Biotite

CAB–calc–alkaline basalt

Cb–Carbonate mineral

Chl–Chlorite

Crd–Cordierite

Czo–Clinozoisite

E–MORB–enriched mid–ocean ridge basalt

Ep–Epidote

Grt–Garnet

Hbl–Hornblende

Hem–Hematite

IAT–island arc tholeiite

Kfs–K–Feldspar

Lm–Limonite

LOI–loss on ignition

MORB–mid–ocean ridge basalt

Ms–Muscovite

N–MORB–normal mid–ocean ridge basalt

OFB–ocean floor basalt

Opq–Opaque

Pl–Plagioclase

Qz–Quartz

Rt–Rutile

Ser–Sericite

Ttn–Titanite

WPA–alkaline within–plate basalt

WPT–within–plate tholeiite

Zo–Zoisite

Zrn–Zircon

AI–within plate basalt

AII–within plate alkali basalt and within plate tholeiite

B–E–type MORB

C–within plate tholeiites and volcanic arc basalt

D–N–type MORB and volcanic arc basalt.

1. INTRODUCTION

The eastern branch of the European Variscan orogeny, which can be traced from the Pyrenees to Turkey (Ziegler, 1986), is the Carpatho–Balkan orogenic belt. The Getic–Supragetic (Bucovinian) nappe sequence that crops out in the South Carpathians in Romania, the Carpatho–Balkanides in Serbia and Balkan units in Bulgaria is a part of the Bucovino–Getic microplate which was separated from the European plate during Jurassic (Săndulescu, 1984; Kräutner, 1996). It has a complex structure of Precambrian and Phanerozoic rocks intruded by Variscan granitoids (Jovanović et al., 2019). The section of the Getic domain studied in this Master Thesis is located in the Kučaj terrane of the East Serbian Carpatho Balkanides.

The Carpathian–Balkan fold belt is rich in ore deposits related to plutons and/or volcano–plutonic complexes (Berza et al., 1998; Jelenković et al., 2008). Documented metal occurrences and deposits (W, Au–W, Au–Ag–W, Pb–Zn) (Kalenić and Hadži–Vuković 1978) were targets of our prospecting. As a part of iTARG3T project, which stands for "Innovative targeting & processing of W–Sn–Ta–Li ores", ore targeting during a three–day field work was carried out, sampling the host rocks of tungsten mineralisation in eastern Serbia. The targeted W, Au–W and Au–Ag–W occurrences in the Proterozoic metamorphic units in vicinity of Blagojev Kamen were prospected in the Pek riverbed, in neighbouring mineshafts and waste rock dumps of old mines. The fourteen samples were selected with the aim to determine: (1) mineralogical and petrological characteristics, (2) geochemical characteristics of major, minor and trace elements, (3) original geotectonic setting and to (4) correlate with similar rocks of Tisza Unit.

2. GEOGRAPHICAL SETTING

Village of Blagojev Kamen is located in the municipality of Kučevo in the Braničevo District of eastern Serbia. Braničevo District is surrounded by the rivers Danube and Great Morava to the north and east, respectively, and by the mountain range of Homolje mountains. Municipality

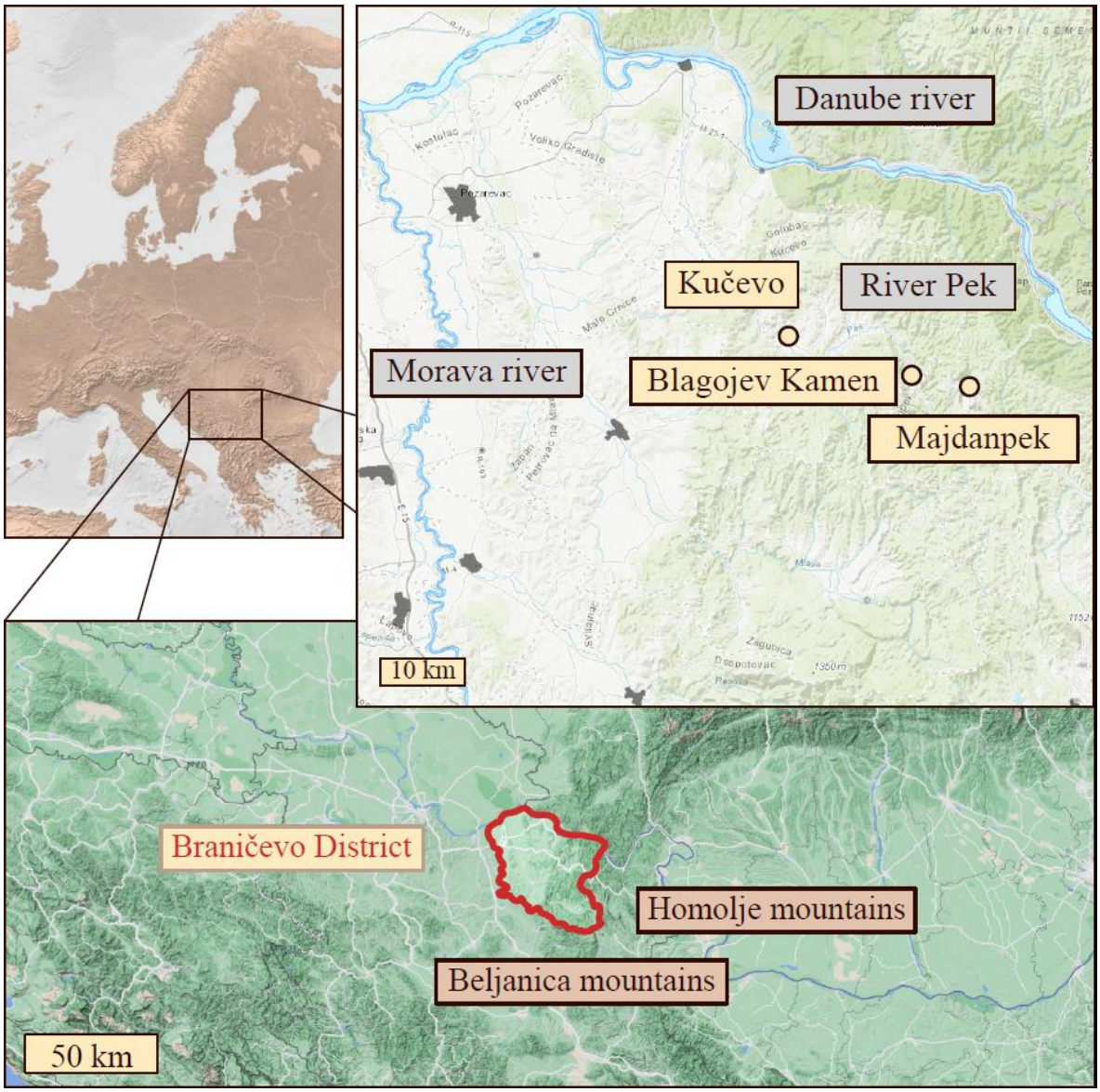

Figure 2-1. Geographical position of the investigated area (Google Maps; Geological Information System of Serbia).

of Kučevo is in hilly to mountainous area at altitudes of 120 to 920 m above sea level. It has a population of 13 851 and the village of Blagojev Kamen has a population of only 26 inhabitants (Vukmirović, 2011). Village of Blagojev Kamen is situated on the river Pek, a 129 km long

tributary of the Danube (Figure 2-1). Village was named after the former gold mine, operating from 1902 to 1953.

In proximity, south–east of Blagojev Kamen is the Majdanpek mine, a large copper open pit mine which, along with copper, produces gold and silver.

3. GEOLOGICAL SETTING

3.1. Geology of the South–Eastern Europe

The South–Eastern Europe is an area south of Ljubljana and the Sava River down to its junction with the Danube River, and further along it all the way to the Black Sea. The southern part is delineated by coastal areas of Aegean, Ionian and Adriatic seas. The South–Eastern Europe region begins along the junction between the south–eastern Alps and the north–western Dinarides and encompasses the entire Dinaride–Albanide–Hellenide, Carpatho–Balkan and Rhodope mountain belts (Cvetković et al., 2016).

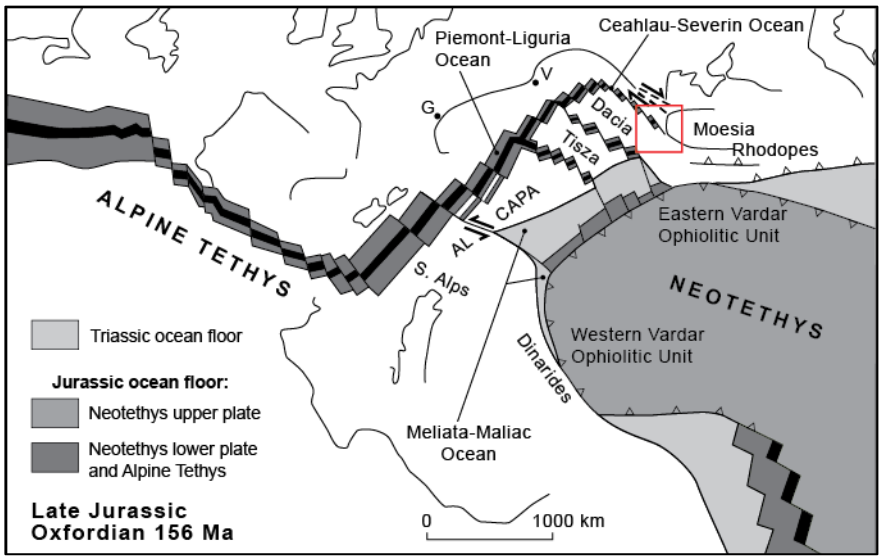

Figure 3–1. Schematic paleogeographic sketch of the opening of the Piemont–Liguria Ocean (Alpine Tethys), leading to the separation of the Adria Plate and Tisza Dacia Mega–Unit from the European continent in Oxfordian time (156 Ma) (Schmid et al., 2008). The area included in the research within this paper is marked with a red rectangle.

Geological history of the South–Eastern Europe is dominated by the single Tethys ocean (Schmid et al., 2008; Borojević Šoštarić et al., 2014) or multiple oceans (Pamić et al., 2002; Karamata, 2006) in–between the Eurasia and Gondwana.

Pre–Tethyan geological evolution refers to a period from Precambrian to Mesozoic times. On the European side it is represented by three tectonic continental blocks: the Moesian Platform, the Tisza–Dacia Mega–Unit and the Rhodopes (Figure 3–1). On the Gondwanan side it includes the Adriatic microplate later incorporated into External Dinarides, the Dalmatian–Ionian Zone and Stable Adria. The Moesian Platform is the stable margin of Europe since the Jurassic Cimmerian orogeny and can be considered as "undeformed European foreland" (Schmid et al., 2008). The Moesian Platform consists of Neoproterozoic metamorphic rocks that locally record a Variscan overprint (Seghedi et al., 2005; Oczlon et al., 2007) and it is in most part covered by younger sediments. The Tisza–Dacia Mega–Unit is the area between the eastern border of the mega–suture or the Eastern Vardar and the Moesian Platform. It includes two nappe systems, the Serbo–Macedonian Massif and the Carpatho–Balkanides.

The Tisza Unit (Prinz, 1926) is a lithospheric fragment bound by the Mid–Hungarian Lineament (Fülöp, 1989) to the north–west, the Sava, Sombor–Bečej and Mureş Lineament (i.e. the north–western border of the Srem–Mureş Ophiolite belt) to the south and the Someş Lineament to the north–east (Haas and Péró 2004). Due to similarities in the crystalline basement, lithofacies and fossil assemblage between certain parts of the Tisza Unit and the Western Carpathian units it is assumed that Tisza Unit could be considered as a continuation of the Inner Carpathian units (Kovács, 1984; Kovács et al., 1989; Haas et al., 1990). The basement outcrops of the Tisza Unit occur in the Slavonian Mountains–Moslavačka Gora, Papuk, Psunj, Krndija (Balen et al., 2006; Pamić et al., 2002), in the South Transdanubian ranges and in the Apuseni Mountains (Haas and Péró 2004).

The Tisza Unit broke off from the southern margin of the European plate during the Middle Jurassic (Channell and Horvath 1976; Balla and Bodrogi 1993; Kovács et al., 1989) and it has a complex movement history and multiple translations and rotations during Mesozoic and Cenozoic times (Csontos, 1995). In the Variscan and early Alpine evolutionary stages the Variscan terrane accretion was accompanied by intensive deformation and progressive regional metamorphism. This was followed by transpressional tectonics in the late and post–Variscan

stages, leading to the development of molasse basins (Haas and Péró 2004). In the mid–Cretaceous, due to the northward motion of the Adria Block and related west to east closure of the westernmost Neotethys basin, and the eastward motion of Moesia, the extensional regime changed into compressional. This change led to the onset of nappe stacking and low–grade regional metamorphism within the Tisza Unit (Haas and Péró 2004). In the early Tertiary the north–eastward interactive motion of the Alcapa and Tisza Dacia Blocks led to the formation of the heterogeneous basement of the Pannonian Basin (Csontos et al., 1992).

The Rhodope massif is the internal Europe–derived geological unit that underwent high to ultra–high pressure metamorphism and was subsequently overprinted by granulite and amphibolite facies (Cvetković et al., 2016).

The Syn–Tethyan geology encompasses geological units, which record the former existence of the Mesozoic oceanic lithosphere, presently mostly represented by ophiolites and trench/accretionary wedge assemblages, formed and reworked in the course of the Tethys Ocean lifespan. Ophiolitic belt is called the Vardar–Tethyan mega suture (Cvetković et al., 2016). In the Vardar–Tethyan mega suture we can distinguish three subparallel belts, commonly named Dinaric, Western Vardar and Eastern Vardar ophiolitic units (Borojević Šoštarić et al., 2014).

The Post–Tethyan geology comprises rocks stratigraphically overlying the Vardar–Tethyan mega suture zone and it is characterized by rapid extension and exhumation, high heat flow, magmatism and lithosphere thinning (Cvetković et al., 2016).

3.2. The Carpatho–Balkan Mountain chain

The Carpatho–Balkan mountain chain (Figure 3–2 a) is an eastern branch of the European Variscan orogeny, a mountain belt extending from the South Carpathians in Romania to the Black Sea in east Bulgaria, surrounding the western margin of the Moesian foreland Platform (Jovanović et al., 2019). In eastern Serbia and western Romania, Carpatho–Balkanides, a N–S to NNW–SSE striking and over 200 km long belt, extends further to the east to Bulgarian Balkan orogen and can also be traced southward, following the eastern rim of the Eastern Vardar Ophiolitic Unit, extending into Northern Greece (Schmid et al., 2008). Geotectonically we can divide it into Serbo–Macedonian Massif, Supragetic unit, Getic unit, Upper and Lower Daunbian and the Severin unit (Figure 3–2 b).

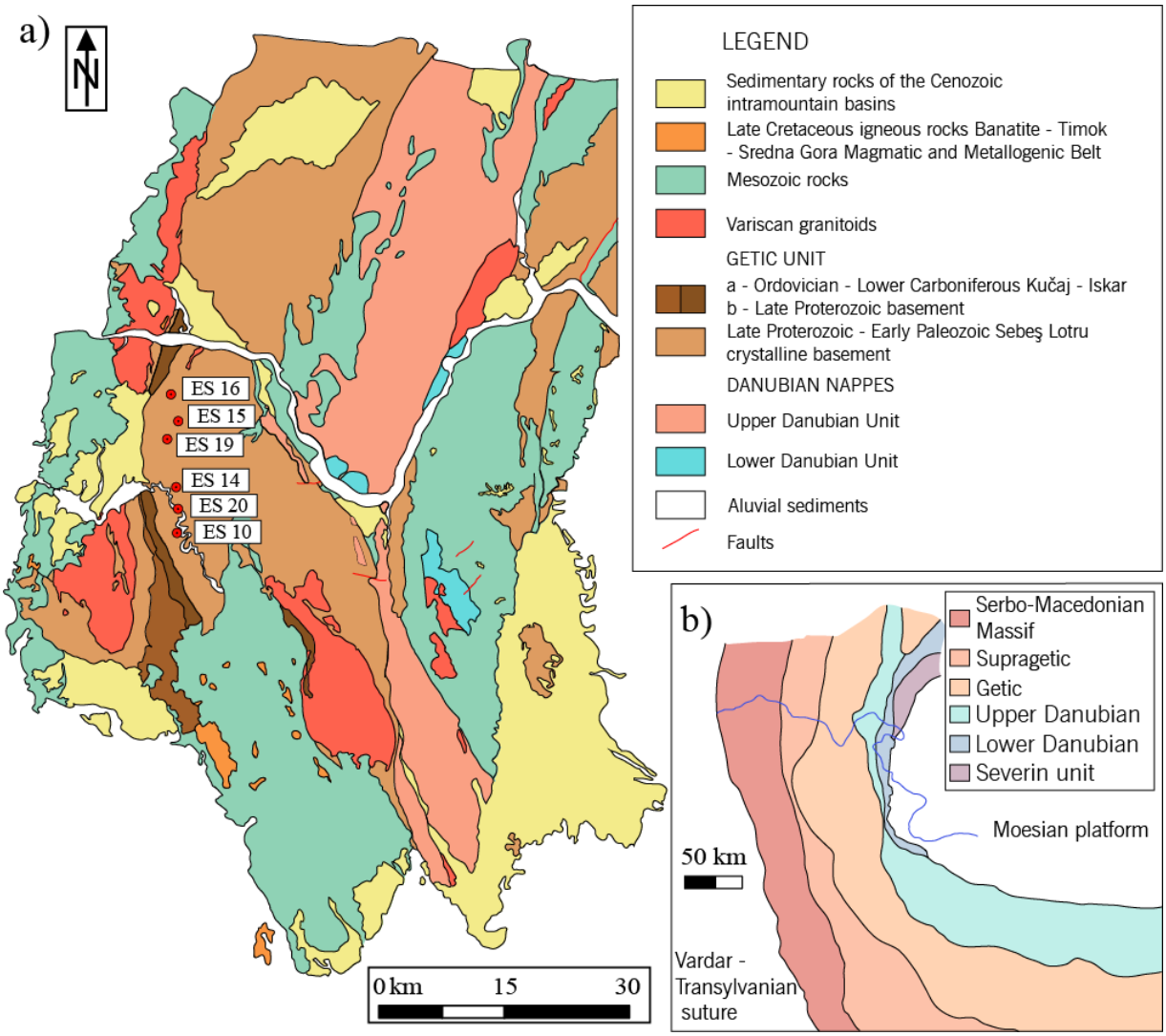

Figure 3–2. (a) Geological map of the investigated area modified after Kräutner and Krstić (2003) and (b) A geotectonic sketch of the Carpathian–Balkan sector (Krstić and Karamata 1992; Karamata, 2006).

Opening and closure of Tethys–Paratethys ocean dominated the tectonic evolution of the Carpatho–Balkanides in the Alpine period (Janković, 1997) and Carpatho–Balkanides owe much of its present day configuration to Alpine tectonics (Gallhofer et al., 2015). The Carpathian–Balkan orogen formed due to subduction of ocean(s) and collision of continental blocks with the European continent, which was driven by the overall convergence between the African and European plates (Csontos and Vörös 2004; Schmid et al., 2008).

Table 3–1. Geotectonic correlation of three sectors of the Carpathian–Balkanides with nomenclature of Alpine units and pre–Alpine basement (Haydoutov 1989; Săndulescu 1994; Kräutner and Krstić 2003; Jovanović et al., 2019).

Romanian South Carpathians		East Serbian Carpatho–Balkanides		Bulgarian Balkan Mountains	
Alpine Unit	Pre–Alpine basement	Alpine Unit	Pre–Alpine basement	Alpine Unit	Pre–Alpine basement
		Supragetic Serbo–Macedonian Massif			Morava unit
Median Dacides – Getic	Sebeş–Lotru terrane (Ordovician, North African orogen, magmatic arc)	Getic	Kučaj terrane (Late Proterozoic to Early Cambrian volcanic arc)	Sredna Gora nappes	Iskar–Svoge
Marginal Dacides – Danubian	Tisovita (Devonian oceanic suture)	Upper Danubian	Stara Planina–Poreč terrane (Proterozoic to Neoproterozoic and Early–Mid Paleozoic; island arc + ophiolites, Deli Jovan)	Balkan nappes	Berkovica Group (Island arc + ophiolites)
	Dragsan terrane (Early Neoproterozoic, Avalonia)	Lower Danubian	Vrška Čuka–Miroč terrane (Neoproterozoic volcanic arc)		Late Proterozoic, Cadomian, Gondwana–derived
	Lainici–Paius terrane (Neoproterozoic, Amazonian Cadomian)				

Table 3–1 summarizes the existing terminology and nomenclature of Alpine Units and Pre–Alpine basement of Romanian, East Serbian and Bulgarian sectors of Carpatho–Balkanides including the information about the pre–Alpine basement, available from tectonostratigraphic reconstructions and terrane analyses. The Carpathian orogen includes the Marginal, Outer and

Median Dacides (Săndulescu, 1984, 1994). In the East and South Carpathians, which are referred to as the Dacia Mega–Unit in the Hungarian literature (Csontos and Vörös 2004), the Median Dacides encompass vast areas of pre–Mesozoic metamorphic–magmatic basement complexes and Mesozoic sedimentary sequences. The Outer Dacides consist of a thrust sheet complex of Cretaceous turbidites and ophiolites, the Marginal Dacides are present only in the South Carpathians and represented by Mesozoic–Paleozoic cover sequences overlaying Precambrian basement (Iancu et al., 2005). The Cerna–Jiu (Berza and Drăgănescu 1988) and Timok (Kräutner and Krstić 2002; Fügenschuh and Schmid 2005), curved strike–slip faults, displace the Cretaceous nappe sequence along the contact between the Dacia Mega–Unit and the Moesian Platform (Schmid et al., 2008).

The Getic–Supragetic and the Danubian units are the two major eastward–facing nappe systems derived from the European continental margin and the Bucovino–Getic microplate (Kräutner and Krstić 2002). The Bucovino–Getic microplate was separated from European plate during Jurassic by the Civcin–Severin rifting and spreading system (Săndulescu, 1984; Kräutner, 1996). These units contain lithospheric fragments originated from northern margin of Gondwana (Nance et al., 2008).

The Danubian nappes, also referred to as Marginal Dacides in Romania (Săndulescu, 1994) and north–facing Balkan nappes in Bulgaria (Haydoutov, 1989), were originally part of the Moesian foreland (Schmid et al., 2008). The Upper Danubian and Lower Danubian are thrusted over the stable Moesian Platform and are structurally in a lower position with respect to the Getic unit. The Stara Planina–Poreč Unit can be correlated with the Devonian oceanic suture zone Tisovita terrane in the South Carpathians (Balintoni et al., 2014) and Berkovica group (Yanev, 2000). Vrška Čuka–Miroč terrane in Serbia is interpreted to be a Neoproterozoic volcanic arc (Krstić and Karamata 1992) similar to Cadomian basement in the Balkan terrane in Bulgaria (Yanev, 2000; Yanev et al., 2005). These terranes can be correlated to Dragsan and Lainici–Paius terranes, representing old crustal fragments in Marginal Dacides in Romania.

3.3. The Getic and Supragetic unit

The Getic unit is a complex Alpine unit that contains old continental fragments in the Romanian South Carpathians (Balintoni et al., 2014), East Serbian Carpatho Balkanides (Krstić and Karamata 1992; Krstić et al., 1974) and in Bulgarian Balkan units (Kräutner and Krstić 2003).

The basement of the Getic–Supragetic nappe sequence consists of medium to high grade Neoproterozoic to Early Paleozoic gneiss and Paleozoic greenschist to sub–greenschist metabasic rocks unconformably overlain by Late Carboniferous to Permian fluvial sediments (Iancu et al., 2005), with detrital material derived from the European continent. The basement is also intruded by Variscan plutons that crop out at many places in Serbia and Bulgaria (Jovanović et al., 2019).

In the Kučaj Unit, acritarchs demonstrate the Upper Cambrian–Lower Ordovician age of the conglomerates which transgressively overly the greenschist rocks. Upper Ordovician system of the Kučaj terrane is marked by quarzitic conglomerates grading toward quartz arenites and siltstones (Krstić and Maslarević 1990; Spahić et al., 2019). This succession of deep basinal metapelites adjoins the shallow Ordovician siliciclastics. Deepwater meta–arenites and metagreywackes mark the Ordovician–Silurian boundary. (Krstić and Maslarević 1990)

The Devonian succession locally transgressively overlies the Supragetic crystalline basement and occasionally is in direct connection with the Upper Silurian (Krstić et al., 2004). Carboniferous sediments are referred to as the "šarena serija" ("variegated series") mostly accompanied by the Permian to Mesozoic cover (Spahić et al., 2019).

The Supragetic basement is differentiated as the system structurally on top (upthrusted sequence) of the Getic unit. Such systematization favours the Alpine structural style (overprint) rather than an original depositional configuration (Spahić et al., 2019). The Supragetic unit metamorphic basement includes various volcano–sedimentary rocks of Ordovician–Silurian protolith age (Krstekanić et al., 2017). In Romania the Supragetic unit is referred to as the Locva and Bocşa units (Năstăseanu et al., 1981) continuing across the Danube into Serbia where these units are known as, from bottom to top, Ranovac and Vlasina units (Kräutner and Krstić 2002). They consist predominantly of low to intermediate–grade Proterozoic and Paleozoic rocks (Karamata, 2006). These units extend into Western Bulgaria, where they are known as the

"Morava Unit" and form the upper plate of the Osogovo–Lisets core complex (Kounov et al., 2004; Schmid et al., 2008).

4. MATERIALS AND METHODS

4.1. Prospecting the Blagojev Kamen area

Prospecting the East Serbian Carpatho–Balkanides was a troublesome task. Pre–Vardar–Tethyan geological history of the area has only fragmentarily exposed geological records, which were later subjected to different periods of tectonic and sedimentary reworking (Cvetković et al., 2016). The literature provides only incomplete data sets obtained by various approaches of terrane analyses (Jovanović et al., 2019). During prospecting we relied on the Basic Geological Map of SFRY (1978) to find metal occurrences. Occurrences of W, Au–W, Au–Ag–W and localities where they were mined in the history, around the village of Blagojev Kamen and the area around the river Pek, are featured on the map (Figure 4–1 b) modified after Kalenić and Hadži–Vuković (1978). We expected to find tungsten and gold occurrences associated with quartz hydrothermal veins (Kalenić et al., 1980). Macrophotographs of veins from different sampling sites can be seen in Figure 4–1 a. In the Pek riverbed, mineshafts and waste rock dumps of old mines 58 samples were sampled (Figure 4–1 b), fourteen of which were selected and analysed in this paper.

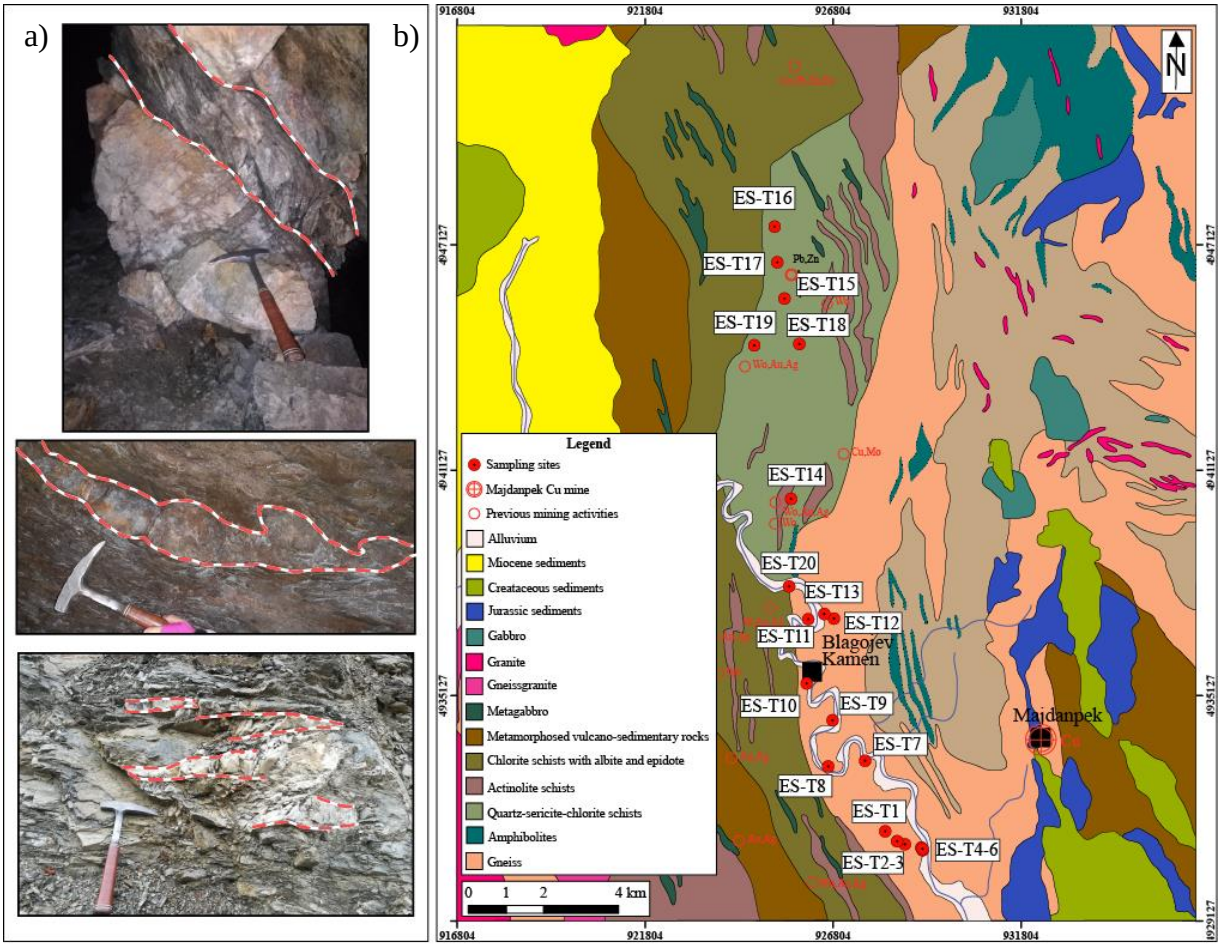

Figure 4–1. (a) Quartz veins with metal sulphides photographed on the field and (b) Geological map of prospected area with sampling location. Geological map of the targeted area modified after the Basic Geological Map of SFRY (Kalenić and Hadži–Vuković 1978).

Table 4–1. The list of samples with their coordinates and field observations. Samples presented in this study are highlighted in colour according to their grouping which can be seen in Table 5–1. Hornblende containing schists are marked in shades of green, the rest of the schists in shades of grey, hornfels in orange colour and quartz vein in light blue.

#	Sample	Field observations	Coordinates
1	ES 1	quartz veins within schists	44°23'49.1" N, 21°52'31.4" E
2	ES 2	quartz veins in schists, possible cassiterite occurrence	
3	ES 3	quartz vein, possible tungsten occurrence	
4	ES 4	mica schist	44°23'32.1" N, 21°53'12.4" E
5	ES 5	gneiss, very altered	44°23'33.8" N, 21°53'12.3" E
6	ES 6	gneiss, very altered	44.392458, 21.886892
7	ES 7	significant silicification	44.392458, 21.886892
8	ES 8	gabbro, contains quartz, mica, albite phenocrystals	
9	ES 9	foliation of chlorites, high quartz content, epidote	
10	ES 10A-1	schist, microfolds	Blagojev Kamen (44°26'00.5" N, 21°51'07.3" E)
11	ES 10A-2	schist, red crystals (?), possible pyrite and chalcopyrite occurrence	Blagojev Kamen (44°26'00.5" N, 21°51'07.3" E)
12	ES 10A-3	quartz vein with (red) alteration	Blagojev Kamen (44°26'00.5" N, 21°51'07.3" E)
13	ES 10A-4		
14	ES 10B	quartz vein with high pyrite content	Blagojev Kamen (44°26'00.5" N, 21°51'07.3" E)
15	ES 10C	amphibolite, foliation, quartz veins, pyrite?	Blagojev Kamen (44°26'00.5" N, 21°51'07.3" E)
16	ES 10D	gneiss, high mica content, pyrite (fresh and altered)	Blagojev Kamen (44°26'00.5" N, 21°51'07.3" E)
17	ES 10E-1	quartz vein with high pyrite content	Blagojev Kamen (44°26'00.5" N, 21°51'07.3" E)
18	ES 10E-2	amphibolite with pyrite	Blagojev Kamen (44°26'00.5" N, 21°51'07.3" E)
19	ES 10F-1	schist, pyrite with variable degree of alteration (can be seen by difference in colour)	Blagojev Kamen (44°26'00.5" N, 21°51'07.3" E)
20	ES 10F-2	quartz	Blagojev Kamen (44°26'00.5" N, 21°51'07.3" E)
21	ES 10G	breccia, quartz vein with host rock fragments	Blagojev Kamen (44°26'00.5" N, 21°51'07.3" E)
22	ES 10H	amphibolite (inerbanding), chalcopyrite/pyrite occurrence	Blagojev Kamen (44°26'00.5" N, 21°51'07.3" E)
23	ES 11	sericite schist, high mica content, altered	44°26'56.0" N, 21°51'15.0" E
24	ES 12-1	altered sample with quartz and feldspar	44°26'59.1" N, 21°51'33.6" E
25	ES 12-2	mica gneiss	
26	ES 13	mica schist, high mica content; quartz	44°26'54.0" N, 21°51'44,5" E
27	ES 14-1	amphibolite, fresh sample	outcrop by the road
28	ES 14-2	amphibolite, altered sample	
29	ES 15A	quartz-sericite-chlorite schist; limonitization	44°31'32.6" N, 21°51'11.6"
30	ES 15B-1	quartz vein, altered sample	44°31'32.6" N, 21°51'11.6"
31	ES 15B-2	quartz	44°31'32.6" N, 21°51'11.6"
32	ES 15B-3	schist	44°31'32.6" N, 21°51'11.6"
33	ES 15B-4	schist	44°31'32.6" N, 21°51'11.6"
34	ES 15B-5	schist, heavily altered	44°31'32.6" N, 21°51'11.6"
35	ES 15B-6	schist, mineralised altered sample	44°31'32.6" N, 21°51'11.6"
36	ES 15B-7	amphibolite	44°31'32.6" N, 21°51'11.6"
37	ES 15B-8	schist	44°31'32.6" N, 21°51'11.6"
38	ES 15C-1	schist, silicified; quartz veins	44°31'32.6" N, 21°51'11.6"
39	ES 15C-2	red alteration around quartz, breccia	44°31'32.6" N, 21°51'11.6"
40	ES 15C-3	fresh quartz from waste rock dump	44°31'32.6" N, 21°51'11.6"
41	ES 15C-4	amphibole schist	44°31'32.6" N, 21°51'11.6"
42	ES 16	schist, altered, pyrite occurrence; outcrop by the road	44°32'35.0" N, 21°50'52.4" E
43	ES 17-1	phyllite	44°32'03.6" N, 21°51'05.7" E
44	ES 17-2	opalisation of quartz	44°32'03.6" N, 21°51'05.7" E
45	ES 18	phyllite, quartz	
46	ES 19A	quartz vein, right tunel	44°30'54.2" N, 21°50'31.8" E
47	ES 19A	before the right tunel	44°30'54.2" N, 21°50'31.8" E
48	ES 19A-1	schist	44°30'54.2" N, 21°50'31.8" E
	ES 19A-2	quartz vein, right tunel, altered	44°30'54.2" N, 21°50'31.8" E
50	ES 19B	1. quartz vein in the left tunel; fresh quartz	44°30'54.2" N, 21°50'31.8" E
51	ES 19B (schaft)	mineralised schist, schaft in the left tunel	44°30'54.2" N, 21°50'31.8" E
52	ES 19B (niche)	weaker mineralisation of the schist, niche in the left tunel	44°30'54.2" N, 21°50'31.8" E
53	ES 20-1	fresh quartz with pyrite and large feldspar crystals	44.460400, 21.842658
54	ES 20-2	amphibolite	44.460400, 21.842658
55	ES 20-3	schist	44.460400, 21.842658
56	ES 21		44.644264, 21.813589
57	ES 21-1	fresh granite, contains biotite	44.644264, 21.813589
58	ES 21-2	granite and carbonates contact	44.644264, 21.813589

4.2. Analytical methods

Fourteen samples in total were analysed in this study, based on field observations nine schists (samples ES 10A–1, ES 15B–6, ES 15B–7, ES 15B–8, ES 15C–4 and ES 16), quartz vein (sample ES 15C–1) and four amphibolites (samples ES 10E–2, ES 10H, ES 20–2 and ES 14–1), were sampled (Table 4–1). They were further divided into groups according to their mineralogical composition (Table 5–1).

Analytical methods used were polarization microscopy and geochemical analysis. Optical examination of samples (Table 5–1) was conducted on microscope Leica Microsystem 020–522 101 DM/LSP, in Department of Mineralogy, Petrology and Mineral Resources of Faculty of Mining, Geology and Petroleum engineering. Camera used for microphotographs is Canon CA–PS700. Abbreviations used are taken from "Abbreviations for names of rock–forming minerals" by Whitney and Evans (2010).

Geochemical analysis was performed at the accredited MS Analytical Laboratory in Langley, Canada. Multielement contents were analysed using inductively coupled plasma–mass spectrometry (ICP–MS) using a 4–acid digestion including hydrochloric, nitric, perchloric and hydrofluoric acids. Hydrochloric, nitric, perchloric and hydrofluoric acids were used for near total digestion. Only the most highly resistant minerals (such as zircon) were not fully dissolved. The detection limits for most analysed elements were in the part per million (ppm). Major oxides analysis was performed using powdered samples which were analysed with inductively coupled plasma–atomic emission spectrometry (ICP–AES) using lithium borate ($LiBO_2$) fusion. Loss on ignition (LOI) was determined by weight difference after ignition at 1000 °C.

5. RESULTS

5.1. Petrography

After optically determining mineralogical composition of samples, names of the rocks were given in accordance with nomenclature by Winkler (1986) and assigned to groups based on their petrographic composition (Table 5–1). Based on their mineralogical composition, epidote–quartz–chlorite schist, quartz–albite–muscovite–chlorite schist, feldspar–biotite–quartz–chlorite schist, biotite–epidote–quartz–chlorite schist and epidote–muscovite–quartz–chlorite schist form a subgroup within the rocks of greenschist metamorphic facies. Samples marked in shades of green are hornblende containing schists. Albite–epidote–chlorite–amphibole schist, epidote–chlorite–feldspar–amphibole schist and chlorite–epidote–albite–amphibole schist form a subgroup within the rocks of amphibolite metamorphic facies.

Table 5–1. Mineralogical composition of analysed samples.

Sample	ES 16	ES 15C–1	ES 10A–1	ES 19A–1	ES 15B–6	ES 15B–8	ES 15C–4	ES 15B–7	ES 10F–1	ES 19B	ES 10E–2	ES 10H	ES 20–2	ES 14–1
	Cordierite–quartz–epidote–chlorite–actinolite hornfels	Quarz vein	Feldspar–biotite–chlorite–muscovite–quartz schist	Epidote–muscovite–quartz–chlorite schist	Epidote–chlorite–quartz schist	Feldspar–biotite–quartz–chlorite schist	Biotite–epidote–quartz–chlorite schist	Quartz–albite–muscovite–chlorite schist	Quartz–chlorite–actinolite–schist	Garnet–epidote–chlorite–quartz–muscovite schist	Albite–epidote–chlorite–amphibole schist	Epidote–chlorite–feldspar–amphibole schist	Chlorite–epidote–albite–amphibole schist	Garnet–quartz–chlorite–amphibole–albite schist
Quartz	+	+	+	+	+	+	+	+	+	+	+	+	+	+
Muscovite	–	–	+	+	–	+	+	+	+	+	–	–	–	–
Plagioclase	–	–	–	+	+	+	+	+	–	–	+	+	+	+
Chlorite	+	–	+	+	+	+	+	+	+	+	+	+	+	+
Biotite	–	–	+	–	–	+	+	+	–	+	–	–	+	+
K–Feldspar	–	–	+	–	–	+	–	–	–	–	+	+	–	+
Carbonate	–	+	+	+	+	+	+	+	+	+	+	+	+	–
Amphibole	Act	–	–	–	–	–	–	–	Act	–	Act,Hbl	Act,Hbl	Hbl	Hbl
Opaque	+	+	+	+	+	+	+	+	+	+	+	+	+	+
Rutile	–	–	+	–	–	+	–	+	–	–	–	–	+	+
Garnet	–	–	–	–	–	–	–	–	–	+	–	–	+	+
Zircon	–	–	–	–	–	–	–	–	–	–	–	–	–	+
Epidote	–	–	–	+	+	+	+	+	–	–	+	–	+	–
Clinozoisite	+	–	–	–	+	–	+	–	–	+	+	+	+	+
Titanite	+	–	–	–	+	–	+	–	–	+	+	+	+	–
Sericite	–	–	+	+	–	–	–	–	+	–	+	+	–	–
Zoisite	+	–	–	–	–	–	+	–	–	+	+	+	–	–
Cordierite	+	–	–	–	–	–	–	–	–	–	–	–	–	–

5.1.1. Cordierite–quartz–epidote–chlorite–actinolite hornfels ES 16

Quartz is occurring as xenoblast, its grain size varies from 0,18x0,04 to 0,01x0,01 millimetres. Larger grains exhibit undulose extinction and are often surrounded by cryptocrystalline quartz. Quartz minerals often form clusters. It occupies 7 vol % of this sample (Figure 5–2).

Chlorite is occurring as xenoblast, its grain size varies from 0,5x0,06 to 0,14x0,06 millimetres. Chlorite has low positive relief and moderate pleochroism in shades of green. It occupies 27 vol % of the sample (Figure 5–2).

Amphibole is occurring as idioblastic porphyroblast and in matrix. It is presented by actinolite, its size varies from 1,52x0,15 to 0,14x0,04 millimetres. It is characterized by pleochroism in green to bluish–green colour. It occupies 33 vol % of this sample (Figure 5–1, Figure 5–2).

Opaque mineral is occurring as xenoblast. Its grain size varies from 0,3x0,15 to 0,075x0,05 millimetres. It occupies 4 vol % of this sample.

Clinozoisite is occurring as subidioblast. Its grain size varies from 0,28x0,06 to 0,12x 0,03 millimetres. It has blue and yellow first order interference colours. It occupies 8 vol % of this sample.

Titanite is occurring as subidioblast. Its grain size varies from 0,2x0,08 to 0,06x0,02 millimetres. It has inequant shapes and high relief. It occupies 5 vol % of this sample.

Zoisite is occurring as idioblast. Its grain size varies from 0,18x0,08 to 0,02x0,02 millimetres. It has prismatic form and high positive relief. It has characteristic blue interference colour. It often has fractures perpendicular to elongation of the grain. It occupies 4 vol % of this sample (Figure 5–1).

Cordierite is occurring as subidioblastic porphyroblast. Its grain size varies from 1,2x0,1 to 0,22x0,04 millimetres. Porphyroblasts have low relief and weak pleochroism in shades of green colour (Figure 5–1, Figure 5–3). It has parallel extinction and grey interference colour of first order. It occupies 7 vol % of this sample.

Hematite appears as xenoblast. Its grain size varies from 0,3x0,2 to 0,04x0,02 millimetres. It has deep red colour. There is around 5 vol % of it in this sample.

Sample ES 16 has a homogenous structure and lepidogranoblastic texture. There are two zones with noticeably different grain size distribution of minerals. Quartz veins intersect the sample. It is determined as a **cordierite–quartz–epidote–chlorite–actinolite hornfels (**Table 5–2**)**.

Table 5–2. Mineralogical description of sample ES 16.

Sample ES 16	Structure	Texture
Cordierite–quartz–epidote–chlorite–actinolite hornfels	homogeneous	porphyroblastic
Quartz	**Chlorite**	**Amphibole**
grain size: 0,18x0,04 - 0,01x0,01 habit: xenoblastic estimation of proportion: 7% alterations: /	grain size: 0,5x0,06 - 0,14x0,06 habit: xenoblastic, fibrous, radiating estimation of proportion: 27% alterations: /	Actinolite grain size: 1,52x0,15 - 0,14x0,04 habit: idioblastic estimation of proportion: 35% alterations: /
Opaque	**Clinozoisite**	**Titanite**
grain size: 0,3x0,15 - 0,075x0,05 habit: xenoblastic estimation of proportion: 4% alterations: /	grain size: 0,28x0,06 - 0,12x 0,03 habit: subidioblastic estimation of proportion: 8% alterations: /	grain size:0,2x0,08 - 0,06x0,02 habit: subidioblastic estimation of proportion: 5% alterations: /
Zoisite	**Cordierite**	**Hematite**
grain size: 0,18x0,08 - 0,02x0,02 habit: idioblastic estimation of proportion: 5% alterations: /	grain size: 1,2x0,1 - 0,22x0,04 habit: subidioblastic estimation of proportion: 7% alterations: /	grain size: 0,3x0,2 - 0,04x0,02 habit: xenoblastic estimation of proportion: 5% alterations: /

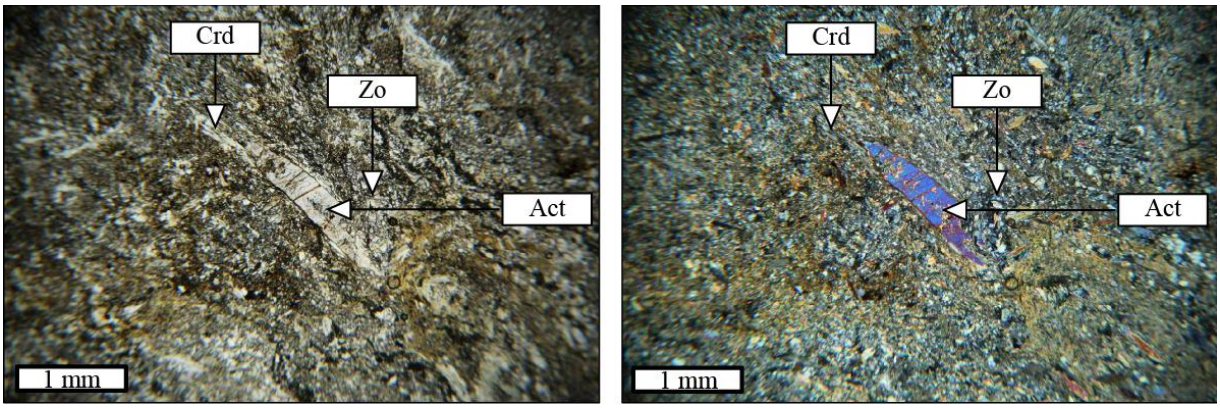

Figure 5–1. Actinolite porphyroblast is surrounded by cordierite and zoisite, lepidogranoblastic texture of cordierite–quartz–epidote–chlorite–actinolite hornfels can be seen.

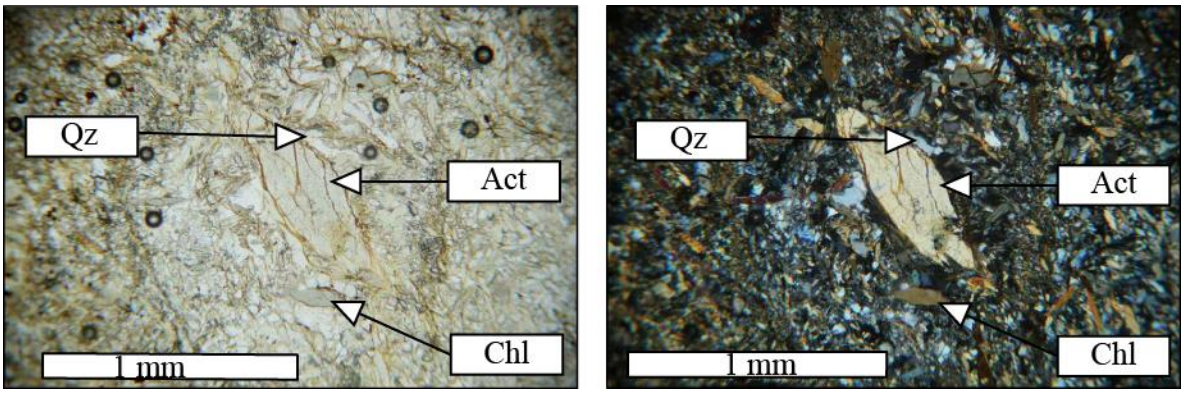

Figure 5–2. Actinolite porphyroblast with quartz and chlorite in the cordierite–quartz–epidote–chlorite–actinolite hornfels **(**sample ES 16). Lepidogranoblastic texture of hornfels can be seen.

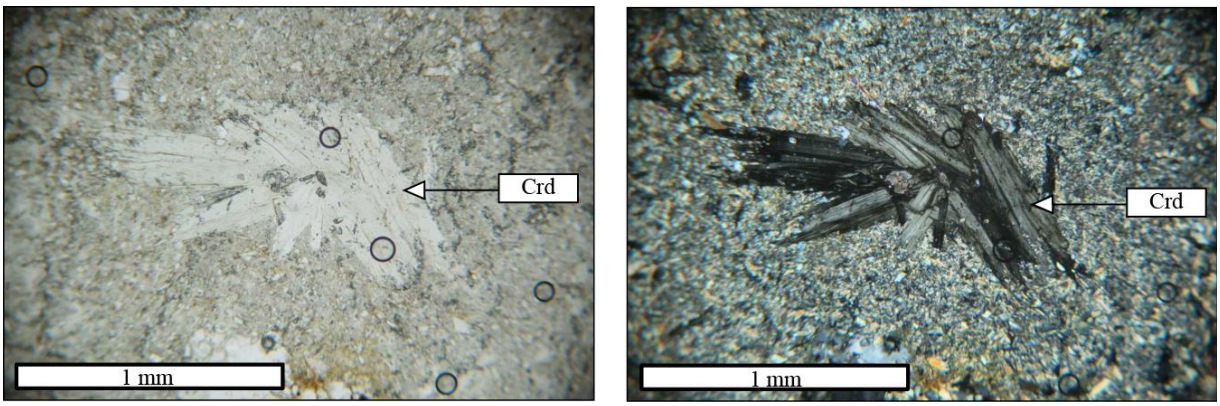

Figure 5–3. Elongated cordierite twins in the cordierite–quartz–epidote–chlorite–actinolite hornfels.

5.1.2. Quartz vein ES 15C–1

Quartz is occurring as xenomorphic grain, its size varies from 4x1,44 to 0,16x0,08 millimetres (Figure 5–4). Quartz has undulose extinction, it is often strained and partly recrystallized, forming polygonal texture. Coarser quartz grains exhibit strain lamellae. It occupies 70 vol % of this sample.

Carbonate mineral is occurring as xenomorphic grain, its size varies from 2,4x2,2 to 0,04x0,24 millimetres (Figure 5–4). It occupies around 20 vol % of this sample.

Opaque mineral is occurring as idiomorphic prismatic mineral. Its grain size varies from 6x0,3 to 0,32x0,08 millimetres. Minerals are appearing in clusters and are randomly oriented (Figure 5–4). Opaque mineral sometimes has carbonate halo. It occupies 10 vol % of this sample.

Sample ES 15C–1 has a granoblastic texture and belongs to a **quartz vein.**

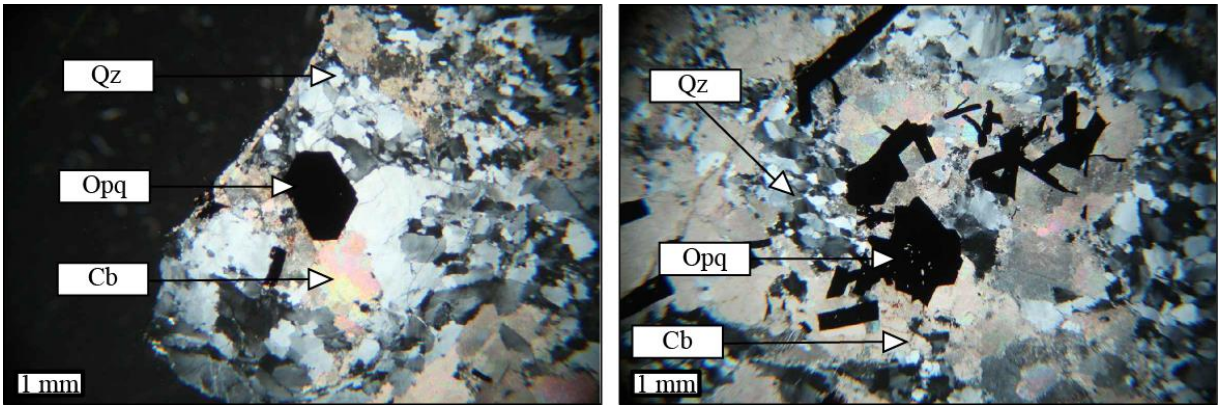

Figure 5–4. Opaque mineral with idiomorphic habit surrounded by carbonate mineral and quartz in the quartz vein.

5.1.3. Feldspar–biotite–chlorite–muscovite–quartz schist ES 10A–1

Quartz occurs as xenoblastic grains (Figure 5–5). Its size varies from 0,05x0,1 to 0,72x0,4 millimetres. Quartz is colourless and has low positive relief. It shows undulose extinction. Edges are corroded due to subgrain rotation and recrystallization. Inequant quartz grains occur in elongated agglomerations of minerals outlined by alignment of sheets of muscovite. Locally, quartz grains are lined by reddish–brown iron (oxy) hydroxides (limonite). Quartz is the main component of the sample occupying 44 vol %.

Muscovite is appearing as xenoblast. Its size varies from 1x0,05 to 0,14x0,02 millimetres. It shows "bird's eye extinction". Grains are often plastically deformed with undulose extinction. Parallelism of muscovite flakes dominates the foliation. Muscovite occupies 18 vol % of the sample.

Chlorite is occurring as xenoblast and as massive and earthy aggregate. Its grain size varies from 0,54x0,22 to 0,08x0,04 millimetres. It exhibits anomalous birefringence and blue interference colours. It occupies about 10 vol % of this sample.

Biotite is occurring as massive platy aggregate. It is altered to chlorite which is why it shows anomalous interference colours. The two often occur as cryptocrystalline aggregate. Biotite occupies 7 vol % of this sample.

K–Feldspar is appearing as subidioblast. Its size varies from 0,4x0,1 to 0,2x0,08 millimetres. It is presented by orthoclase. It is colourless in plain polarised light but seems cloudy due to alterations. It is sericitized. It occupies around 10 vol % of the sample.

Carbonate mineral is appearing as xenoblast. Its size varies from 0,16x0,06 to 0,4x0,32 millimetres. Carbonate mineral forms veins which are intersecting quartz lenses. This gives evidence that carbonate mineral crystallized last. Carbonate mineral occupies around 4 vol % of the sample.

Opaque mineral is appearing as idioblast to xenoblast. Its size varies from 4x1,68 to 0,15x0,1 millimetres (Figure 5–5). It is occurring as large idioblastic porphyroblast and in the form of smaller xenoblastic equigranular to minerals in the matrix. Porphyroblasts often have fractures perpendicular to elongation of the grain. They are limonitized and have inclusions of hematite with average size of 0,05x0,05 millimetres. Opaque mineral occupies around 5 vol % of the sample.

Rutile is occurring as xenoblast, its size varies from 0,24x0,24 to 0,04x0,02 millimetres. Rutile exhibits weak pleochroism in yellowish brown colour. It has high relief and extreme birefringence. There is around 2 vol % of it in the sample.

Opaque veins are intersecting the sample (Figure 5–5). Vein minerals are limonite and hematite. Opaque fragments are sometimes intercalated in between foliated micaceous minerals. There are quartz veins, intersected by opaque veins. Structure of the rock is foliated, texture is porphyroblastic. In this sample we have a polyphase paragenesis, after initial crystallisation muscovite and quartz crystallised and in the third stage carbonate mineral crystallised.

Sample ES 10A–1 is determined as **feldspar–biotite–chlorite–muscovite–quartz schist** (Table 5–3).

Table 5–3. Mineralogical description of sample ES 10A–1.

Sample ES 10A-1	Structure	Texture
Feldspar–biotite–chlorite–muscovite–quartz schist	foliated	porphyroblastic
Quartz	**Muscovite**	**Chlorite**
grain size: 0,05x0,1 - 0,72x0,4 habit: xenoblastic estimation of proportion: 45% alterations: undulose extinction	grain size: 1x0,05 - 0,14x0,02 habit: xenoblastic estimation of proportion: 19% alterations: undulose extinction	grain size: 0,54x0,22 - 0,08x0,04 habit: xenoblastic, massive, earthy estimation of proportion: 10% alterations: /
Biotite	**K-Feldspar**	**Carbonates**
habit: massive platy aggregate estimation of proportion: 7% alterations: chloritized	grain size: 0,4x0,1 - 0,2x0,08 habit: subidioblastic estimation of proportion: 10% alterations: sericitization	grain size: 0,4x0,32 - 0,16x0,06 habit: xenoblastic estimation of proportion: 4% alterations: /
Opaque	**Rutile**	**Hematite**
grain size: 4x1,68 - 0,15x0,1 habit: idioblastic porphyroblasts and xenoblasts estimation of proportion: 5% alterations: /	grain size: 0,24x0,24 - 0,04x0,02 habit:xenoblastic estimation of proportion: 2% alterations: /	inclusions in opaque minerals of average size 0,05x0,05

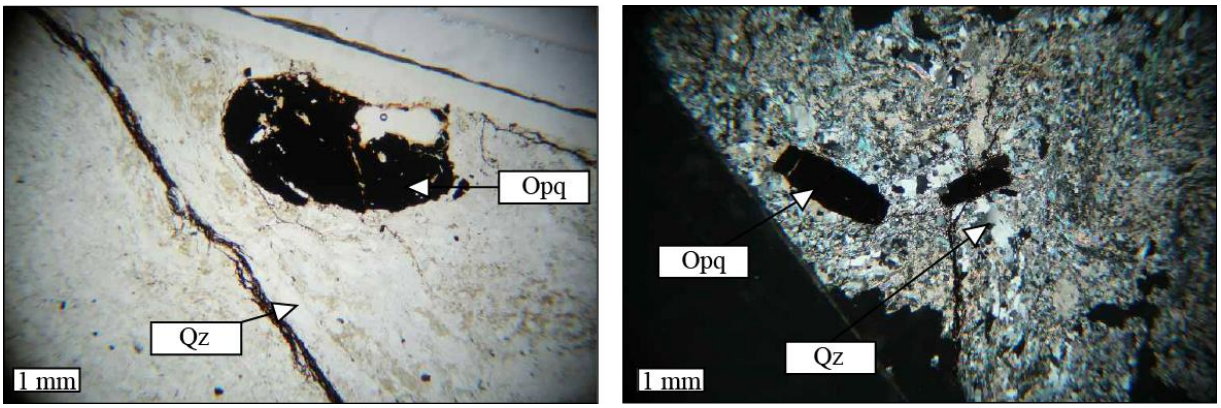

Figure 5–5. Porphyroblastic texture can be observed in the figure. Opaque mineral, quartz and opaque veins in the feldspar–biotite–chlorite–muscovite–quartz schist.

5.1.4. Schists ES 19A–1, ES 15B–6, ES 15B–8, ES 15C–4 and ES 15B–7

Quartz is occurring as xenoblast (Figure 5–7). Its grain dimension greatly varies from 1,2x0,57 to 0,025x0,01 millimetres. Quartz shows undulose extinction and white and blue interference colours of first order. Interpenetrating boundaries are formed due to subgrain rotation and bulging. Cryptocrystalline quartz forms laths and contributes to the foliation of the rock. Deformation lamellae in quartz give evidence to high stress that the rock has been exposed to.

In sample ES 15B–6 some grains are occurring as porphyroblasts with pressure shadow containing predominately chlorite. Quartz occupies 5 to 40 vol % of the samples.

Muscovite is occurring in samples ES 19A–1, ES 15B–6, ES 15B–8, ES 15C–4 and ES 15B–7. It has xenoblastic to subidioblastic habit and its grain size varies from 0,75x0,025 to 0,025x0,01 millimetres (Figure 5–8). Muscovite exhibits pale green colour under plane polarized light and interference colours of second order under crossed polars (Figure 5–6). Flakes of muscovite are subparallel and are contributing to the foliation of the sample. It occupies from 3 to 25 vol % of the samples.

Plagioclase is occurring in samples as xenoblast, its grain size varies from 0,38x0,14 to 0,11x0,05 millimetres. Plagioclase is kaolinized, sericitized and prehnitized. It occupies 10 to 16 vol % of this sample.

Chlorite is occurring as xenoblast and as fibrous, radiating aggregate. Its dimensions vary from 0,72x0,06 to 0,03x0,01 millimetres (Figure 5–6, Figure 5–7 and Figure 5–8). Chlorite has leafy habit and green pleochroism. It often shows anomalous brown and purple interference colour. In sample ES 15B–8 chlorite in contact with opaque veins is affected by limonitization. In sample ES 15C–4 it is possible to see relicts of biotite in the middle of chlorite minerals This is manifesting as brown fibres along chlorite habit. It occupies 25 to 30 vol % of the samples.

Biotite is occurring in samples ES 15B–8, ES 15C–4 ES and 15B–7 as massive, platy aggregate and as grains of xenoblastic habit. Its grain size varies from 0,16x0,08 to 0,035x0,02 millimetres. It exhibits strong pleochroism in brown colour. It has interference colours of high order. It is altered to chlorite and muscovite. Biotite occupies 3 to 5 vol % of the samples.

K–Feldspar is occurring in sample ES 15B–8 as xenoblast, its grain size varies from 0,7x0,4 to 0,05x0,03 millimetres. It is sericitized and prehnitized. It is scarce and occupies only about 5 vol % of the sample.

Carbonate mineral is occurring as xenoblastic grain which varies in size from 0,39x0,3 to 0,02x0,01 millimetres. Carbonate mineral shows change of relief with rotation and high order colours under crossed polars. Samples are intersected with veins filled with large, recrystallised calcite grains and large quartz grains. Calcite shows lamellar twinning in plane polarized light.

Dimensions of calcite mineral varies in different veins. Carbonate mineral occupies from 8 to 20 vol % of the samples.

Opaque mineral is occurring as xenoblast. Its grain size varies from 1,4x0,86 to 0,02x0,005 millimetres (Figure 5–6, Figure 5–7 and Figure 5–8). In the middle of some opaque grains red hematite is detected. Opaque mineral in samples ES 15B–7 (Figure 5–6) and ES 15B–8 is forming veins and is often accompanied by iron oxides and hydroxides of reddish–brown colour. Elongated minerals are parallel to foliation. It can be partially epidotized. Opaque mineral occupies 7 to 14 vol % of the samples.

Rutile is occurring as subidioblastic to xenoblastic grains in samples ES 15B–7 and ES 15B–8. Its grain size varies from 0,16x0,14 to 0,03x0,025 millimetres. It is characterized by very high relief and extreme birefringence. Rutile is often accompanied by titanite. It occupies 2 to 5 vol % of the samples.

Epidote is occurring as xenoblastic to subidioblastic grain, its grain size varies from 0,12x0,07 to 0,005x0,005 millimetres. Epidote has pale pleochroism in shades of green and interference colours of higher order (Figure 5–7 and Figure 5–8). It has a very high relief and yellow colour under plane polarised light. It is often appearing in the middle of opaque minerals. It occupies 3 to 5 vol % of the samples.

Clinozoisite is occurring in samples ES 15B–6 and ES 15C–4 as xenoblast. Its grain size varies from 0,08x0,06 to 0,03x0,02 millimetres. It has elongated habit and is colourless under plane polarised light and yellow and blue in cross–polarized light. It occupies 7 vol % of the samples.

Titanite is occurring in samples ES 15B–6 and ES 15C–4. Its subidioblastic grains vary in size from 0,045x0,02 to 0,02x0,015 millimetres. It has very high relief and elongated rhomb–shaped to rounded habit. It occupies 3 vol % of the sample.

Zoisite is occurring as subidioblast in sample ES 15C–4. Its grain size varies from 0,09x0,035 to 0,05x0,025 millimetres (Figure 5–7 and Figure 5–8). It has columnar shape and high relief. It is colourless and has a distinct blue interference colour. It occupies 3 vol % of the sample.

Sample ES 19A–1 has foliated structure and lepidogranoblastic texture. It has thick quartz veins which are intersected by thinner calcite veins. Some calcite veins have been limonitized.

Sample ES 15B–6 has foliated structure intersected by carbonate and limonite veins and homeoblastic texture.

Samples ES 15B–8 and ES 15C–4 have foliated structure and lepidogranoblastic texture. Sample ES 15B–8 has elements of banded texture, interchanging of quartz + carbonate mineral bands and mostly chlorite bands. Thin opaque veins in the samples are pathways for limonitization.

Sample ES 15B–7 has foliated structure and granolepidoblastic texture (Figure 5–6). Carbonate veins formed after the rock cooled down enough to be brittle and got fractured. Fractures were later filled with carbonate solutions which later crystallised, forming carbonate veins which intersect the foliation of the sample.

Sample ES 19A–1 is determined as **epidote–muscovite–quartz–chlorite schist** (Table 5–4). Sample ES 15B–6 is determined as **epidote–quartz–chlorite schist** (Table 5–4). Sample ES 15B–8 is determined as **feldspar–biotite–quartz–chlorite schist** (Table 5–4). Sample ES 15C–4 is determined as **biotite– epidote–quartz–chlorite schist** (Table 5–4). Sample ES 15B–7 is determined as **quartz–albite–muscovite–chlorite schist** (Table 5–4).

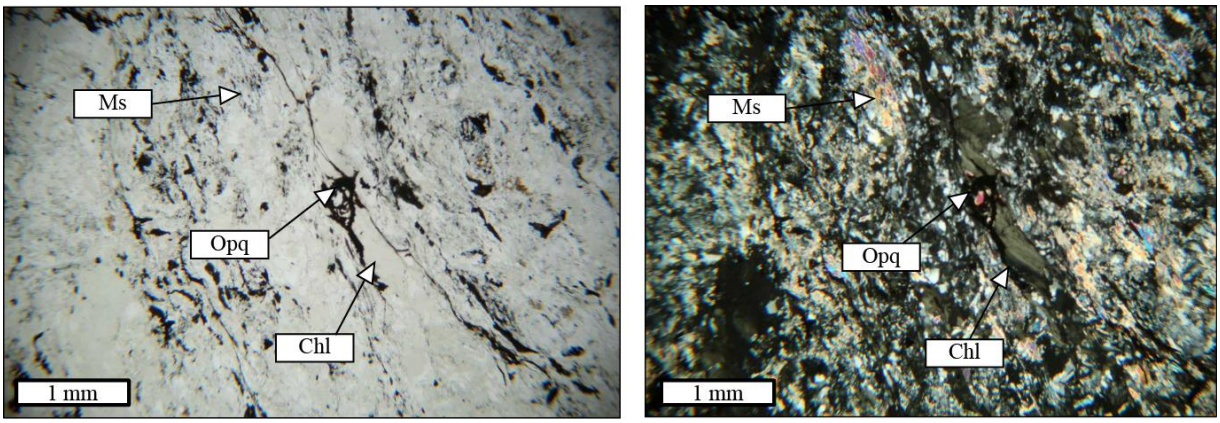

Figure 5–6. Opaque mineral, chlorite and muscovite in sample ES 15B–7, determined as quartz–albite–muscovite–chlorite schist. Granolepidoblastic texture of sample can be seen.

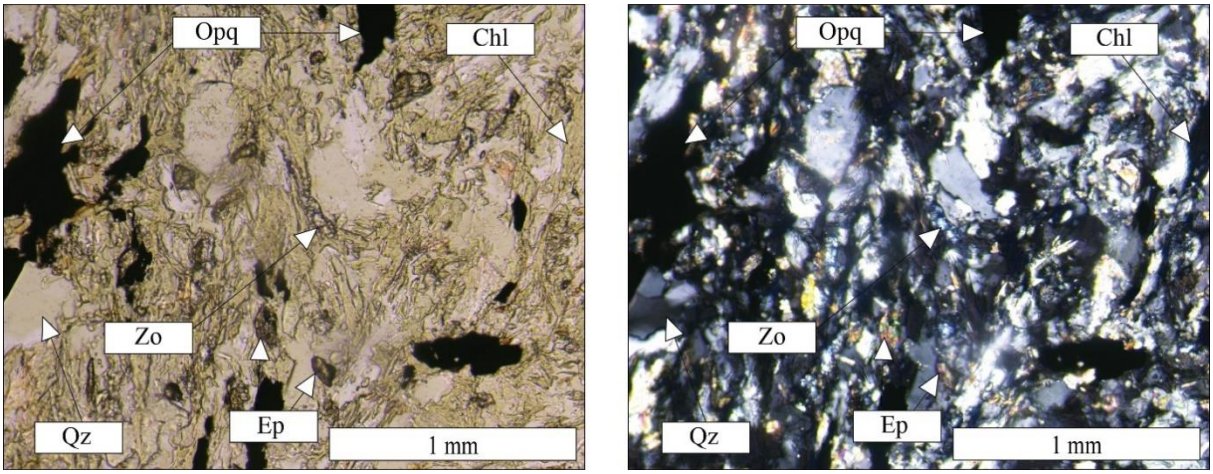

Figure 5–7. Epidote, opaque mineral, chlorite, quartz and zoisite in sample ES 15C–4. Biotite–epidote–quartz–chlorite schist with lepidogranoblastic texture.

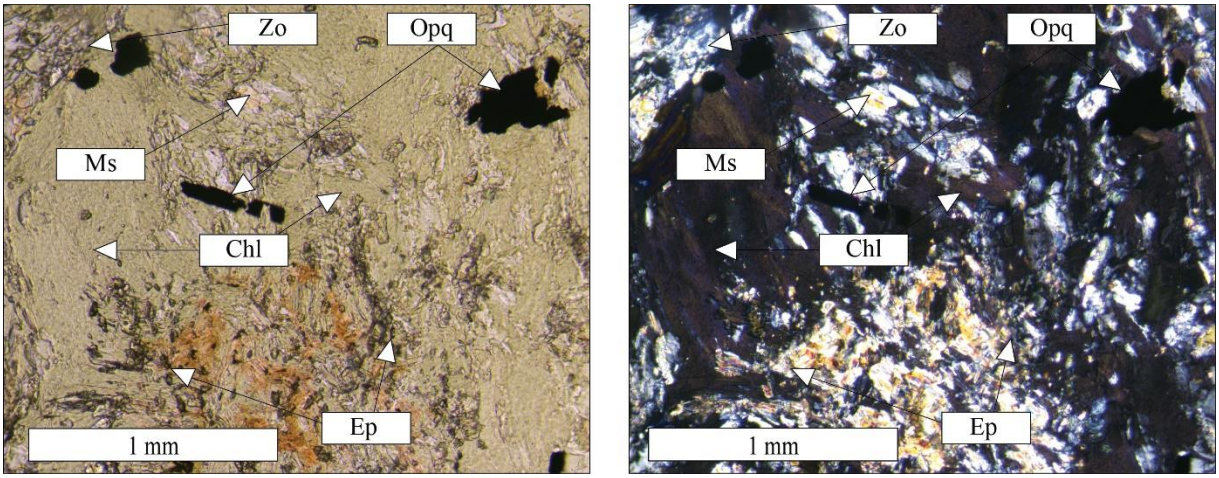

Figure 5–8. Epidote, opaque mineral, chlorite, zoisite and muscovite in sample ES 15C–4. Biotite– epidote–quartz–chlorite schist with lepidogranoblastic texture.

Table 5–4. Mineralogical description of samples ES 19A–1, ES 15B–6, ES 15B–8, ES 15C–4 ES and 15B–7.

Sample	ES 19A-1	ES 15B-6	ES 15B-8	ES 15C-4	ES 15B-7
	Epidote–muscovite–quartz–chlorite schist	Epidote–quartz-chlorite schist	Feldspar–biotite–quartz–chlorite schist	Biotite– epidote–quartz–chlorite schist	Quartz–albite–muscovite–chlorite schist
Structure	foliated	foliated	foliated	foliated	foliated
Texture	lepidogranoblastic	homeoblastic	lepidogranoblastic	lepidogranoblastic	granolepidoblastic
Quartz	grain size: 1,04x0,56 - 0,04x0,02 habit: xenoblastic estimation of proportion: 24% alterations: /	grain size: 0,12x0,06 - 0,025x0,01 habit: xenoblastic estimation of proportion: 18% alterations: undulose extinction	grain size: 1,2x0,57 - 0,05x0,03 habit: xenoblastic estimation of proportion: 10% alterations: undulose extinction	grain size: 0,12x0,08 - 0,04x0,04 habit: xenoblastic estimation of proportion: 10% alterations: /	grain size: 0,65x0,5 - 0,04x0,02 habit: xenoblastic grains, porphyroblasts estimation of proportion: 5% alterations: undulose extinction
Muscovite	grain size: 0,3x0,08 - 0,12x0,028 habit: subidioblastic estimation of proportion: 10% alterations: /		grain size: 0,75x0,025 - 0,025x0,01 habit: xenoblastic estimation of proportion: 3% alterations: /	grain size: 0,06x0,01 - 0,05x0,015 habit: xenoblastic estimation of proportion: 3% alterations: intergrowth with chlorite	grain size: 0,28x0,06 - 0,1x0,02 habit: subidioblastic estimation of proportion: 25% alterations: /
Plagioclase	grain size: 0,3x0,18 - 0,1x0,05 habit: xenoblastic estimation of proportion: 16% alterations: prehnitization	grain size: 0,35x0,2 - 0,11x0,09 habit: xenoblastic estimation of proportion: 12% alterations: prehnitization	grain size: 0,31x0,1 - 0,12x0,06 habit: xenoblastic estimation of proportion: 10% alterations: prehnitization	grain size: 0,28x0,15 - 0,1x0,04 habit: xenoblastic estimation of proportion: 15% alterations: prehnitization	grain size: 0,38x0,14 - 0,11x0,05 habit: xenoblastic estimation of proportion: 10% alterations: kaolinitization, prehnitization
Chlorite	grain size: 0,72x0,06 - 0,06x0,02 habit: xenoblastic, fibrous estimation of proportion: 15% alterations: /	grain size: 0,1x0,05 - 0,03x0,01 habit: xenoblastic estimation of proportion: 27% alterations: /	grain size: 0,44x0,32 - 0,03x0,01 habit: xenoblastic estimation of proportion: 20% alterations: /	habit: fibrous, radiating aggregate estimation of proportion: 30% alterations: /	grain size: 0,44x0,28 - 0,1x0,02 habit: xenoblastic estimation of proportion: 30% alterations: /
Biotite			grain size: 0,16x0,08 to 0,035x0,02 habit: xenoblastic estimation of proportion: 5% alterations: chloritization	grain size: 0,16x0,08 - 0,035x0,02 habit: xenoblastic estimation of proportion: 5% alterations: chloritized	habit: massive, platy aggregate estimation of proportion: 3% alterations: chloritization, interlayering with muscovite and chlorite
K-Feldspar			grain size: 0,7x0,4 - 0,05x0,03 habit: xenoblastic estimation of proportion: 5% alterations: sericitization, prehnitization		
Carbonates	grain size: 0,18x0,1 - 0,06x0,03 habit: xenoblastic estimation of proportion: 10% alterations: /	grain size: 0,12x0,08 - 0,02x0,01 habit: xenoblastic estimation of proportion: 20% alterations: /	grain size: 0,32x0,3 - 0,1x0,08 habit: xenoblastic estimation of proportion: 15% alterations: /	grain size: 0,2x0,12 - 0,15x0,1 habit: xenoblastic estimation of proportion: 10% alterations: /	grain size: 0,39x0,3 - 0,16x0,8 habit: xenoblastic estimation of proportion: 8% alterations: /
Opaque	grain size: 0,56x0,32 - 0,025x0,02 habit: xenoblastic estimation of proportion: 10% alterations: /	grain size: 0,08x0,04 - 0,02x0,005 habit: xenoblastic estimation of proportion: 8% alterations: /	grain size: 0,24x0,2 - 0,08x0,02 habit: xenoblastic estimation of proportion: 7% alterations: /	grain size: 0,5x0,25 - 0,15x0,1 habit: xenoblastic estimation of proportion: 10% alterations: epidotization	grain size: 1,4x0,86 - 0,16x0,08 habit: xenoblastic grains and veins estimation of proportion: 14% alterations: hematitization limonitization
Rutile			grain size: 0,16x0,14 - 0,06x0,02 habit: xenoblastic estimation of proportion: 5% alterations: titanitization		grain size: 0,1x0,035 - 0,03x0,025 habit:subidioblastic estimation of proportion: 2% alterations: titanitization
Epidote	grain size: 0,03x0,015 - 0,02x0,01 habit: xenoblastic estimation of proportion: 5% alterations: /	grain size: 0,04x0,02 - 0,02x0,02 habit: xenoblastic estimation of proportion: 5% alterations: /	grain size: 0,01x0,01 to 0,005x0,005 habit: subidioblastic estimation of proportion: 4% alterations: /	grain size: 0,12x0,07 - 0,05x0,01 habit: xenoblastic estimation of proportion: 5% alterations: /	grain size: 0,04x0,01 - 0,02x0,035 habit: subidioblastic estimation of proportion: 3% alterations: /
Clinozoisite		grain size: 0,06x0,04 - 0,03x0,02 habit: xenoblastic estimation of proportion: 7% alterations: /		grain size: 0,08x0,06 - 0,04x0,01 habit: xenoblastic estimation of proportion: 7% alterations: /	
Titanite		grain size: 0,045x0,02 - 0,02x0,015 habit: subidioblastic estimation of proportion: 3% alterations: /		grain size: 0,05x0,02 - 0,02x0,009 habit: subidioblastic estimation of proportion: 15% alterations: /	
Zoisite				grain size: 0,09x0,035 - 0,05x0,025 habit: subidioblastic estimation of proportion:3% alterations: /	
Hematite					grain size: 0,1x0,06 -0,04x0,02 habit:subidioblastic estimation of proportion: 1% alterations: /

5.1.5. Quartz–chlorite–actinolite schist ES 10F–1

Quartz is appearing as xenoblast, its grain size varies from 0,16x0,14 to 0,06x0,04 millimetres (Figure 5–9 and Figure 5–12). It shows undulose extinction. Quartz is also occurring in its fibrous form, usually known as “quartz–wings” or “feather–quartz” (Figure 5–10). It forms due

to extension in the plane of schistosity which pulls the matrix from the sides of the porphyroblasts. Quartz occupies around 8 vol % of this sample.

Muscovite is appearing as xenoblastic flakes whose dimensions vary from 0,145x0,01 to 0,04x0,01 millimetres. There is an acicular intergrowth of colourless muscovite with green chlorite (Figure 5–9, Figure 5–10, Figure 5–11 and Figure 5–12). Muscovite, as opposed to chlorite has a change of relief with rotation and higher interference colours. Muscovite occupies 4 vol % of the sample.

Chlorite is appearing as fibrous, radiating and massive aggregate and as xenoblast (Figure 5–9, Figure 5–10, Figure 5–11 and Figure 5–12). It has a pleochroism in shades of green and "Berlin–blue" interference colour. Its size varies from 0,22x0,04 to 0,05x0,01 millimetres. It occupies around 30 vol % of the sample.

Carbonate mineral is occurring as xenoblast (Figure 5–9, Figure 5–10, Figure 5–11 and Figure 5–12). It shows high relief that changes with rotation and pale, high order interference colours. Its grain size varies from 0,41x0,2 to 0,04x0,04 millimetres. It occupies 10 vol % of this sample.

Amphibole is appearing as fibrous aggregate and hipidioblast. It is presented by actinolite, and it is recognizable by its pale pleochroism in shades of green and fibrous habit. It exhibits extinction angle of around 9 ° parallel to the fibres. Its size varies from 0,17x0,01 to 0,025x0,005 millimetres. It occupies 40 vol % of this rock.

Opaque mineral is occurring as a phase with idioblastic habitus and as xenoblastic grains (Figure 5–9 and Figure 5–10, Figure 5–11 and Figure 5–12). Idioblasts are appearing as pre–cinematic porphyroblasts and have a pressure shadow of fibrous quartz. Xenoblastic grains often appear in elongated clusters which display the preferred orientation of the rock. Opaque mineral grain size varies from 0,4x0,16 to 0,04x0,04 millimetres. It occupies 8 vol % of this sample.

Sericite is abundant in the sample, it completely altered some mineral grains. There are several fractures which were a pathway for limonite. Fractures are surrounded by carbonate mineral. Rock has foliated structure and porphyroblastic texture. It is determined as **quartz–chlorite–actinolite schist** (Table 5–5).

Table 5–5. Mineralogical description of sample ES 10F–1.

Sample ES 10F-1 **Quartz–chlorite–actinolite schist**	Structure foliated	Texture porphyroblastic
Quartz	**Muscovite**	**Chlorite**
grain size: 0,16x0,14 - 0,06x0,04 habit: xenoblastic estimation of proportion: 5% alterations: undulose extinction alterations: /	grain size: 0,145x0,01 - 0,04x0,01 habit: xenoblastic flakes estimation of proportion: 4% alterations: /	grain size: 0,22x0,04 - 0,05x0,01 habit: xenoblastic, fibrous, radiating, massive estimation of proportion: 30% alterations: /
Carbonates	**Amphibole**	**Opaque**
grain size: 0,41x0,2 - 0,04x0,04 habit: xenoblastic estimation of proportion: 10% alterations: /	Actinolite grain size: 0,17x0,01 - 0,025x0,005 habit: hipidioblastic, fibrous aggregate estimation of proportion: 40% alterations: /	grain size: 0,4x0,16 - 0,04x0,04 habit: phase with idioblastic habit and second phase with xenoblastic habit (grainy) estimation of proportion: 8% alterations: /

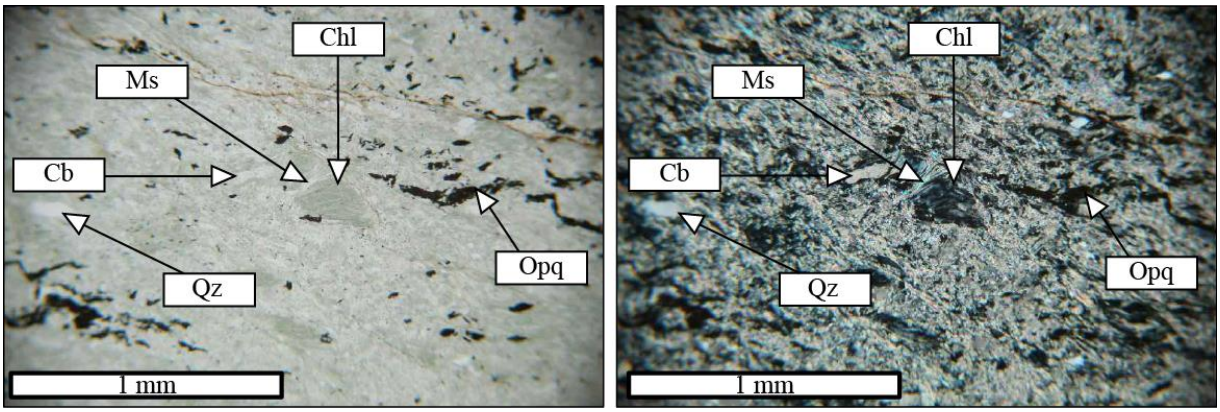

Figure 5–9. Muscovite, chlorite, carbonate mineral, quartz and opaque mineral in the porphyroblastic quartz–chlorite–actinolite schist.

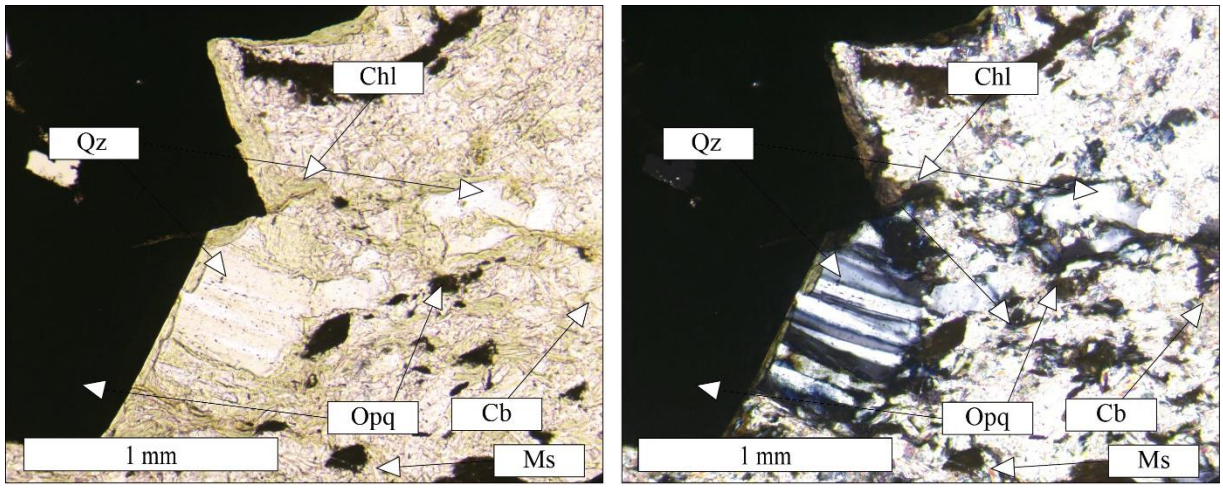

Figure 5–10. Pre–cinematic opaque porphyroblast with pressure shadow of fibrous quartz, chlorite, carbonate mineral and muscovite in the quartz–chlorite–actinolite schist, sample ES 10F–1.

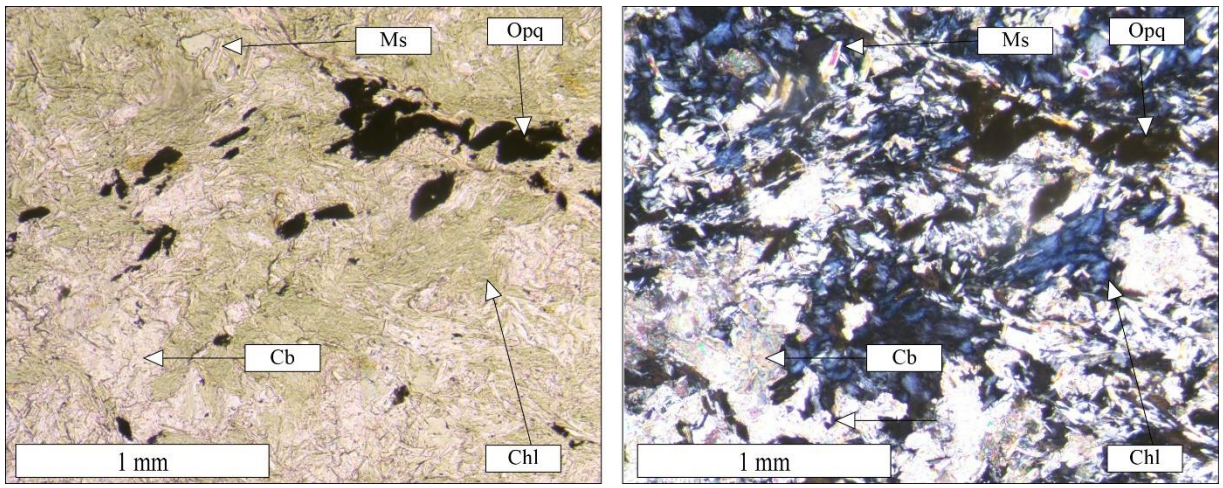

Figure 5–11. Chlorite, muscovite, carbonate mineral and opaque mineral in the Quartz–chlorite–actinolite schist, sample ES 10F–1.

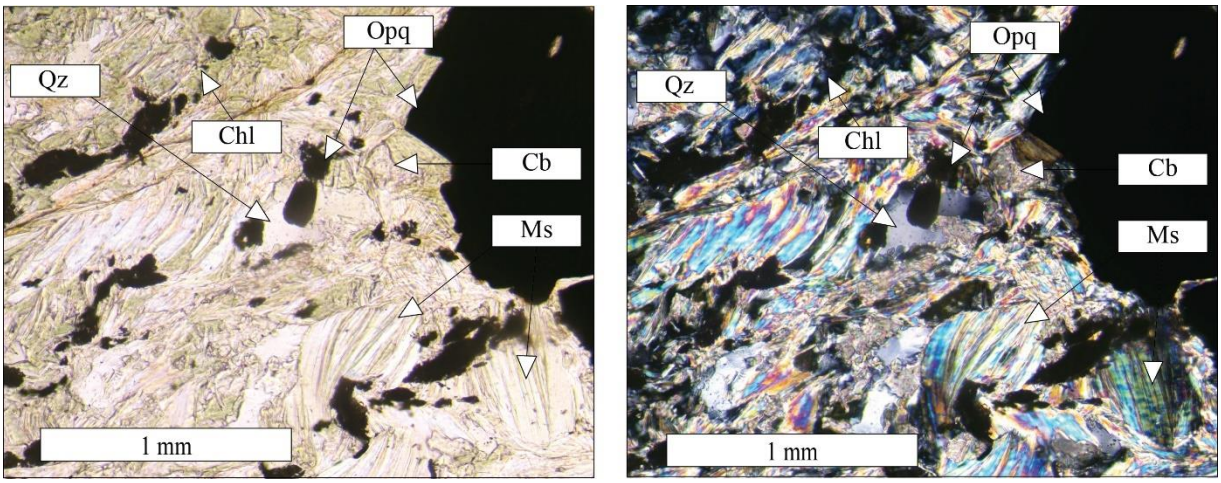

Figure 5–12. Chlorite, muscovite, carbonate mineral, quartz and opaque mineral in the quartz–chlorite–actinolite schist.

5.1.6. Garnet–epidote–chlorite–quartz–muscovite schist ES 19B

Quartz is occurring as xenoblast, its grain size varies from 0,24x0,16 to 0,08x0,04 millimetres (Figure 5–13). Quartz grains are forming laths. Coarser quartz has curved to narrow grain boundaries some of which are intersecting at approximately 120°. This is a result of recrystallization driven by the reduction in system energy. Finer quartz has inequant, largely elongated grains with undulose extinction and interpenetrating boundaries. Quartz occupies around 20 vol % of this rock.

Muscovite is occurring as xenoblast, its grain size varies from 1x0,05 to 0,15x0,01 millimetres. It has vivid interference colours of high order. Some muscovite flakes are folded, contributing to foliation of the rock. It occupies 20 vol % of this rock.

Chlorite is occurring as xenoblast, its grain size varies from 0,34x0,08 to 0,1x0,03 millimetres. It has weak pleochroism in green colour. It has anomalous, very dark brown and “Berlin–blue” interference colours. It occupies 17 vol % of this rock.

Biotite is occurring as xenoblast, its grain size varies from 0,3x0,12 to 0,04x0,01 millimetres (Figure 5–13). Biotite has strong pleochroism in brown colour. It has vivid interference colours of high order. It is partly altered to chlorite. It occupies 3 vol % of this rock.

Carbonate mineral is occurring as xenoblast, its grain size varies from 0,8x0,4 to 0,06x0,04 millimetres. Carbonate mineral is colourless and shows lamellar twinning in plane polarized light. It has high order birefringence colours. It occupies 5 vol % of this rock.

Opaque mineral is occurring as xenoblast, its grain size varies from 0,7x0,25 to 0,05x0,02 millimetres (Figure 5–13). There is a titanitization in the middle of opaque grains and along the edge. It occupies 5 vol % of this rock.

Garnet is occurring as xenoblast, its grain size varies from 3,2x1,6 to 0,72x0,32 millimetres. Garnet shows intense retrograde alteration along veins and fractures. It is replaced with lower temperature minerals such as chlorite, muscovite and biotite (Figure 5–13). It also contains zoisite and opaque mineral with titanite rim. It occupies 12 vol % of this sample.

Clinozoisite is occurring as subidioblast, its grain size varies from 0,2x0,05 to 0,08x0,04 millimetres. Clinozoisite is colourless in plain polarized light and shows first order colours under cross–polarized light and. It occupies 8 vol % of this rock.

Titanite is occurring as idioblast, its grain size varies from 0,22x0,06 to 0,06x0,04 millimetres. It has tan brown colour under plane polarized light. Titanite often incorporates opaque inclusions. It occupies 5 vol % of this rock.

Zoisite is occurring as subidioblast, its grain size varies from 1,2x0,08 to 0,2x0,05 millimetres. Minerals are of prismatic shape and show perfect cleavage. It occupies 5 vol % of this sample.

In this rock, deformation partitioning resulted in the division into less strained and more intensely strained domains. Less strained domains are characterized by noticeably larger quartz grains outlined by mica flakes, while more intensely strained domains have smaller, stretched quartz grains and smaller mica flakes.

Foliation of the sample, caused by muscovite flakes is intersected by opaque veins. Opaque veins are limonitized. Rock has foliated structure. Texture is porphyroblastic. Sample is determined as **garnet–epidote–chlorite–quartz–muscovite schist** (Table 5–6).

Table 5–6. Mineralogical description of sample ES 19B.

Sample ES 19B	Structure	Texture
Garnet–epidote–chlorite–quartz–muscovite schist	foliated	porphyroblastic
Quartz	**Muscovite**	**Chlorite**
grain size: 0,24x0,16 - 0,08x0,04 habit: xenoblastic estimation of proportion: 15% alterations: /	grain size: 1x0,05 - 0,15x0,01 habit: xenoblastic estimation of proportion: 20% alterations: /	grain size: 0,34x0,08 - 0,1x0,03 habit: xenoblastic estimation of proportion: 15% alterations: /
Biotite	**Carbonates**	**Opaque**
grain size: 0,3x0,12 - 0,04x0,01 habit: xenoblastic estimation of proportion: 3% alterations: chloritized	grain size: 0,8x0,4 - 0,06x0,04 habit: xenoblastic estimation of proportion: 5% alterations: /	grain size: 0,7x0,25 - 0,05x0,02 habit: xenoblastic estimation of proportion: 5% alterations: titanitization
Garnet	**Clinozoisite**	**Titanite**
grain size: 3,2x1,6 - 0,72x0,32 habit: xenoblastic estimation of proportion: 10% alterations: chloritization, titanitization	grain size: 0,2x0,05 - 0,08x0,04 habit: subidioblastic estimation of proportion: 8% alterations: /	grain size: 0,22x0,06 - 0,06x0,04 habit: idioblastic estimation of proportion: 5% alterations: /
Zoisite		
grain size: 1,2x0,08 - 0,2x0,05 habit: subidioblastic estimation of proportion: 5% alterations: /		

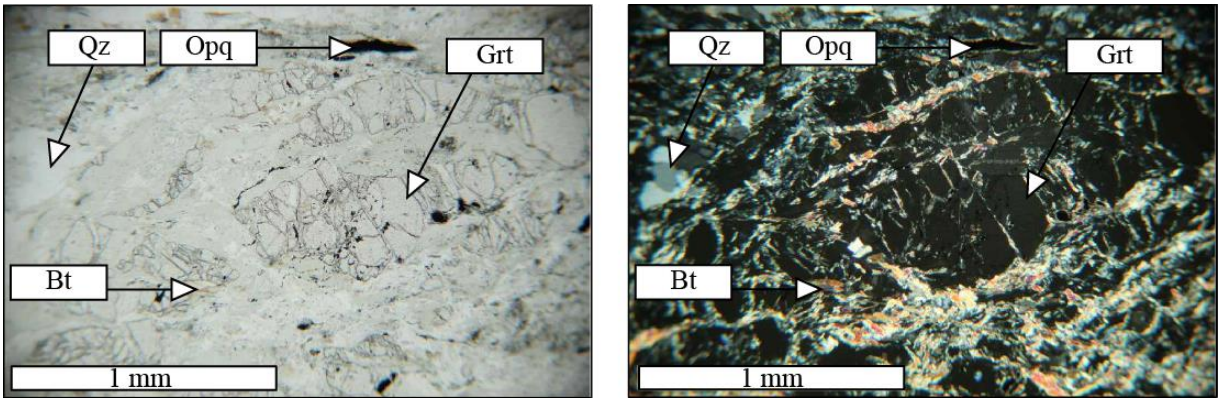

Figure 5–13. Garnet showing retrograde alteration along veins and fractures which consist of chlorite, muscovite, biotite and zoisite and opaque mineral with titanite rim in sample ES 19B.

5.1.7. Amphibole schists: ES 10E–2, ES 10H and ES 20–2

Amphibole in sample ES 10E–2 occurs as subidioblast in the matrix and as porphyroblast (Figure 5–14, Figure 5–15, Figure 5–16 and Figure 5–17). Its elongated, prismatic grains vary in size from 4,8x4,4 to 0,08x0,04 millimetres. In samples ES 10H and ES 20–2 grain size varies from 0,55x0,5 to 0,1x0,04 millimetres. It is presented by hornblende and actinolite, both of

which are characterized by pleochroism in green to yellowish green colour. Hornblende shows high relief and perfect cleavage with 56° and 124° cleavage intersections. Actinolite has columnar, more elongated habit and often shows orange to pink interference colours of second order.

Amphibole porphyroblasts in sample ES 10E–2 show moderate relief and high interference colours of second order. They have cracks filled with calcite and others filled with chlorite. Cracks could have been pathways for quartz to enter and recrystallize in the porphyroblast. Some grains show a resorption texture. Porphyroblasts preserve inclusion trails that are not continuous with matrix foliation. They have quartz–dominated strain shadow with minerals from the matrix. In this sample we have a pre–kinematic porphyroblast. Hornblende is partially altered to clinozoisite. Amphibole occupies up from 38 vol % to 58 vol % of the samples.

Plagioclase occurs as xenoblast. Grain size varies form 0,8x0,75 to 0,11x0,05 millimetres. Plagioclase has lamellae and is sericitized and prehnitized. In sample ES 10H plagioclase has many zoisite inclusions. It occupies from 7 to 10 vol % of the samples.

Chlorite occurs both as porphyroblast with idioblastic to subidioblastic habit and as massive and foliated aggregates (Figure 5–14, Figure 5–15, Figure 5–16). Chlorite dimensions varies from 2,2x1,4 to 0,26x0,8 millimetres. It shows pleochroism in shades of green. Chlorite also exhibits anomalous, dark purple to dark brown interference colours. Which indicate that it has high iron and magnesium content, and it is probable that it is a chamosite. Porphyroclast has inclusions of irregular grains of titanite, epidote and quartz. Its inclusions do not show alignment, but orientation of the grain is not coextending with matrix foliation. A pressure shadow consists of syn–cinematic quartz and minerals from the matrix. It is a pre–kinematic porphyroblast. Fan–shaped aggregate of chlorite is surrounding the limonitized vein which is intersecting the ES 20–2 sample. Chlorite occupies up from 5 vol % to 19 vol % of the samples.

Biotite occurs as xenoblast in sample ES 20–2. Its grain size varies form 0,04x0,02 to 0,02x0,01 millimetres. It occupies around 3 vol % of the sample.

Quartz has xenoblastic habit and grain size varies from 0,95x0,88 to 0,08x0,04 millimetres (Figure 5–14, Figure 5–15, Figure 5–16 and Figure 5–17). Quartz appears randomly dispersed along the samples and in sample ES 10E–2 it also forms clusters with orthoclase and plagioclase

forming lath leucocratic textures. In such lenses there are often many zoisite and clinozoisite minerals. Grains show undulose extinction and contacts between quartz grains are sutured. Quartz is partially recrystallized, subgrain rotation and bulging of quartz is detected in the sample. In sample E 20–2 there is a quartz–carbonate vein. There is around 3 to 4 vol % of quartz in the samples.

Orthoclase appears in samples ES 10E–2 and ES 10H. It shows subidioblastic habit and its grain size varies from 0,5x0,1 to 0,08x0,04 millimetres. Orthoclase is sericitized, alteration occurring on grain edges and kaolinized (starting from the middle of the grain), it often has many zoisite and clinozoisite inclusions (Figure 5–15). Orthoclase occupies 3 to 10 vol % of the samples.

Carbonate mineral occurs as xenoblast (Figure 5–14, Figure 5–15), predominately in veins. Its grain size varies from 0,54x0,22 to 0,07x0,07 millimetres. It shows change of relief with rotation and high order colours under crossed polars. It occupies 2 vol % of the rock.

Opaque mineral appears both as xenoblast and as idioblast in sample ES 10E–2. In sample ES 10H it has idioblastic habit and in sample ES 20–2 it appears as xenoblast which often has epidote minerals along their rims. Its grain size varies from 0,8x0,24 to 0,05x0,04 millimetres (Figure 5–14, Figure 5–15, Figure 5–16 and Figure 5–17). Its orientation is random, and it is not aligned with matrix foliation. It often contains inclusions of matrix minerals. It occupies around 4 vol % of the samples.

Rutile occurs in sample ES 20–2. It has xenoblastic habit and varies in size from 0,18x0,1 to 0,08x0,05 millimetres. Rutile has very high relief and interference colours masked by rich minerals yellowish brown colour. It is accompanied by ilmenite. There is around 3 vol % of it in the sample.

Garnet occurs as xenoblast in sample ES 20–2 (Figure 5–16), its size varies from 1,2x0,8 to 0,7x0,45 millimetres. It is heavily altered. Along its irregular fractures and around the rims, there are many alteration minerals such as chlorite, epidote, amphibole. This group of alteration minerals is known as kelyphitic alteration rim. Garnet occupies up to 4 vol % of the sample.

Titanite occurs as subidioblast, its size varies from 0,07x0,04 to 0,02x0,01 millimetres. It has pleochroism from almost colourless to pale yellow colour and high–order white (cream)

interference colour. It is often forming elongated bundles aligned with the matrix foliation. There is around 5 vol % of it in the samples.

Zoisite appears in samples ES 10E–2 and ES 10H (Figure 5–15). It has subidioblastic habit with characteristic elongated rhomb–shaped minerals with very high relief. Its size varies from 0,22x0,1 to 0,08x0,03 millimetres. It has perfect cleavage and distinct blue interference colour. It occupies around 4 vol % of the samples.

Clinozoisite occurs as subidioblast, its size varies from 0,8x0,44 to 0,08x0,04 millimetres (Figure 5–14Figure 5–15). Mineral is colourless and elongated and yellow and blue in cross–polarized light. Along with zoisite, it often appears as inclusions in orthoclase. In sample ES 20–2 it has an alteration texture which resembles readsorption. It occupies around 4 vol % of the samples.

Epidote occurs as idioblast in samples ES 10E–2 and ES 20–2, its size varies from 0,32x0,1 to 0,04x0,02 millimetres. It has high relief and live interference colours of second order. There is 3 to 8 vol % of it in the samples (Figure 5–14, Figure 5–15, Figure 5–16 and Figure 5–17).

In sample ES 10E–2 prismatic amphibole grains and titanite elongated bundles are contributing to the foliation of the texture. Several veins are intersecting the matrix. Veins consist of fibrous chlorite and of recrystallized quartz and calcite but various minerals from the matrix are also imbedded in the veins. There are also veins consisting predominately of limonite. There are pre–cinematic porphyroblast of amphibole and chlorite and opaque mineral. Rock has a foliated structure and relict porphyroblastic texture.

Sample ES 10H has leucocratic vein which separates finer–grained and coarser–grained segments. Finer–grained part of the sample is more homogenous and coarser–grained part of the sample has interchange of predominately amphibole and leucocratic (quartz + orthoclase + plagioclase) layers. Rock has a foliated structure and granonematoblastic texture.

Sample ES 20–2 contains a thick vein, predominately composed of quartz grains of different sizes and calcite. From it, a smaller limonite veins are intruding into the other part of the sample composed predominately of amphibole. Limonite veins are partly filled or surrounded by a fan–shaped chlorite aggregate and in part carbonate mineral. Interlocking, randomly orientated

prismatic amphibole minerals form a decussate structure. Sample has relict intergranular doleritic texture.

Sample ES 10E–2 is an **albite–epidote–chlorite–amphibole schist**. Sample ES 10H is determined as **epidote–chlorite–feldspar–amphibole schist**. Sample ES 20–2 is a **chlorite–epidote–albite–amphibole schist** (Table 5–7).

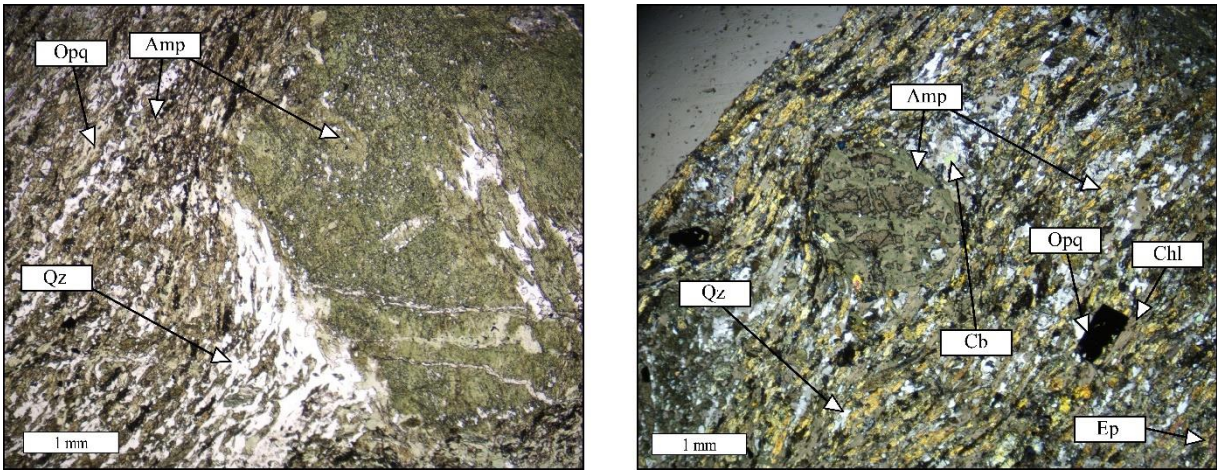

Figure 5–14. Amphibole porphyroblast, chlorite, opaque mineral, epidote, carbonate mineral, quartz and other matrix minerals in the albite–epidote–chlorite–amphibole schist (sample ES 10E–2) with relict porphyroblastic texture.

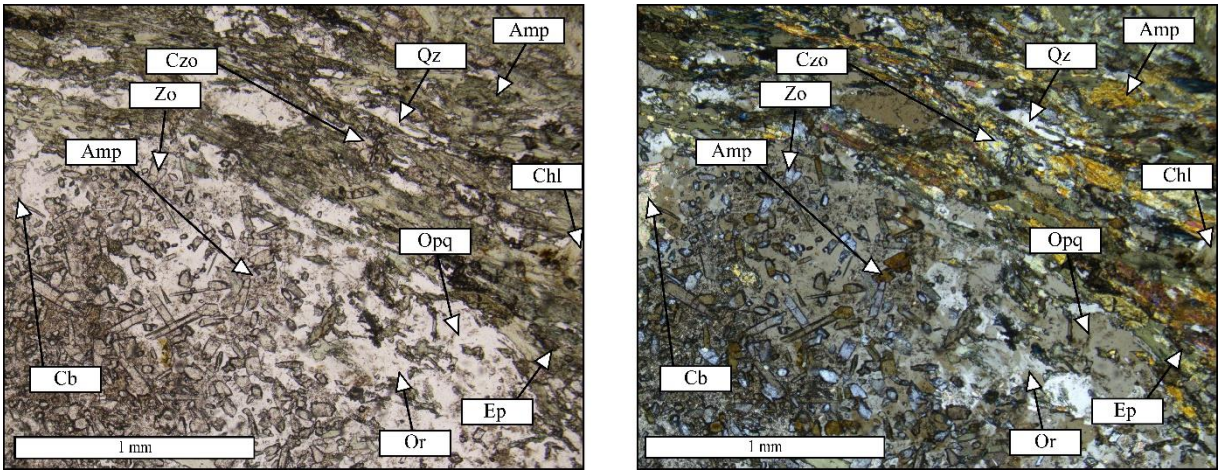

Figure 5–15. Amphibole, chlorite, opaque mineral, zoisite, clinozoisite, epidote, orthoclase, quartz and carbonate mineral in the epidote–chlorite–feldspar–amphibole schist (sample ES 10H) with relict granonematoblastic texture.

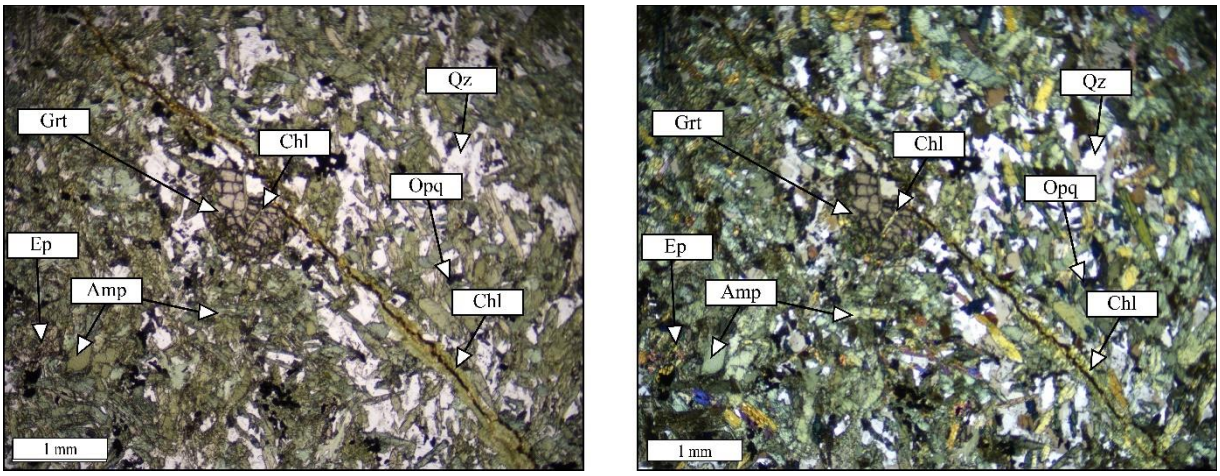

Figure 5–16. Amphibole, chlorite, opaque mineral, garnet, epidote and quartz in the chlorite–epidote–albite–amphibole schist (sample ES 20–2) with relict intergranular doleritic texture.

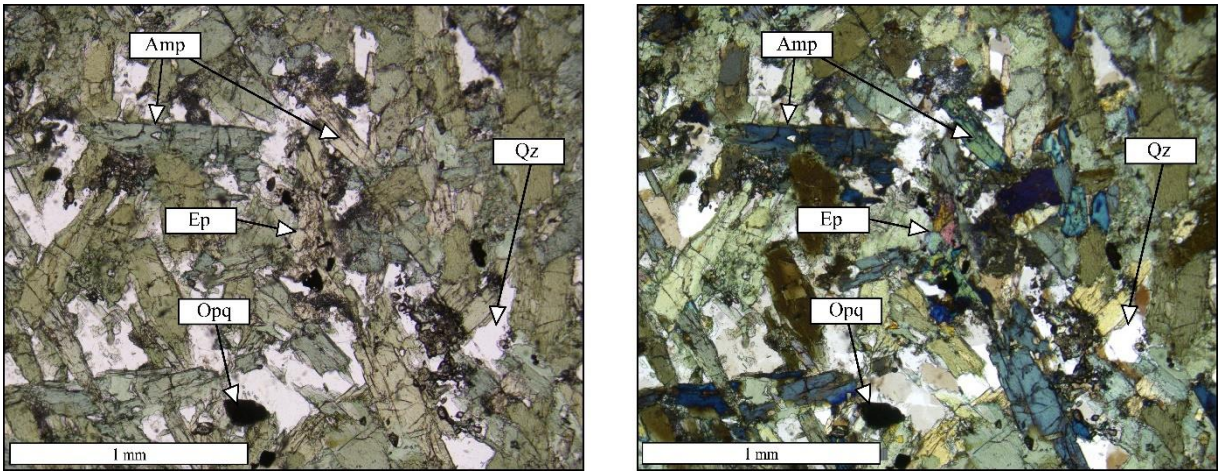

Figure 5–17. Amphibole, opaque mineral, epidote and quartz in the chlorite–epidote–albite–amphibole schist (sample ES 20–2) with intergranular doleritic texture.

Table 5–7. Mineralogical description of samples ES 10E–1, ES 10H and ES 20–2.

Sample	ES 10E-2	ES 10H	ES 20-2
	Albite–epidote–chlorite–amphibole schist	**Epidote–chlorite–feldspar–amphibole schist**	**Chlorite–epidote–albite–amphibole schist**
Structure	foliated	foliated	decussate
Texture	porphyroblastic	lepidogranonematoblastic	relict intergranular texture
Quartz	grain size: 0,2x0,1 - 0,08x0,04 habit: xenoblastic estimation of proportion: 3%	grain size: 0,22x0,16 - 0,14x0,06 habit: xenoblastic estimation of proportion: 4% alterations: /	grain size: 0,95x0,88 - 0,72x0,6 habit: xenoblastic estimation of proportion: 4%
Plagioclase	grain size: 0,28x0,1 - 0,7x0,15 habit: xenoblastic grains estimation of proportion: 10% alterations: sericitization	grain size: 0,8x0,75 - 0,14x0,4 habit: xenoblastic estimation of proportion: 10% alterations: sericitization	grain size: 0,3x0,11 - 0,11x0,05 habit: xenoblastic estimation of proportion: 7% alterations: sericitization, prehnitization
Chlorite	grain size: 2,2x1,4 - 0,26x0,8 habit: massive, earthy, large xenoblastic porphyroblasts estimation of proportion: 19% alterations: /	grain size: 0,58x0,4 - 0,2x0,04 habit: xenoblastic estimation of proportion: 10% alterations: /	grain size: 0,1x0,04 - 0,04x0,01 habit: massive, earthy estimation of proportion: 5% alterations: /
Biotite			grain size: 0,04x0,02 - 0,02x0,01 habit: xenoblastic estimation of proportion: 3% alterations: /
K-Feldspar	Orthoclase grain size: 0,5x0,1 - 0,08x0,04 habit: subidioblastic estimation of proportion: 3% alterations: sericitization, kaolinization	grain size: 0,2x0,25 - 0,08x0,05 habit: subidioblastic to xenoblastic estimation of proportion: 10% alterations: sericitization, prehnitization	
Calcite	grain size: 0,54x0,22 - 0,08x0,04 habit: xenoblastic estimation of proportion: 2% alterations: /	grain size: 0,36x0,14 - 0,07x0,07 habit: xenoblastic estimation of proportion: 2% alterations: /	grain size: 0,5x0,2 - 0,1x0,06 habit: xenoblastic estimation of proportion: 2% alterations: /
Amphibole	Actinolite, hornblende grain size: 0,42x0,04 - 0,08x0,04 porphyroblast: 4,8x4,4 habit: subidioblastic estimation of proportion: 38% alterations: /	Actinolite, hornblende grain size: 0,55x0,5 - 0,25x0,05 habit: xenoblastic estimation of proportion: 48% alterations: /	Actinolite, hornblende grain size: 0,4x0,09 - 0,1x0,04 habit: subidioblastic estimation of proportion: 58% alterations: hornblende altered to cinozoisite
Opaque	grain size: 0,65x0,5 - 0,1x0,035 habit: idioblastic estimation of proportion: 4% alterations: /	grain size: 0,4x0,24 - 0,16x0,08 habit: idioblastic estimation of proportion: 4% alterations: /	grain size: 0,8x0,24 - 0,05x0,04 habit: xenoblastic estimation of proportion: 4% alterations: epidotization
Rutile			grain size: 0,18x0,1 - 0,08x0,05 habit: xenoblastic estimation of proportion: 3% alterations: /
Garnet			grain size: 1,2x0,8 - 0,7x0,45 habit: xenoblastic estimation of proportion: 4% alterations: epidotization
Epidote	grain size: 0,1x0,08 - 0,04x0,02 habit: idioblastic estimation of proportion: 8% alterations: /		grain size: 0,32x0,1 - 0,09x0,04 habit: idioblastic estimation of proportion: 3% alterations: /
Titanite	grain size: 0,07x0,04 - 0,02x0,01 habit: xenoblastic estimation of proportion: 5% alterations: /	grain size: 0,05x0,04 - 0,02x0,01 habit: xenoblastic estimation of proportion: 4% alterations: /	grain size: 0,04x0,02 - 0,02x0,01 habit: xenoblastic estimation of proportion: 4% alterations: /
Clinozoisite	grain size: 0,65x0,05 - 0,08x0,04 habit: subidioblastic estimation of proportion: 4% alterations: /	grain size: 0,6x0,05 - 0,16x0,08 habit: subidioblastic estimation of proportion: 4% alterations: /	grain size: 0,8x0,44 - 0,16x0,08 habit: subidiblastic estimation of proportion: 3% alterations: /
Zoisite	grain size: 0,22x0,1 - 0,08x0,03 habit: subidioblastic estimation of proportion: 4% alterations: /	grain size: 0,26x0,09 - 0,06x0,02 habit: subidioblastic estimation of proportion: 4% alterations: /	

5.1.8. Garnet–quartz–chlorite–amphibole–albite schist ES 14–1

Amphibole is presented by hornblende and occurs as subidioblast. Its grain size varies from 1,76x0,96 to 0,95x0,48 millimetres. Hornblende has strong pleochroism in green, yellow and brown colours. It has perfect cleavage sets which intersect at 56°and 124°. In cross–polarized light it shows yellow and green interference colour of second order. Amphibole is chloritized and epidotized. Hornblende incorporates rounded quartz grains, opaque mineral, chlorite and rutile (Figure 5–20, Figure 5–21, Figure 5–22). Hornblende occupies up to 19 vol % of this sample.

Plagioclase occurs as xenoblast. Grain dimensions varies form 0,95x0,55 to 0,3x0,1 millimetres (Figure 5–19, Figure 5–20, Figure 5–21). Plagioclase has lamellae and grains are sericitized (Figure 5–22). It occupies 32 vol % of this sample.

Chlorite occurs as subidioblast. Chlorite dimensions varies from 1,52x0,24 to 0,2x0,08 millimetres (Figure 5–18, Figure 5–19, Figure 5–20, Figure 5–21, Figure 5–23). It has perfect cleavage and pleochroism in green to yellowish–green colours. Chlorite exhibits anomalous "Berlin–blue" interference colour. This indicates an iron–rich chlorite. Some grains exhibit anomalous purple interference colour. Chlorite often incorporates various inclusions, isometric quartz grains, opaques, garnets, clinozoisite and cryptocrystalline minerals. It is often formed by alteration of biotite. Chlorite occupies up to 10 vol % of this sample.

Quartz has xenoblastic habit and grain size varies from 0,45x0,05 to 0,15x0,05 millimetres (Figure 5–18, Figure 5–19, Figure 5–20, Figure 5–21, Figure 5–22, Figure 5–23). Quartz grains are clear and show undulose extinction. Grain contacts are mostly concave–convex and contoured by red hematite. There is around 17 vol % of quartz in this sample.

Orthoclase shows xenoblastic habit and its grain size varies from 1,2x1,4 to 0,4x0,16 millimetres. Orthoclase is sericitized (Figure 5–21). It occupies 5 vol % of this sample.

Biotite occurs as idioblast. Its grain size varies from 0,32x0,2 to 0,23x0,17 millimetres. Biotite shows perfect cleavage and has pleochroism in brown shades. It is chloritized (Figure 5–19, Figure 5–23) and limonitized. It occupies up to 3 vol % of this sample.

Opaque mineral appears as xenoblast. Its grain size varies from 0,48x0,22 to 0,24x0,1 millimetres (Figure 5–18, Figure 5–20, Figure 5–22). It is epidotized. Some grains have a dark

brown colour in the centre and their rims are completely black. Opaque mineral occupies 5 vol % of this sample.

Rutile appears as subidioblast. Its grain size varies from 0,12x0,05 to 0,08x0,05 millimetres (Figure 5–20). Rutile has extinct cleavage and reddish–brown colour. Minerals have black rim. It occupies 1 vol % of this sample.

Garnet appears as idioblast. Rounded grains are distinguishable by their high relief and isometric habit (Figure 5–18, Figure 5–19, Figure 5–20, Figure 5–21). Its grain size varies from 0,92x0,34 to 0,3x0,14 millimetres. It is partly limonitized and has a kelyphitic alteration rim. It occupies 7 vol % of this sample.

Clinozoisite occurs as subidioblast, its size varies from 0,42x0,16 to 0,11x0,04 millimetres (Figure 5–18). It is often accompanied by epidote and chlorite. Several grains contain inclusion of an idioblastic relict mineral, completely altered to limonite. It occupies around 2 vol % of this sample.

Zircon appears as idioblastic inclusions in quartz and hornblende (Figure 5–22). Its grain size is from 0,07x0,03 to 0,07x0,045 millimetres. It is colourless it has a very high relief and live interference colours of high order. It occupies less than 1 vol % of this sample.

The sample is containing limonite and hematite, which occur along cleavage fractures of amphibole and chlorite. Based on xenoblastic, rounded quartz grain which are often in amphibole grains, we can assume that quartz crystallized later. Texture of the rock is lepidonematogranoblastic. Structure of the rock is banded. This sample is determined as garnet–quartz–chlorite–amphibole–albite schist.

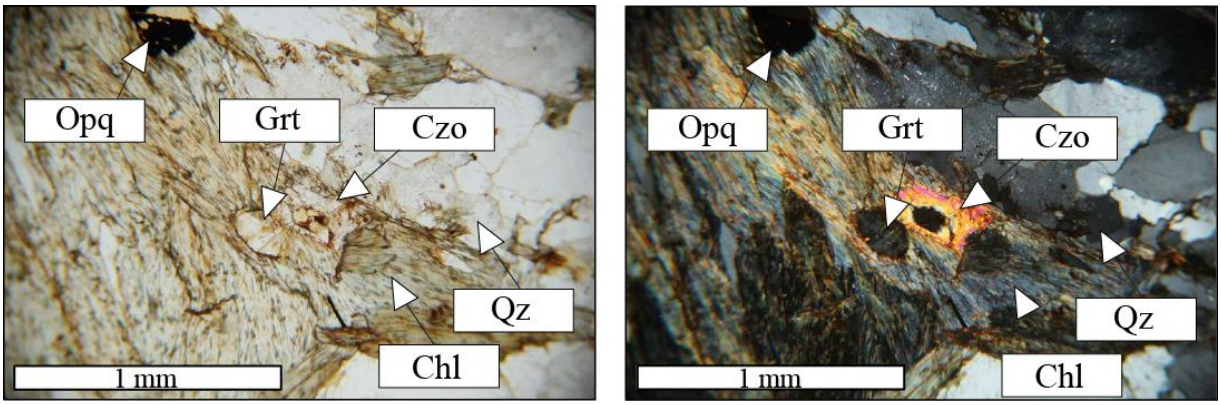

Figure 5–18. Chlorite incorporating opaque mineral, garnet, clinozoisite, quartz and cryptocrystalline minerals in the garnet–quartz–chlorite–amphibole–albite schist with lepidonematogranoblastic texture.

Table 5–8. Mineralogical description of sample ES 14–1.

Sample ES 14-1	Structure	Texture	
Garnet–quartz–chlorite–amphibole–albite schist	banded	lepidonematogranoblastic	
Quartz	**Plagioclase**	**Chlorite**	**Biotite**
grain size: 0,45x0,05 - 0,15x0,05 habit: xenoblastic estimation of proportion: 17% alterations: undulose extinction	grain size: 0,95x0,55 - 0,3x0,1 habit: xenoblastic estimation of proportion: 32% alterations: sericitization	grain size: 1,52x0,24 - 0,2x0,08 habit: subidioblastic estimation of proportion:10% alterations: /	grain size: 0,32x0,2 - 0,23x0,17 habit: idioblastic estimation of proportion: 3% alterations: chloritization, limonitization
K-Feldspar	**Amphibole**	**Opaque**	**Rutile**
grain size: 1,2x1,4 - 0,4x0,16 habit: xenoblastic estimation of proportion: 5% alterations: sericitization	Hornblende grain size: 1,76x0,96 - 0,95x0,48 habit: subidioblastic estimation of proportion: 19% alterations: chloritization, epidotization	grain size: 0,48x0,22 - 0,24x0,1 habit: xenoblastic estimation of proportion: 5% alterations: epidotization, titanitization	grain size: 0,12x0,05 - 0,08x0,05 habit: subidioblastic estimation of proportion: 1% alterations: titanization
Garnet	**Zircon**	**Clinozoisite**	
grain size: 0,92x0,34 - 0,3x0,14 habit: idioblastic estimation of proportion: 7% alterations:kelyphitic alteration rim, limonitized	grain size: 0,08x0,03 - 0,07x0,045 habit: idioblastic estimation of proportion: < 1% alterations: /	grain size: 0,42x0,16 - 0,11x0,04 habit: xenoblastic estimation of proportion: 2% alterations: /	

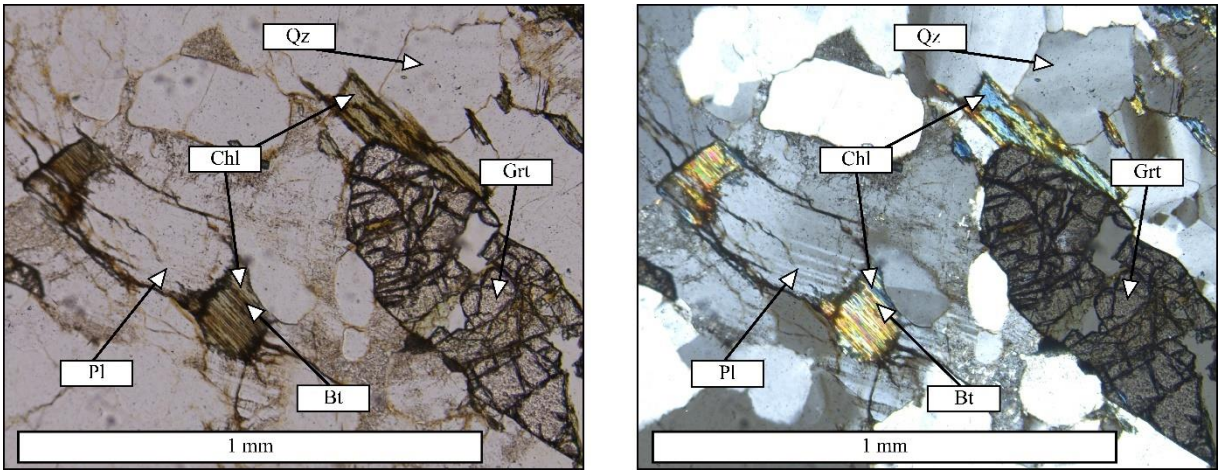

Figure 5–19. Quartz, garnet, plagioclase, chloritized biotite and in the garnet–quartz–chlorite–amphibole–albite schist with lepidonematogranoblastic texture.

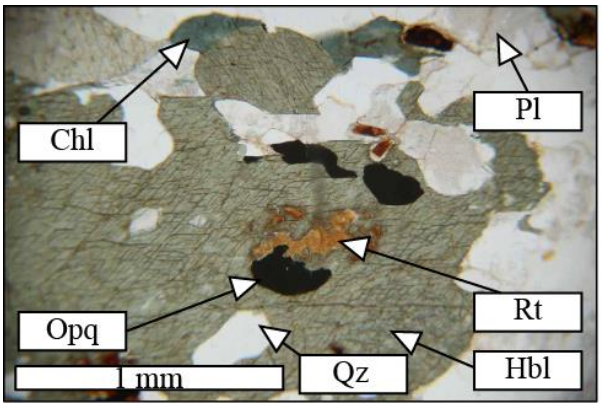

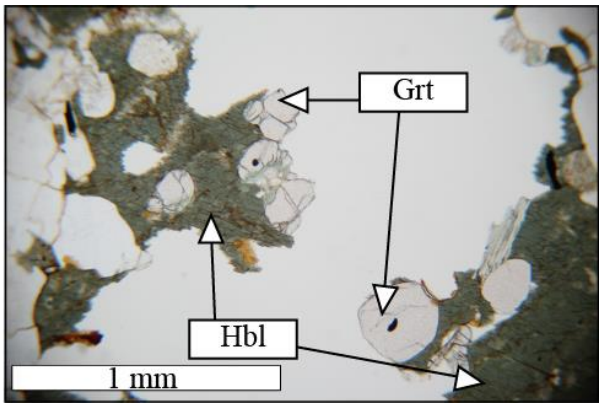

Figure 5–20. Hornblende incorporates rounded opaque mineral, rutile, quartz and garnet in the garnet–quartz–chlorite–amphibole–albite schist. There are also plagioclase and chlorite.

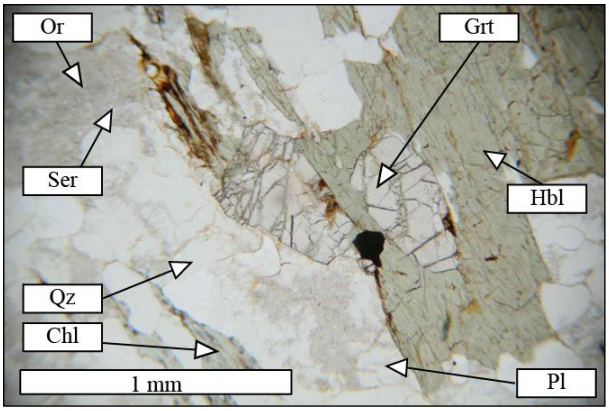

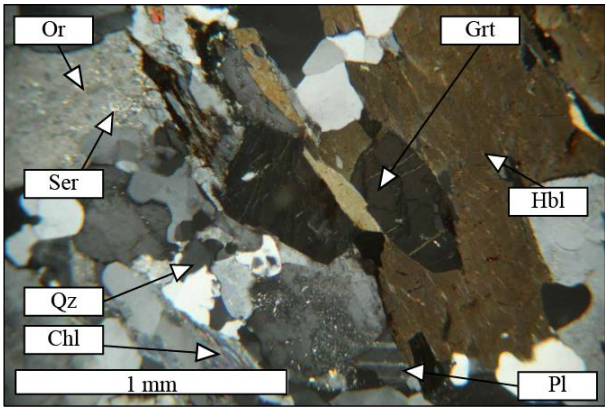

Figure 5–21. Garnet, hornblende, plagioclase, orthoclase, sericite, chlorite and quartz in the garnet–quartz–chlorite–amphibole–albite schist with lepidonematogranoblastic texture.

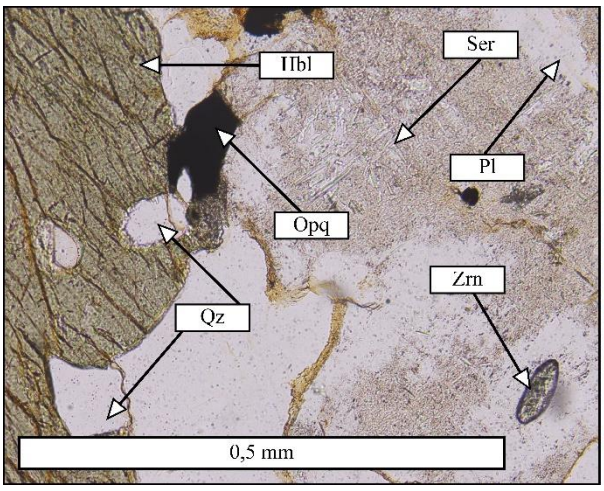

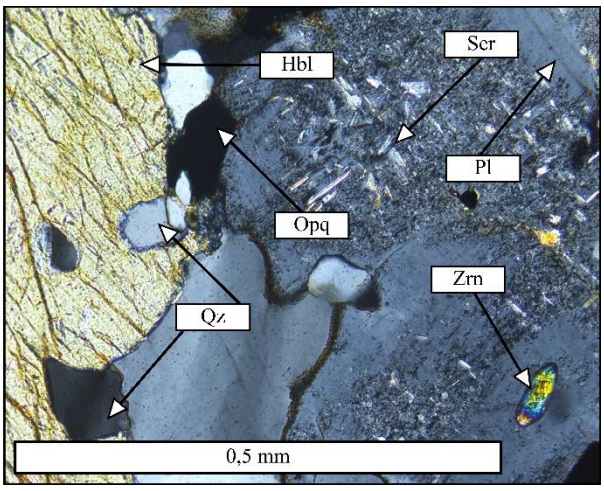

Figure 5–22. Zircon, quartz, hornblende, opaque mineral and plagioclase with sericite in the garnet–quartz–chlorite–amphibole–albite schist with lepidonematogranoblastic texture.

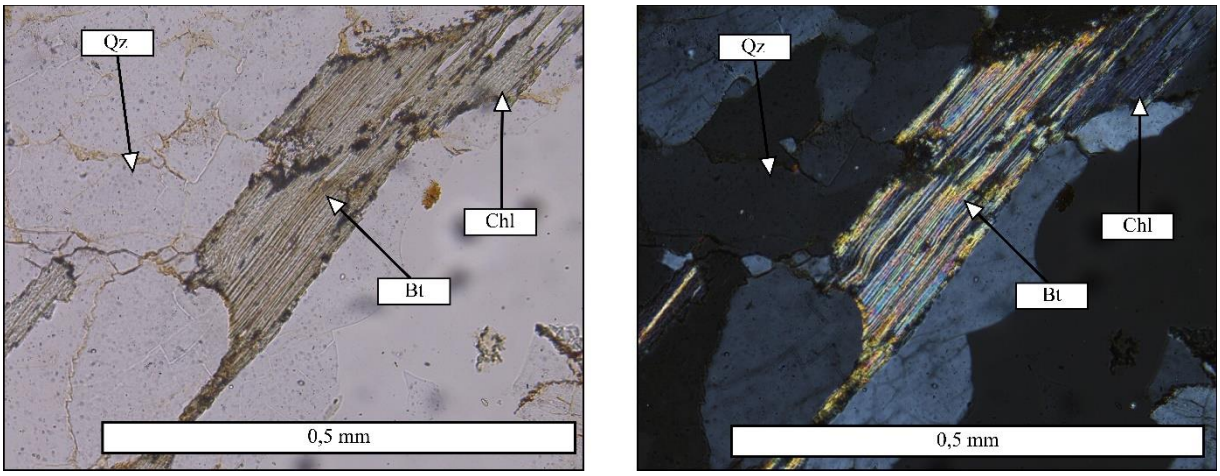

Figure 5–23. Quartz and chloritized biotite and in the garnet–quartz–chlorite–amphibole–albite schist with lepidonematogranoblastic texture.

5.2. Whole–rock chemistry

5.2.1. Major oxides

The major oxide compositions are listed in Table 5–9.

Table 5–9. The major oxide composition of samples. Samples are highlighted in colour according to their grouping which can also be seen in Table 5–1.

	SiO_2	TiO_2	Al_2O_3	Fe_2O_3	Cr_2O_3	CaO	MgO	MnO	K_2O	Na_2O	P_2O_5	SrO	BaO	LOI	Total
ES 10E-2	48,17	2,18	13,76	12,21	0,02	9,71	6,47	0,2	0,11	2,41	0,22	0,02	<0,01	4,84	100,31
ES 10H	48,15	1,66	15,09	10,89	0,03	10,11	6,83	0,17	0,23	3,12	0,17	0,03	<0,01	3,27	99,76
ES 20-2	48,96	1,88	13,33	11,97	0,03	9,07	7,09	0,18	0,53	2,45	0,18	0,02	<0,01	4,23	99,91
ES 14-1	59,19	1,51	12,42	11,44	0,05	5,4	4,3	0,26	0,66	3,39	0,23	0,01	0,02	1,95	100,83
ES 16	48,86	2,43	14,65	11,26	0,05	9,17	6,54	0,15	0,76	2,16	0,35	0,05	0,07	2,96	99,47
ES 15C-1	74,44	0,19	2,76	4,15	0,06	7,75	0,74	0,16	0,78	0,03	0,05	0,01	0,02	6,45	97,59
ES 10A-1	53,62	1,10	14,03	7,46	0,03	8,43	2,04	0,11	3,17	1,11	0,17	<0,01	0,07	7,57	98,92
ES 19A-1	65,77	0,65	12,46	5,37	0,04	2,87	2,32	0,07	1,45	2,87	0,16	0,01	0,05	4,60	98,70
ES 15B-6	44,77	1,73	15,68	7,00	0,04	10,56	3,65	0,13	1,07	4,06	0,32	0,05	0,03	11,19	100,28
ES 15B-8	41,82	2,34	13,97	12,62	0,03	8,59	7,77	0,21	0,46	1,69	0,37	0,02	0,02	10,65	100,55
ES 15B-7	47,29	1,73	13,34	10,71	0,03	7,12	5,92	0,20	1,08	1,48	0,29	0,02	0,06	9,19	98,46
ES 10F-1	35,61	2,49	19,06	12,45	0,05	8,09	7,22	0,13	3,62	0,13	0,23	0,02	0,03	11,02	100,16
ES 19B	60,06	0,82	15,77	7,49	0,04	1,57	2,91	0,10	2,54	2,62	0,16	0,03	0,24	3,88	98,23

5.2.1.1. Rocks of greenschist metamorphic facies

Compositional ranges of SiO_2 are wide for schists and hornfels, ranging from 35,61 to 65,77 wt %.

TiO_2 content ranges from 0,65 to 2,49 wt % for schists and hornfels.

Al_2O_3 content of hornfels is 14,65 wt %, and of schists it is from 13,34 to 19,06 wt %.

Total alkalis ($K_2O + Na_2O$) concentration is 2,92 wt % for hornfels and ranging from 0,8 to 5,16 wt % for schists.

Fe_2O_3 content ranges from 4,15 to 12,62 wt % for schists and is 11,26 wt % for hornfels.

MgO content ranges from 0,74 to 7,77 wt % for hornfels and schists.

CaO content of hornfels and schists ranges from 1,57 to 10,56 wt %.

P_2O_5 content ranges from 0,05 to 0,37 wt % for hornfels and schists.

MnO content ranges from 0,07 to 0,21 wt % for hornfels and schists.

Loss on ignition (LOI) is somewhat higher for hornfels and schists than for schists containing hornblende, ranging from 2,96 to 11,19 wt %, this could be due to higher content of aluminosilicates.

5.2.1.2. Rocks of amphibolite metamorphic facies

Compositional ranges of SiO_2 for rocks of amphibolite metamorphic facies is 48 wt %, with the exception of garnet–quartz–chlorite–amphibole–albite schist (sample ES 14–1) which contains 59 wt % of SiO_2. This is due to high amount of recrystallised quartz (17%, Figure 5–18. Chlorite incorporating opaque mineral, garnet, clinozoisite, quartz and cryptocrystalline minerals in the garnet–quartz–chlorite–amphibole–albite schist with lepidonematogranoblastic texture.

Table 5–8) in this sample.

TiO_2 values range from 1,51 to 2,18 wt %. Cr_2O_3 content is less than 0,05 wt % for all hornblende containing schists. Cr values ranging from 172 to 361 ppm and TiO_2 values ranging from 1,51 to 2,18 wt % indicate that they all have igneous protoliths (Leake, 1964). The relationship between TiO_2–Cr is plotted in Figure 6–10.

Al_2O_3 content of the garnet–quartz–chlorite–amphibole–albite schist is 12,42 wt %, and for other hornblende containing schists it ranges from 13,33 wt % to 15,09 wt %.

Total alkalis ($K_2O + Na_2O$) concentration is 4,5 wt % for garnet–quartz–chlorite–amphibole–albite schist. Alkalis concentrations for other amphibolite metamorphic facies samples is from 2,52 to 3,33 wt %.

Fe_2O_3 content ranges from 10,89 to 12,21 wt %.

MgO content of garnet–quartz–chlorite–amphibole–albite schist is 4,3 wt % and from 6,47 to 7,09 wt % for other samples of the group.

CaO content of garnet–quartz–chlorite–amphibole–albite schist is the lowest at 5,4 wt % and for other hornblende containing schists s it ranges from 9,07 to 10,11 wt %.

P_2O_5 value is from 0,17 to 0,23 wt % for hornblende containing schists.

MnO content ranges from 0,17 to 0,26 wt % for hornblende containing schists.

Loss on ignition for garnet–quartz–chlorite–amphibole–albite schist is 1,95 wt% and for other hornblende containing schists it is from 3,27 to 4,84 wt %.

5.2.2. Trace elements

The Rare Earth Elements are amongst the least soluble trace elements. In most cases they stay immobile during low–grade metamorphism and weathering which is why they reflect the original composition of the protolith (Rollinson 2014).

Trace elements of the samples are listed in the Table 5–10 and are expressed in ppm (parts per million).

In order to interpret them, the REE concentrations are normalized to a reference standard and relationship between elements is shown graphically in a multi–element plot.

Normal Mid–Ocean Ridge Basalt (NMORB) normalized multi–element plots (Sun and McDonough 1989) are plotted for cordierite–quartz–epidote–chlorite–actinolite hornfels in Figure 6–1 a, for quartz vein in Figure 6–4 a, for rocks of greenschist metamorphic facies (Barrow, 1893; Yardley, 1989) in Figure 6–9 a, Figure 6–8 a, Figure 6–9 a and Figure 6–9 a; for rocks of amphibolite metamorphic facies in the Figure 6–11 a.

Measured distribution of REE are normalized to the reference standard of chondritic meteorite (Boynton, 1984) and shown for cordierite–quartz–epidote–chlorite–actinolite hornfels in Figure

6–1 b, for quartz vein in Figure 6–4 b, for rocks of greenschist metamorphic facies in Figure 6–9 b, Figure 6–8 b, Figure 6–9 b and Figure 6–9 b; and for rocks of amphibolite metamorphic facies in the Figure 6–11 b. All of the normalized multi–element plots in this paper were made in GeoChemical Data toolkit (GCDkit) software (Janoušek et al., 2006).

Table 5–10. Trace elements and rare earth elements data. Samples are highlighted in colour according to their grouping which can also be seen in Table 5–1.

	Li	Cs	Rb	Sr	Ba	Be	Sn	Ta	W	Ni	Cr	Pb	Zn	Cu	Co	Mn	Mo	Ag	Th	U
ES 16	11,2	0,46	15,4	435,1	593,6	1,84	<5	1,3	<1	375,1	380	6,1	116	39,2	46,1	1211	1,07	0,17	2,4	2,0
ES 15C-1	1,3	0,34	21,2	132,8	171,1	0,42	<5	0,5	5	1198,1	455	505,1	172	18,1	4,4	1350	2,48	0,34	1,2	0,5
ES 10A-1	9,1	1,75	101,7	82,2	599,1	1,74	<5	0,7	7	283,6	214	14,9	42	14,4	17,0	837	2,28	0,12	4,3	1,0
ES 19A-1	9,9	1,35	40,7	137,9	428,7	1,82	<5	0,8	6	693,6	333	12,8	93	9,0	13,6	608	1,25	0,08	4,4	0,9
ES 15B-6	16,2	0,66	36,6	434,2	238,1	0,81	<5	0,7	1	191,4	305	10,3	67	1,7	38,8	1050	0,85	0,05	0,7	0,9
ES 15B-8	**20,5**	0,34	11,9	167,0	179,4	0,75	<5	1,0	2	308,2	258	6,0	163	26,9	47,4	1609	1,45	0,09	1,8	1,0
ES 15B-7	14,4	0,62	27,2	142,9	464,7	0,88	<5	0,9	1	347,2	262	7,4	146	46,9	34,4	1614	4,45	0,17	2,4	1,6
ES 10F-1	**19,4**	1,41	107,6	211,9	268,9	1,67	<5	0,8	**41**	163,2	363	4,4	92	14,5	52,2	947	0,78	0,10	0,4	1,0
ES 19B	11,6	2,07	55,9	246,3	2260,7	1,01	<5	0,9	3	624,8	306	12,5	99	130,1	25,5	811	6,78	0,18	9,1	3,3
ES 10E-2	9,6	0,19	2,1	152,8	24,3	0,48	<5	0,6	4	299	172	4,2	102	178,4	40,8	1524	0,4	0,15	0,4	0,1
ES 10H	7,7	0,15	4,7	223,8	60	0,62	<5	0,5	6	259,7	256	6,5	82	44	36,8	1289	0,65	0,06	0,5	0,3
ES 20-2	10,3	0,92	13,2	188,9	74,3	0,99	<5	0,7	2	369,5	239	3	89	43,8	38,7	1430	1,03	0,04	0,4	0,3
ES 14-1	12,7	0,41	10,4	107,9	207,3	1,38	<5	0,8	2	1078,3	361	4,4	218	79,3	27,5	2064	1,17	0,12	6,4	1,6

	La	Ce	Pr	Nd	Sm	Eu	Gd	Tb	Dy	Ho	Er	Tm	Yb	Lu	Y	Zr	Hf	Ta
ES 16	21,9	45,9	5,99	24,7	5,40	1,79	5,43	0,82	4,94	0,90	2,49	0,34	2,02		24,9	160	3,8	1,3
ES 15C-1	5,3	11,1	1,47	5,9	1,48	0,65	1,71	0,31	2,22	0,42	1,31	0,19	1,18	0,17	13,4	46	1,2	0,5
ES 10A-1	20,8	44,8	5,70	23,7	5,55	1,40	5,51	0,91	5,28	1,04	2,91	0,44	2,77	0,47	31,0	112	3,0	0,7
ES 19A-1	18,0	37,5	4,70	18,1	3,83	0,93	3,64	0,55	3,54	0,70	2,09	0,31	1,97	0,30	20,6	138	3,4	0,8
ES 15B-6	6,6	16,3	2,48	11,7	3,37	1,21	3,87	0,69	4,67	0,94	2,67	0,40	2,50	0,39	26,7	108	2,8	0,7
ES 15B-8	17,8	38,7	5,06	21,1	4,67	1,25	4,48	0,68	4,16	0,78	2,28	0,34	2,05	0,34	22,0	163	3,8	1,0
ES 15B-7	12,6	26,6	3,51	14,3	3,31	1,04	3,80	0,71	4,79	1,04	3,05	0,47	2,84	0,46	29,7	135	3,4	0,9
ES 10F-1	7,7	20,7	3,01	14,5	3,91	1,17	5,02	0,94	6,93	1,42	4,19	0,63	3,72	0,58	41,3	137	3,4	0,8
ES 19B	33,1	69,1	8,36	31,7	6,70	1,55	5,87	0,97	5,74	1,14	3,61	0,51	3,45	0,51	30,4	152	4,4	0,9
ES 10E-2	5,4	15,5	2,7	14	4,45	1,54	5,45	1,01	6,88	1,39	4,13	0,64	3,86	0,61	40	130	3,4	0,6
ES 10H	5	13,5	2,33	11,9	3,74	1,3	4,59	0,83	5,65	1,11	3,33	0,51	3,13	0,51	33,8	107	2,8	0,5
ES 20-2	6	14,4	2,52	12,6	3,78	1,25	4,65	0,84	5,87	1,19	3,5	0,57	3,33	0,5	35,8	111	2,9	0,7
ES 14-1	21,8	60,7	7,14	29,8	7,9	1,82	8,88	1,65	11,06	2,26	7,03	1,13	7,12	1,16	69,8	282	7,5	0,8

	As	Bi	Cd	Ga	Ge	In	Nb	P	Re	Sb	Sc	Se	Te	Tl	V
ES 16	3,4	0,04	0,28	22,5	<0,05	0,087	24,4	1545	0,004	0,7	31,5	<1	<0,05	0,17	293
ES 15C-1	6,9	0,06	2,93	4,6	<0,05	0,022	3,8	206	0,004	0,7	4,3	1	<0,05	0,13	35
ES 10A-1	2,9	0,29	0,19	17,0	0,05	0,054	6,6	743	0,009	0,7	24,7	<1	<0,05	0,81	164
ES 19A-1	4,7	0,02	0,22	18,9	0,06	0,065	10,4	718	0,003	<0,5	16,1	<1	<0,05	0,19	132
ES 15B-6	50,8	0,01	0,20	19,5	<0,05	0,076	8,1	1386	0,005	0,6	42,0	<1	<0,05	0,21	239
ES 15B-8	27,2	0,06	0,28	19,7	<0,05	0,068	16,0	1602	0,004	<0,5	25,3	<1	<0,05	0,08	217
ES 15B-7	1,9	0,09	0,34	19,7	<0,05	0,075	12,7	1269	0,008	<0,5	24,9	<1	<0,05	0,15	218
ES 10F-1	56,1	0,05	0,09	25,2	<0,05	0,055	4,9	964	0,005	1,3	44,1	<1	<0,05	0,63	344
ES 10E-2	8,5	0,03	0,17	17,4	<0,05	0,095	3,3	931	0,005	0,7	40,1	<1	<0,05	0,03	328
ES 10H	10,2	0,03	0,12	17,2	<0,05	0,081	3,1	743	0,006	0,7	35,4	<1	<0,05	0,04	266
ES 20-2	2,2	0,02	0,1	17,8	<0,05	0,086	3,5	809	0,005	<0,5	41,9	<1	<0,05	0,09	299
ES 14-1	3,7	0,08	0,46	18,7	0,06	0,137	9,4	985	0,008	1,1	29,4	<1	<0,05	0,08	190

6. DISCUSSION

6.1. Contact metamorphism

There are several factors that indicate the contact metamorphic origin of the cordierite–quartz–epidote–chlorite–actinolite hornfels. Contact metamorphism occurs when temperature rises in rocks adjacent to magmatic intrusion of local extent. The cordierite–quartz–epidote–chlorite–actinolite hornfels exhibits two zones with different sizes of minerals, so it could be possible that the zone with larger minerals is the one closer to the intrusion and exposed to higher temperatures. It is known that the surrounding area of the hornfels was intruded by Variscan granitic plutons that crop out at many places and are occasionally associated to skarn–related ore occurrences (Jovanović et al., 2019). Andalusite + cordierite ± corundum and actinolite + chlorite + epidote ± zoisite hornfels mineral assemblage is mentioned in the Banatitic Magmatic and Metallogenic Belt (Berza et al., 1998), as being of contact metamorphic origin but also pointing to hydrothermal alteration (Ilinca, 2012). The cordierite–quartz–epidote–chlorite–actinolite hornfels has a homogenous structure and lepidogranoblastic texture which is characteristic for contact metamorphosed rocks which are usually exposed to low pressures.

The cordierite–quartz–epidote–chlorite–actinolite hornfels is at the border of the Supragetic and Getic units (Figure 6–3) in proximity of the Poniasca granitoid, a 4 km long and around 500 m wide body on the right bank of the Danube, described by Jovanović et al. (2019). Antonijević et al. (1970) and Kalenić et al. (1976) consider the pluton Cambrian in age. The cordierite–quartz–epidote–chlorite–actinolite hornfels could be a result of contact metamorphic effect caused by the Poniasca granitoid (Jovanović et al., 2019).

The cordierite–quartz–epidote–chlorite–actinolite hornfels consists of porphyroblasts of cordierite and actinolite, and of chlorite, quartz, clinozoisite, zoisite, opaque mineral and titanite in the matrix. The actinolite + chlorite mineral assemblage indicates that this sample belongs to albite–epidote hornfels facies (Turner, 1981; Butler, 1990). The absence of muscovite is characteristic in contact hornfelses, suggesting pressure and temperature conditions above those for the muscovite–out reaction, probably above 600 °C (Nicolescu and Cornell 1999). The temperature of magma forming granitic intrusions is generally 700–800°C (Butler, 1990).

Cordierite is a common contact metamorphic and high grade regional metamorphic mineral. It appears in two polymorphic forms; low–temperature orthorhombic–cordierite and high temperature hexagonal form–indialite (Miyashiro, 1957). The colourless cordierite in hornfels has been described (Kikuchi, 1889; Floyd, 1965) and its appearance indicates pelitic protolith of the rock (Alderton, 2020).

Cordierite–quartz–epidote–chlorite–actinolite hornfels N–MORB normalized multi–variation diagram shows that LILE are enriched in comparison to HFSE with positive anomalies of the following fluid mobile elements (Gamal El Dien et al., 2019; Leeman, 1996) Cs, Ba, U and Pb (Figure 6–1 a). The Pb anomaly could indicate crustal influence (Rollinson, 2014) or be the result of contamination due to the Pb–Zn occurrence (Jelenković et al., 2002) in the vicinity of the sampling location (Figure 4–1 b).

Cordierite–quartz–epidote–chlorite–actinolite hornfels shows enrichment in light and middle Rare Earth Elements in comparison to the heavy REE without noticeable deviations (Figure 6–1 b).

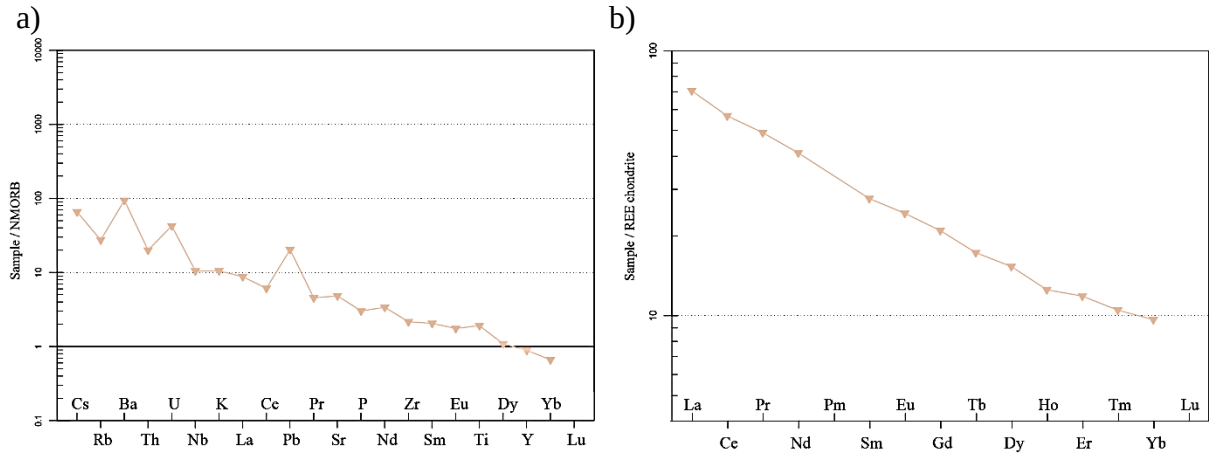

Figure 6–1. (a) N–MORB normalized multi–variation diagram (Sun and McDonough 1989) and (b) Chondrite normalized pattern of REE distribution (Boynton, 1984) of the cordierite–quartz–epidote–chlorite–actinolite hornfels.

6.2. Barrovian metamorphism

Based on petrological analysis of metamorphic rocks, a Barrovian–type metamorphic sequence is recognized. During the metamorphism of protolith rocks newly formed minerals appear in a definite sequence with increasing metamorphic grade; these minerals were designated as index

minerals (Barrow, 1893). This sequence is characterized by following index–minerals: chlorite, epidote, biotite, amphibole and garnet.

Medium and high–pressure Barrovian mineral assemblages, consequence of the Variscan continental collision event, have already been documented in the Getic unit or Sebeş–Lotru composite terrane (Balintoni et al., 2010; Iancu et al., 1998; Horváth and Árkai 2002).

A pressure and temperature chart of the analysed samples is created to show affiliation of the samples to metamorphic facies (Figure 6–2). Feldspar–biotite–chlorite–muscovite–quartz schist (sample ES 10A–1) doesn't contain clinozoisite and zoisite but contains muscovite, biotite and chlorite, placing it at the boundary between the chlorite and biotite zones (Winkler, 1965).

Samples ES 19A–1, ES 15B–6, ES 15B–8, ES 15C–4 and ES 15B–7 belong to greenschist metamorphic facies as they all contain epidote. Samples ES 19A–1, ES 15B–8, ES 15C–4 and ES 15B–7 contain muscovite and samples ES 15B–8, ES 15C–4 and ES 15B–7 biotite. Quartz–chlorite–actinolite schist (sample ES 10F–1) is differentiated from the previously mentioned samples by having around 40 vol % of actinolite.

Garnet–epidote–chlorite–quartz–muscovite schist belongs to greenschist metamorphic facies but to a higher temperature range than the previously mentioned samples. Almandine–rich garnet in pelitic rocks first appears at higher temperature part of greenschist metamorphic facies, but, the first appearance of a garnet depends on its composition so there is no sharp boundary regarding temperature and pressure (Winkler, 1965).

The muscovite–out reaction isograd separates the medium and high–grade metamorphism (Winkler, 1965), as amphibolite facies rocks (samples ES 10E–2, ES 10H, ES 20–2 and ES 14–1) don't contain muscovite, they could belong to medium or high–grade metamorphism.

Samples ES 10E–2, ES 10H and ES 20–2 contain hornblende ± actinolite + plagioclase + orthoclase + clinozoisite + titanite + zoisite + opaque mineral, sample ES 10E–2 also contains epidote. This mineral assemblage belongs to medium grade metamorphism and epidote amphibolite facies (Eskola, 1939; Winkler, 1965; Barrow, 1893). Garnet–quartz–chlorite–amphibole–albite schist (sample ES 14–1) with hornblende + plagioclase + garnet + biotite + rutile + clinozoisite + chlorite + orthoclase + zircon + quartz + opaque mineral, belongs to high–grade, almandine–amphibolite facies (Winkler, 1965).

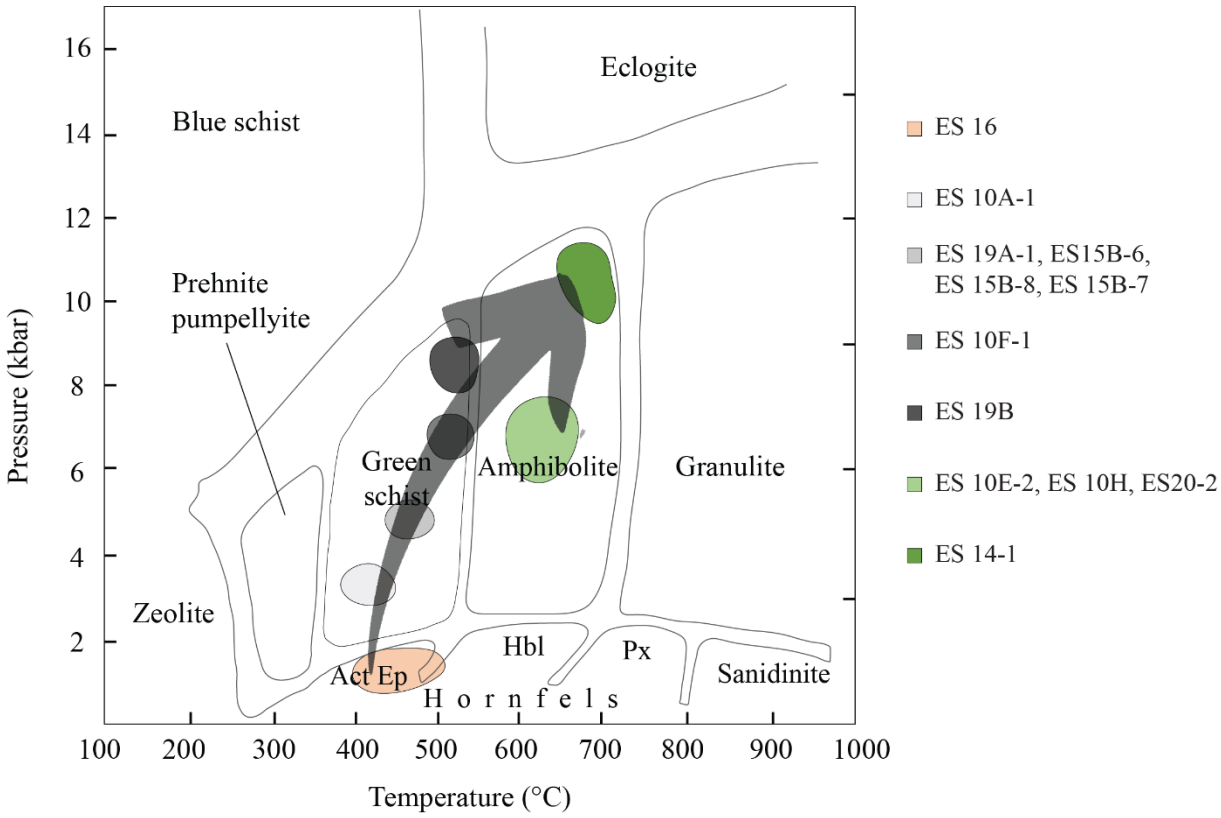

Figure 6–2. Pressure and temperature path of analysed samples with fields of metamorphic facies, modified after (Yardley 1989).

The samples affiliated to the metamorphic facies (Figure 6–2) are shown on the map to determine a zoned distribution of index minerals within the prograde metamorphic sequence of the samples (Figure 6–3).

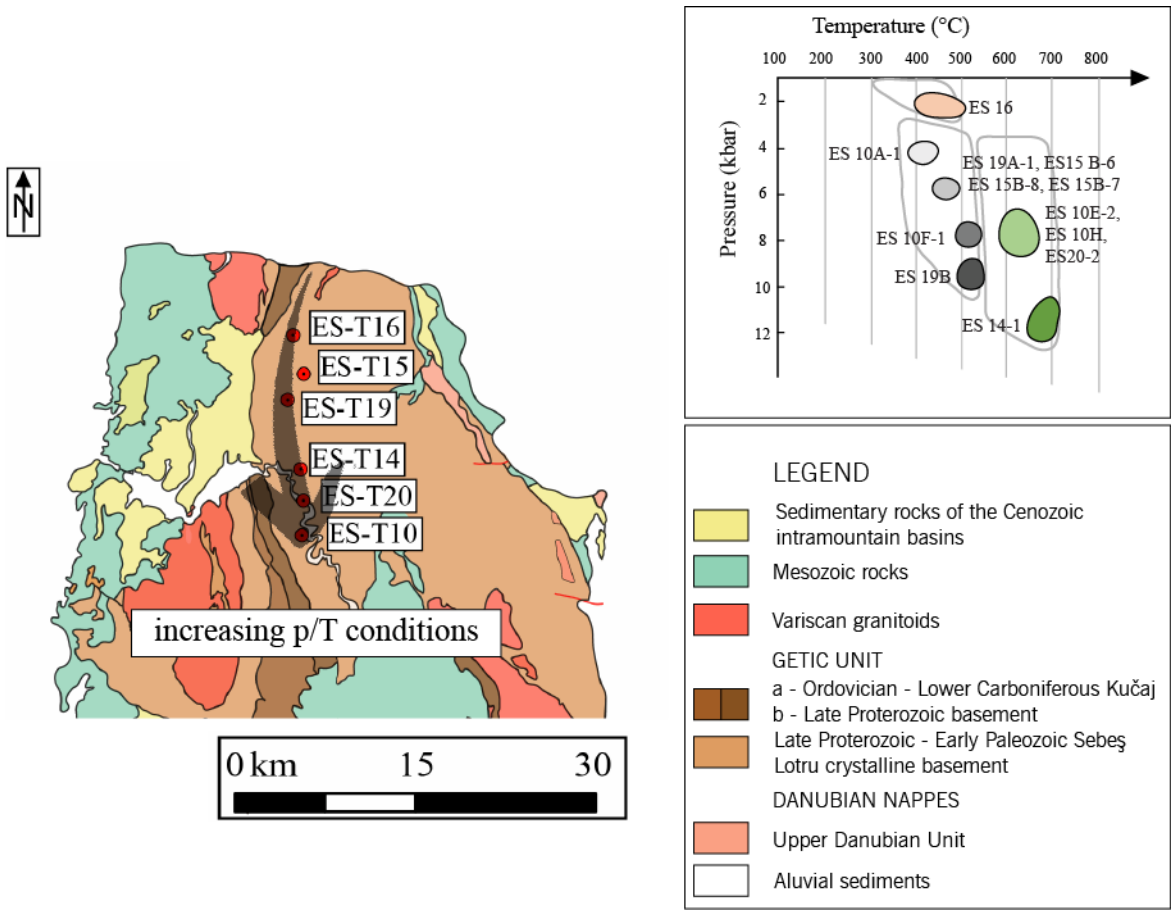

Figure 6–3. Map with the locations of analysed samples, affiliated to greenschist and amphibolite metamorphic facies. Arrow marks the increasing pressure and temperature conditions.

6.3. Retrograde metamorphism and deformation

Signs of post metamorphic cooling after reaching peak temperature are common in the samples as well as fracture zones, results of multiple deformation processes the rocks have been subjected, that provide easy access for H_2O and CO_2 bearing fluids

Chlorite is a low–grade alteration products of biotite and appears parallel to the biotite cleavage. In the quartz–albite–muscovite–chlorite schist (sample ES 15B–7) and garnet–quartz–chlorite–amphibole–albite schist (sample ES 14–1) biotite is heavily altered (Figure 5–19 and Figure 5–23). The biotite/chlorite equilibrium reactions can be related to the function $[K^+]/[H^+]$. Its value can indicate whether a reaction is a result the fluid phase pervading the system, or if the system is closed to potassium–progressive metamorphism (McNamara, 1966; Hemley and Jones 1964).

Plagioclase in samples ES 19A–1, ES 15B–6, ES 15B–8, ES 15C–4, ES 15B–7ES 10E–2, ES 10H and ES 20–2 is altered to sericite and/or prehnite.

Titanite usually forms rims around rutile (samples ES 15B–8, ES 15B–7 and ES 14–1).

Actinolite and chlorite are retrograde alteration of hornblende (samples ES 10E–2 and ES 10H).

Opaque mineral is altered to epidote in samples ES 15C–4 and ES 20–2, and in hematite/limonite in sample ES 15B–7.

Garnet is altered to chlorite and titanite in garnet–epidote–chlorite–quartz–muscovite schist (sample ES 19B), while in garnet–quartz–chlorite–amphibole–albite schist (sample ES 14–1) it has a kelyphitic alteration rim and alteration minerals along fractures (Figure 5–13). The retrograde alteration mineral assemblage of epidote + chlorite + amphibole ± carbonate mineral ± quartz is mentioned in the literature as a result of the greenschist overprint (Ilinca, 2012).

The medium–grade metamorphic rocks were subsequently overprinted by a retrograde greenschist facies metamorphic event (Spahić et al., 2021).

Frequent occurrence of cracks, later filled with minerals (quartz, carbonate mineral, opaque mineral, hematite) but also ductile deformations of micaceous minerals (muscovite, biotite, chlorite) make evident multiple deformation processes to which the rocks were exposed. Retrograde alteration along fractures and cracks is regularly observed. In sample ES 15B–8 chlorite in contact with opaque veins is affected by limonitization, some veins are completely enclosed with retrograde chlorite. In the albite–epidote–chlorite–amphibole schist (sample ES 10E–2) deformation event occurred but cracks are filled with matrix minerals. Often cracks or veins are intersecting each other, so it is possible to determine the relative age of one vein in comparison to the other. Within the feldspar–biotite–chlorite–muscovite–quartz schist, we had observed following sequence of secondary veins formation, opaque vein (2) is intersecting the carbonate vein (1) and the quartz vein (3) stops at opaque vein. This means that carbonate veins (1) were formed first, then opaque veins (2) and quartz veins (3) are the youngest. In the schists ES 15B–7, ES 15B–8 and ES 19A–1 younger carbonate veins are intersecting previously formed opaque veins.

In albite–epidote–chlorite–amphibole schist (sample ES 10E–2) and quartz–chlorite–actinolite schist (sample ES 10F–1) there are microstructures which give a relative sense of shear. Porphyroblasts depict interaction between growth of the porphyroblast and deformation. Geometry of the pre–cinematic porphyroblasts and pressure shadows indicate that porphyroblast growth and foliation forming deformation occurred before the rotation of the porphyroblast and mineral inclusions inside of it. After porphyroblast growth it partitions the deformation in a way that zones of intensified foliation are developed which wrap around the porphyroblast whilst the porphyroblast and its strain shadow undergo little deformation. Porphyroblast strain shadows comprise syn–cinematic quartz and matrix minerals and are probably formed by a solution transfer during deformation.

In albite–epidote–chlorite–amphibole schist (sample ES 10E–2) there are pre–cinematic porphyroblasts of amphibole, chlorite and opaque mineral (Figure 5–14). Their pressure shadows consist of syn–cinematic quartz and minerals from the matrix. Opaque mineral in the quartz–chlorite–actinolite schist is a pre–cinematic porphyroblast with a pressure shadow of fibrous quartz (Figure 5–10).

6.4. Hydrothermal metamorphism

Throughout the samples mineralogical, chemical and textural changes, resulting from the interaction of hot aqueous fluids with the rocks were observed. In the quartz vein, along with quartz and carbonate mineral, idioblastic prismatic opaque mineral is present. Based on its habit, microscopical occurrence and indications we assume it is pyrite, formed as a hydrothermal by–product.

N–MORB normalized multi–variation diagram of quartz vein (Figure 6–4 a) exhibits a general decreasing trend from LILE to HFSE with a significant positive anomaly of Pb. There are positive anomalies of U and K, and a depletion of Th, Nb, La, Ce, P and Ti in comparison to other REE.

Chondrite normalized pattern of REE distribution of quartz vein (Figure 6–4 b) shows enrichment in LREE and modest depletion in HREE, a positive Eu anomaly and a slight negative Ho anomaly.

The rocks which have experienced fluid dominated alteration show the following REE pattern changes; (La/Lu) > 1, and, if Eu occurs as Eu^{2+}, a positive Eu anomaly (Bau, 1991; Torres–Alvarado et al., 2007) both of which is true for quartz vein (Figure 6–4 b).

The presence of positive Pb anomaly could suggest the influence of subduction zone fluids in the composition of the parental magmas since Pb is efficiently extracted from subducting slabs by fluids (Dorais and Tubrett 2008) but could indicate crust contamination (Rollinson, 2014).

According to the metallogenic map of Serbia (Jelenković et al., 2008) the Pb–Zn mineralisation is related to the granitoid bodies which are in the vicinity of the sampling location of the quartz vein. They could be the source of possible Pb contamination of our samples.

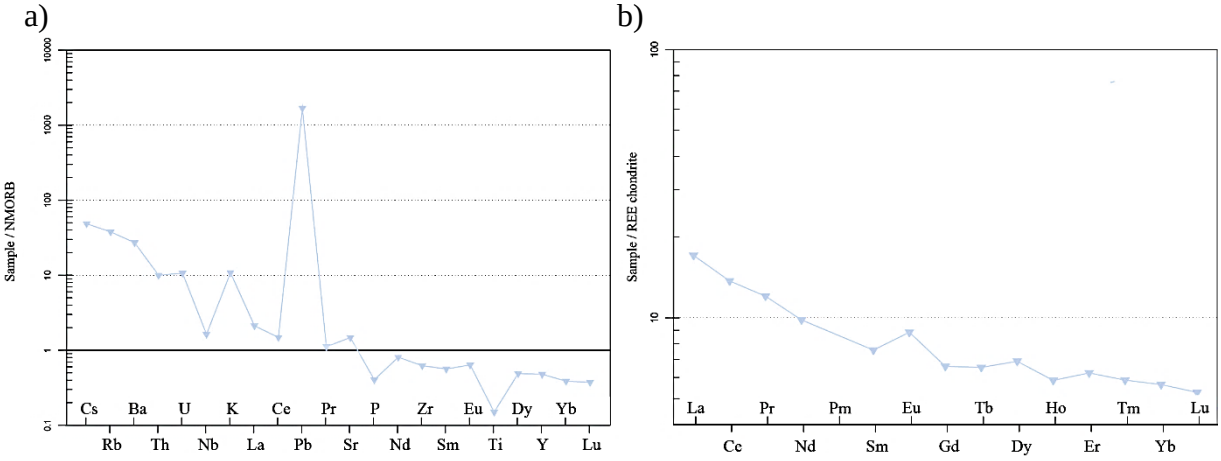

Figure 6–4. (a) N–MORB normalized multi–variation diagram (Sun and McDonough 1989) and (b) Chondrite normalized pattern of REE distribution (Boynton, 1984) of the quartz vein.

The Carpatho–Balkan metallogenic province (Jelenković et al., 2002), in particular the area of Blagojev Kamen, has gold–quartz deposits of hydrothermal origin connected to mobilization of the gold from the rocks of green shist facies during metamorphic processes and deposition in the fracture zones (Kalenić et al., 1980). Granitoid intrusions intruded into the metamorphic rocks of greenschist facies gave the thermal energy necessary for movement of the hydrothermal solutions (Janković, 1990). Often hydrothermal deposits related to volcano–intrusive complexes, hydrothermal metasomatic veins, locally porphyry–Cu and stockwork–disseminated–Mo types can be found. The dominant metals in these deposits are Pb–Zn, Sb, Bi, Ag, As, but small resources of tungsten concentrated in the quartz veins (scheelite) are also mentioned (Jelenković et al., 2008).

6.5. Greenschist facies metamorphic rocks

Figure 6–5. Percentage of minerals in selected schists. belonging to the greenschist metamorphic facies is shown (Figure 6–5).

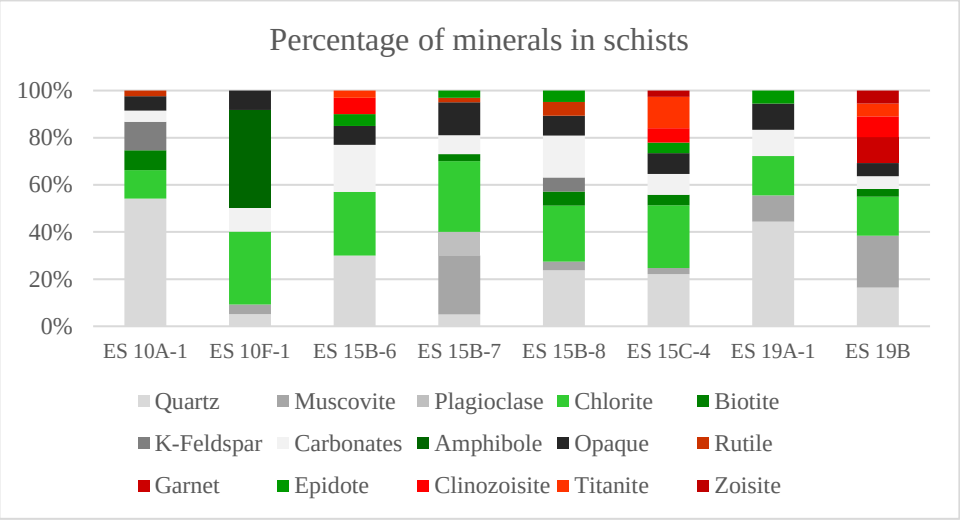

Figure 6–5. Percentage of minerals in selected schists.

N–MORB normalized multi–variation diagram of feldspar–biotite–chlorite–muscovite–quartz schist (Figure 6–6 a) shows significant positive anomalies of compatible elements K and Pb and negative anomalies of Nb and Sr. Chondrite normalized pattern of REE distribution of feldspar–biotite–chlorite–muscovite–quartz schist (Figure 6–6 b) shows significant enrichment in LREE in comparison to HREE with negative Eu anomaly.

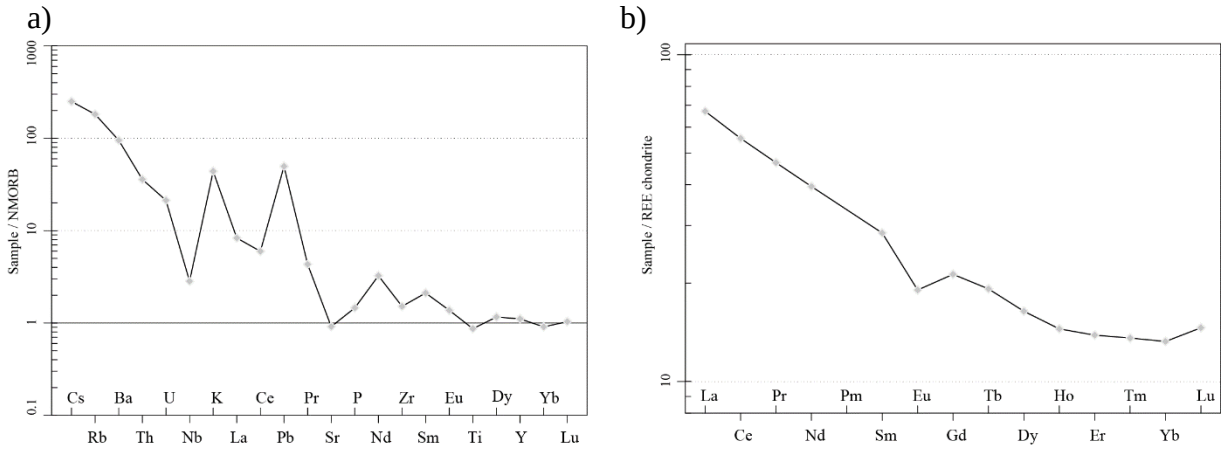

Figure 6–6. (a) N–MORB normalized multi–variation diagram (Sun and McDonough 1989) and (b) Chondrite normalized pattern of REE distribution (Boynton, 1984) of the feldspar–biotite–chlorite–muscovite–quartz schist.

N–MORB normalized multi–variation diagram of samples ES 19A–1, ES 15B–6, ES 15B–7 and ES 15B–8 (Figure 6–7 a) shows a general decreasing trend from LILE to HFSE with a major positive Pb anomaly and Ba, U and K anomalies in all the samples. Sample ES 15B–6 deviates from other sample, which is most visible in the REE distribution diagram. La/Lu ratio which describes enrichment in LREE is much lower for ES 15B–6 than for samples ES 19A–1, ES 15B–7 and ES 15B–8, which is manifested in a milder slope (Figure 6–7 b). In addition, sample ES 15B–6 doesn't have a negative Eu anomaly and samples ES 19A–1, ES 15B–7 and ES 15B–8 do. Chondrite normalized pattern of REE distribution of samples ES 19A–1, ES 15B–7 and ES 15B–8 (Figure 6–7) shows enrichment in LREE in comparison to HREE with a negative Eu anomaly. Mineralogically, sample ES 15B–6 is the only sample from this group that doesn't contain muscovite (Table 5–1).

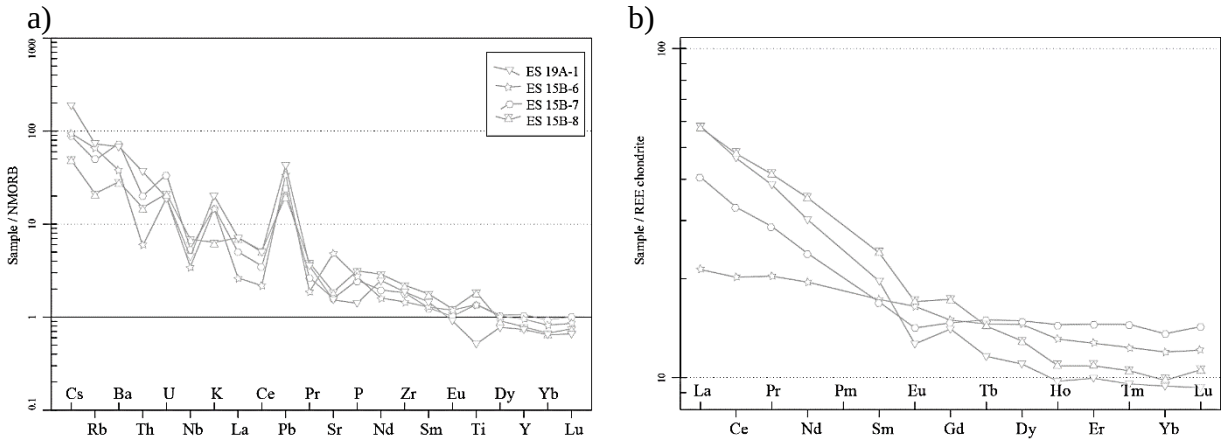

Figure 6–7. (a) N–MORB normalized multi–variation diagram (Sun and McDonough 1989) and (b) Chondrite normalized pattern of REE distribution (Boynton, 1984) of samples ES 19A–1, ES 15B–6, ES 15B–7 and ES 15B–8. Sample ES 15B–6 stands out from the rest.

N–MORB normalized multi–variation diagram of quartz–chlorite–actinolite schist (Figure 6–8 a) shows significant positive anomalies of U, K and Pb. Chondrite normalized pattern of REE distribution of quartz–chlorite–actinolite schist (Figure 6–8 b) shows a flat curve with negative Eu anomaly.

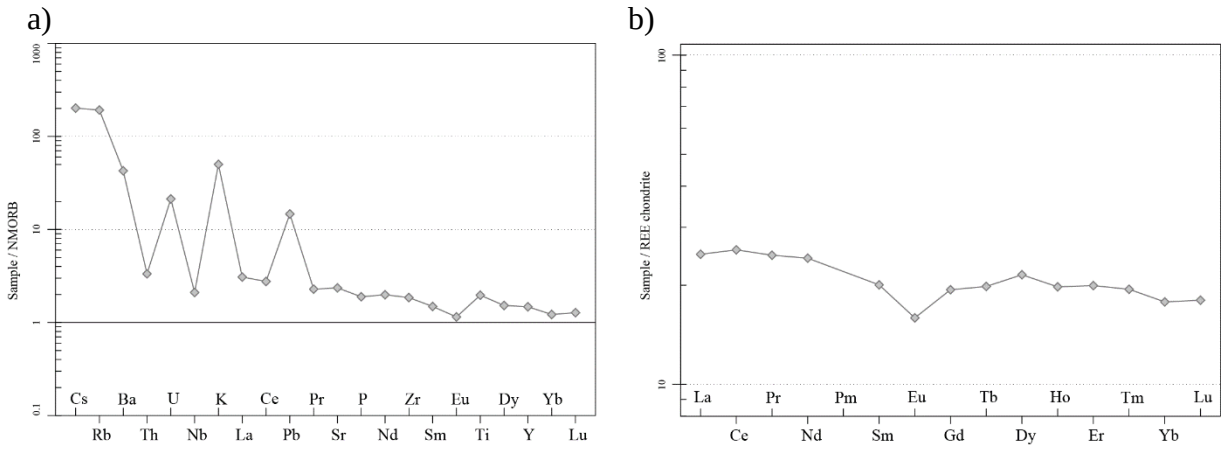

Figure 6–8. (a) N–MORB normalized multi–variation diagram (Sun and McDonough 1989) and (b) Chondrite normalized pattern of REE distribution (Boynton, 1984) of the quartz–chlorite–actinolite schist.

N–MORB normalized multi–variation diagram of garnet–epidote–chlorite–quartz–muscovite schist (Figure 6–9 a) shows significant increase of LILE regarding HFSE. A positive Ba and Pb anomalies can be seen and a negative Nb, P and Ti anomaly. Chondrite normalized pattern of REE distribution of garnet–epidote–chlorite–quartz–muscovite schist (Figure 6–9 b) shows an enrichment in LREE and a negative Eu anomaly.

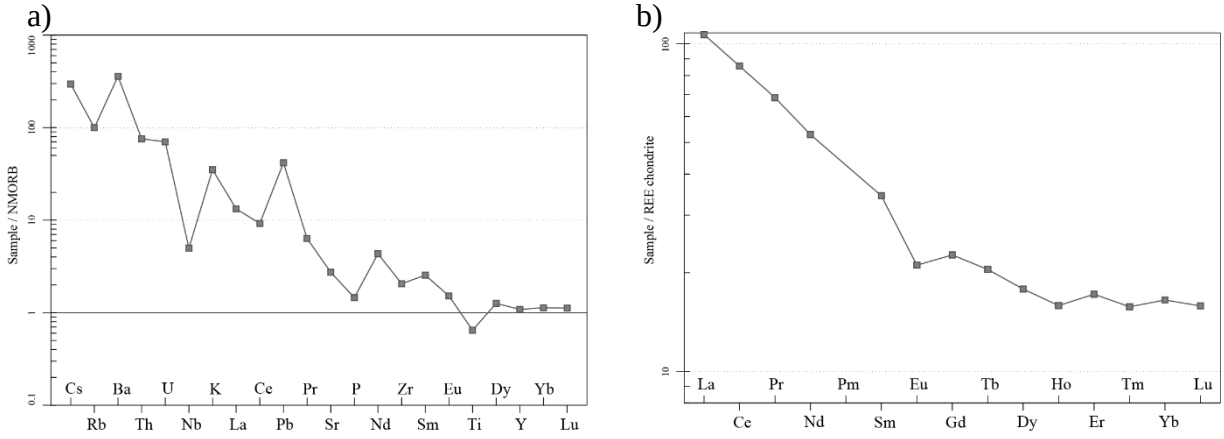

Figure 6–9. (a) N–MORB normalized multi–variation diagram (Sun and McDonough 1989) and (b) Chondrite normalized pattern of REE distribution (Boynton, 1984) of the garnet–epidote–chlorite–quartz–muscovite schist.

In the multi–variation diagrams (Figure 6–6, Figure 6–7, Figure 6–8 and Figure 6–9) all of the greenschist metamorphic facies schist samples show enrichment of LILE relative to HFSE with negative Nb and positive K and Pb anomalies. These patterns are similar to subduction–related

rocks but could also imply slab or crustal influence (Dostal and Durning 1998; Hooper and Hawkesworth 1993).

6.6. Amphibolite facies metamorphic rocks

The major and trace element contents of the samples ES 10E–2, ES 10H, ES 20–2 and ES 14–1 show that they originated from igneous rocks. The high Cr content and low Na_2O and K_2O content indicate an igneous origin (Moazzen and Oberhansli 2008). The TiO_2 versus Cr diagram (Leake, 1964) also confirms the igneous protolith for the hornblende containing schists (Figure 6–10).

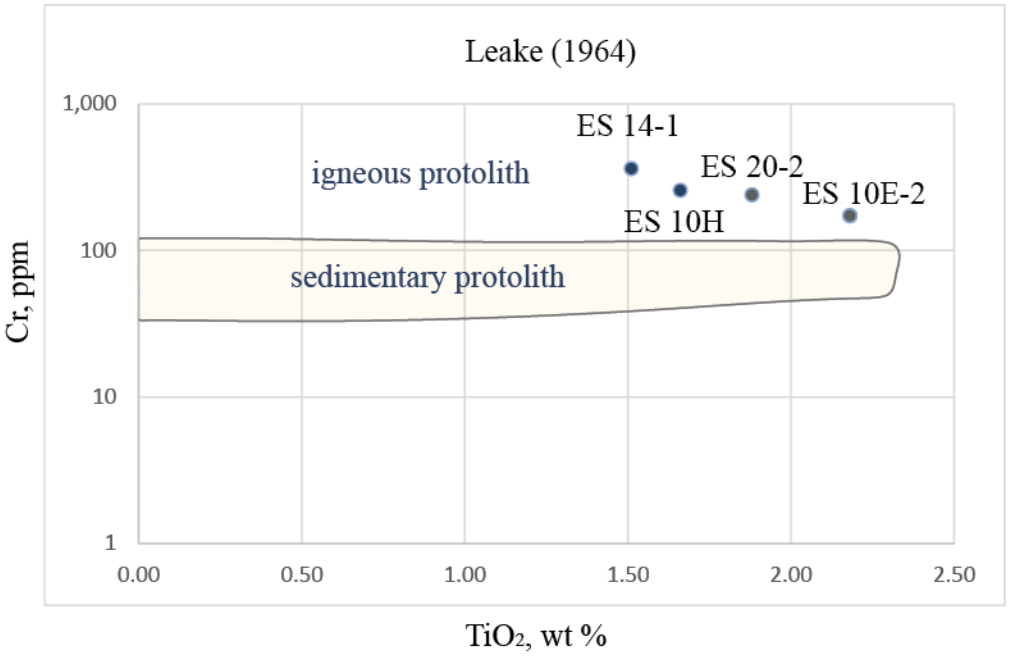

Figure 6–10. The TiO_2 versus Cr diagram (Leake, 1964) to distinguish between sedimentary and igneous protolith of hornblende containing schists. All studied samples plot in the igneous protolith field.

Normal Mid–Ocean Ridge Basalt (NMORB) normalized multi–element plot of amphibolite facies metamorphic rocks (Sun and McDonough 1989) can be seen in Figure 6–11 a. There is an enrichment in LILE in comparison to HFSE. There is a significant positive Pb anomaly in all hornblende containing schists. Samples ES 10E–2, ES 10H and ES 20–2 show similar trends whereas sample ES 14–1 is distinctly different.

In Figure 6–11 b the distribution of REE, normalized to the reference standard of chondritic meteorite values (Sun and McDonough 1989) of amphibolite facies metamorphic rocks is shown. The REE values of samples ES 10E–2, ES 10H and ES 20–2 are enriched around 20 times in comparison to chondrite. REE patterns of samples ES 10E–2 and ES 10H are similar. Sample ES 14–1 has significantly higher REE values and exhibits LREE enrichment. It has a slight, positive cerium anomaly and distinct negative europium anomaly. Cerium anomaly could be explained by incorporation of Ce^{4+} into zircon due to the similar ionic radius and same charge of Ce^{4+} and Zr^{4+} (Thomas et al., 2003). Europium anomaly is caused by the partition of europium between plagioclase feldspar and magmatic liquid and is inherited from primary magmatic host. Eu in its divalent form substitutes for Ca^{2+}, leaving the magmatic fluid depleted in this element after the removal of plagioclase from it (Rollinson, 2014; Weill and Drake 1973).

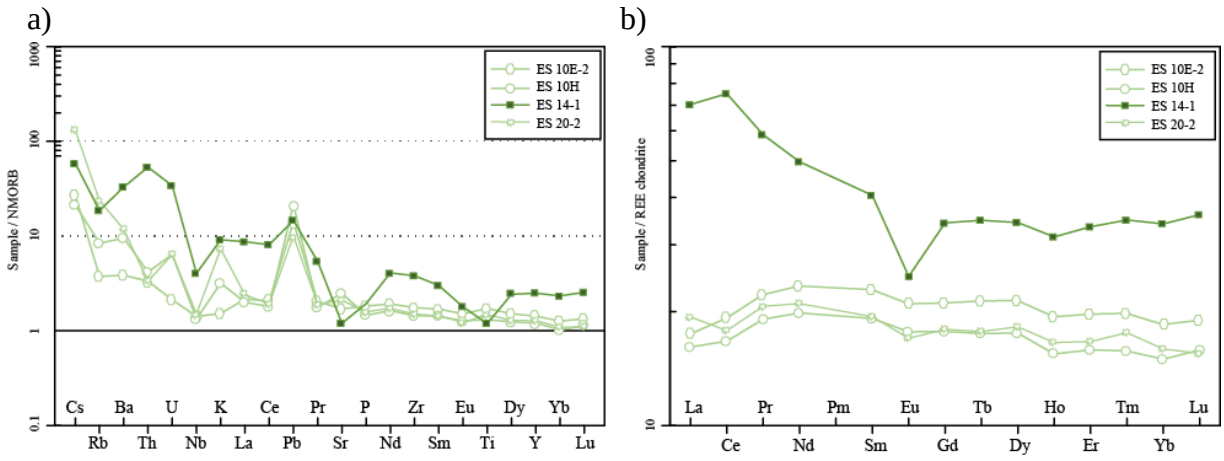

Figure 6–11. (a) N–MORB normalized multi–variation diagram (Sun and McDonough 1989) and (b) Chondrite normalized pattern of REE distribution (Boynton, 1984) of four hornblende containing schists.

Discrimination diagrams for the discrimination of different magma series and their differential products were made after Winchester and Floyd (1977). Samples ES 10E–2, ES 10H and ES 20–2 are projected in the field of basalt andesite (Figure 6–12 a) and subalkaline basalt (Figure 6–12 b). Sample ES 14–1 is in both diagrams projected in the field of andesite (Figure 6–12 a and b).

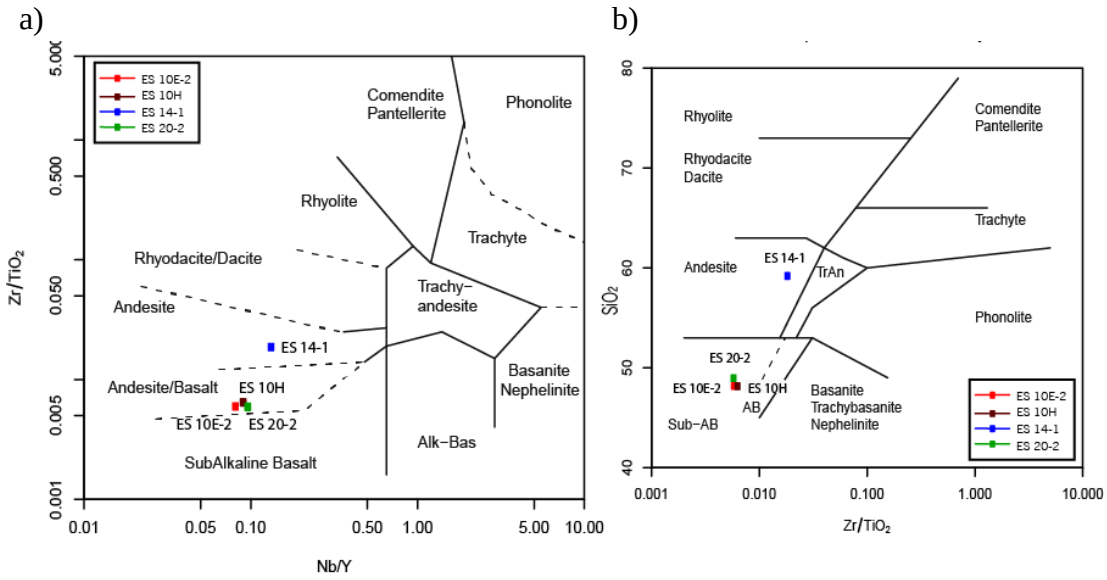

Figure 6–12. (a) Nb/Y–Zr/TiO_2 plot and (b) Zr/TiO_2–SiO_2 plot after Winchester and Floyd (1977).

Figure 6–13 and Figure 6–14 are used to determine possible tectonic setting for the protoliths of rocks belonging to the amphibolite metamorphic facies. In Ti–Zr discrimination diagram (Pearce, 1982) samples ES 10E–2, ES 10H and ES 20–2 are projected in the field of mid–ocean ridge basalt (MORB) and sample ES 14–1 in Within–Plate Lavas (Figure 6–13 a). Ti–V basalt discrimination diagram (Shervais, 1982) in Figure 6–13 b places all the samples belonging to amphibolite metamorphic facies in the ocean–floor basalt field with the garnet–quartz–chlorite–amphibole–albite schist (sample ES 14–1) having border values between ocean–floor basalt field and ocean islands and alkali basalts field (OIB and AB).

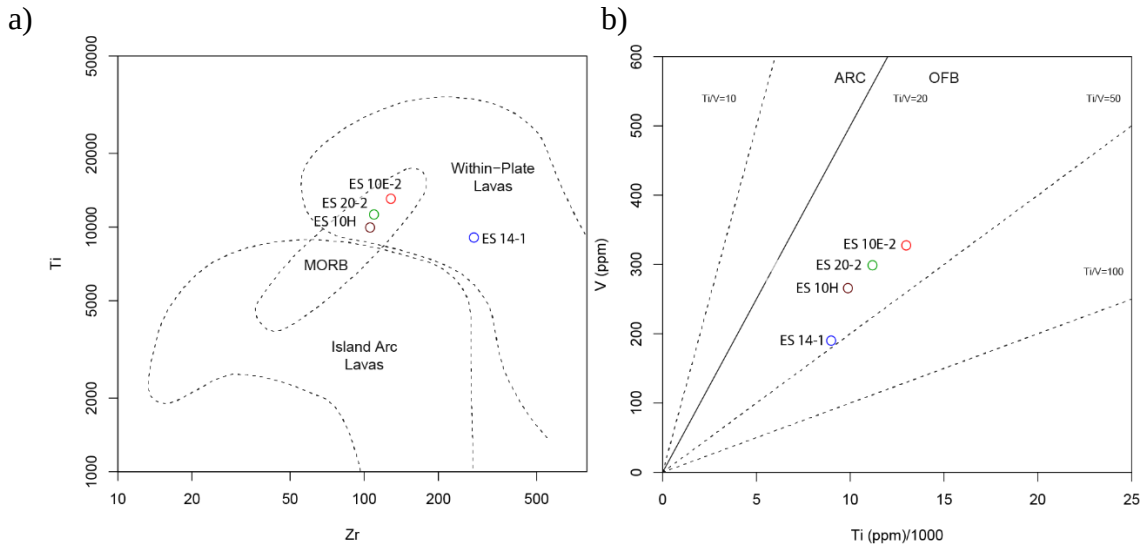

Figure 6–13. (a) Zr–Ti diagram after Pearce (1982) and b) Ti/V diagram based on data from Shervais (1982).

Zr/4–2Nb–Y plot projects all of the amphibolite facies samples in the N–type MORB and volcanic arc basalts, with sample ES 14–1 being on the border with the field of within plate tholeiites and volcanic arc basalts (Figure 6–14 a). Triangular diagram of the Th–Hf–Ta–Zr–Nb system (Figure 6–14 b) shows samples ES 10E–2, ES 10H and E S20–2 in E–MORB within–plate tholeiites field and sample ES 14–1 in calc–alkaline basalts field.

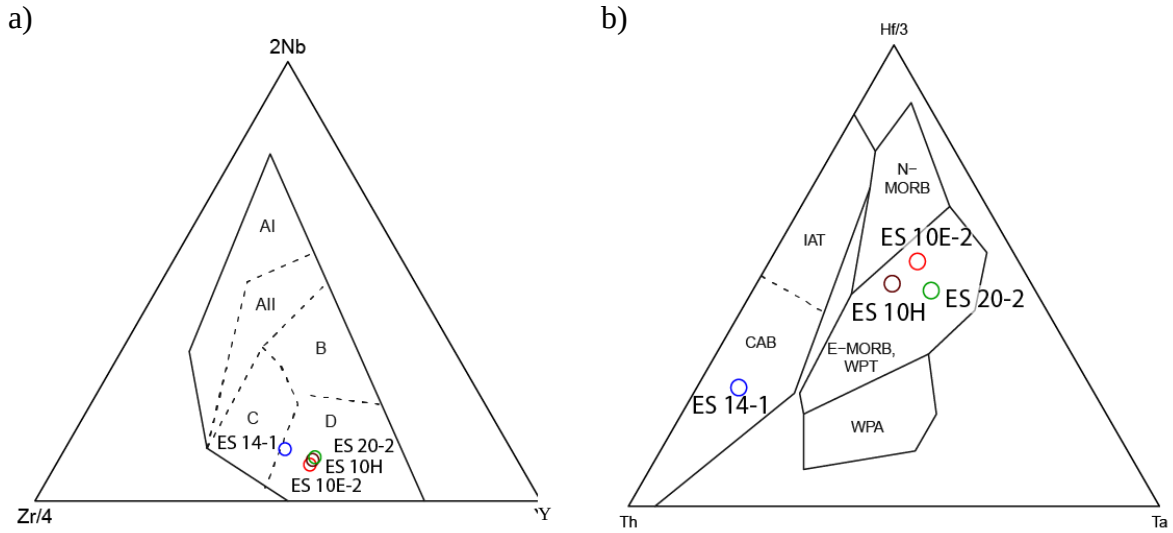

Figure 6–14. (a) Zr/4–2Nb–Y after Meschede (1986) and b) Th–Hf/3–Ta plot after Wood (1980).

6.7. Correlation with the Tisza–Dacia margin

The presented petrological and geochemical data could be correlated with available reconstructions obtained in the nearby parts of the Tisza–Dacia Mega–Unit in the Croatian and Hungarian part of the Pannonian Basin (Balen et al., 2006; Pamić et al., 2002) and in the Romania (Haas and Péró 2004) and Bulgaria.

The first metamorphic event recorded in the Tisa Unit is the Barrow–type amphibolite facies regional metamorphism which is considered pre–Variscan (Lelkes–Felvári and Sassi 1981). Although no isotopic ages older than Variscan (Lelkes–Felvári et al., 1996) are available from the metamorphic basement of the Tisza Unit, this can be partly explained by the intense Variscan heating (Arkai et al., 1999). Árkai (1984; 1985) calculated peak conditions of 500–600 °C and 5–9 kbar for the first Barrow–metamorphism of crystalline basement of the Neogene depression of the Somogy—Drava Basin (southwestern Hungary). The peak metamorphic conditions for mica schist, paragneiss and amphibolite from the Slavonian Mountains according to Balen (2006) were 600–650 °C and 8–11 kbar. Obtained Th–U–Pb ages of around 444 and 428 Ma indicate a pre–Variscan event (Ordovician–Silurian) and are attributed to the particular tectonometamorphic event which resulted in formation of foliation and the peak metamorphic assemblage (Balen et al., 2006).

The Barrow–metamorphism was overprinted by a low–pressure Variscan event with grades varying from subgreenschist facies up to amphibolite facies, closely related to granitoid magmatism (Lelkes–Felvári and Sassi 1981). The age of the greenschist retrograde overprint is considered to be early Carboniferous (Dimitrijević, 1963; Petrović, 1969; Krstić and Karamata 1992; Karamata et al., 1996). Karamata and Krstić (1996) attribute the amphibolite–greenschist assemblage to Baikalian (859–650 Ma) or Caledonian orogenic events. The event occurring at temperatures of 300–350°C (Krstekanić et al., 2017) or 450–500°C (Antić et al., 2017) and at pressures of 3–5 kbar.

As shown by the discussed microscopic observations the samples were affected by the overprint at greenschist facies conditions, however with the limited data it stays a challenge to derive pressure–temperature conditions and to separate pre–Variscan and Variscan metamorphism.

7. CONCLUSION

- The cordierite–quartz–epidote–chlorite–actinolite hornfels, located in the quartz–sericite–chlorite schists unit, belongs to the albite–epidote hornfels facies, formed at temperature little above 600 °C and at low pressure. It was formed as a result of contact metamorphism, probably of the pelitic protolith–which can be assumed based on the specific colourless appearance of cordierite. The event of contact metamorphism most likely occurred when Variscan granitoids intruded into crystalline basement of the Kučaj terrane.
- Insight into the Barrovian–type metamorphic sequence is given through petrological and geochemical analysis of metamorphic rocks of greenschist facies and amphibolite facies. A direction of increase of pressure and temperature conditions within the prograde metamorphic sequence towards the south is proposed, with peak temperatures from 400°C to around 700°C and pressures from 4 to 12 kbar.
- Multiple deformation episodes, which resulted in both brittle and ductile microstructures are observed in the thin sections. Pre–cinematic porphyroblast of amphibole and its pressure shadow consisting prevailingly of quartz possibly indicate a non–coaxial simple shear deformational event that caused rotation of porphyroblast (and its mineral inclusions), which postdates the porphyroblast growth.
- Documented regional greenschist facies overprint is recognized in most samples.
- Quartz vein is located in the quartz–sericite–chlorite schists unit. Presence of positive Pb anomaly in the N–MORB normalized multi–variation diagram of quartz vein implies possible Pb contamination, most likely linked to the proximity of the Pb–Zn mineralisation (related to the granitoid bodies).
- All hornblende containing schists originate from an igneous precursor. Samples ES 10E–2, ES 10H and ES 20–2 are located in the gneiss unit, their protoliths were andesitic or subalkaline basalts. Samples ES 10E–2, ES 10H and ES 20–2 display typical N–MORB characteristics similar to the values of basalts from volcanic arc settings. Based on the values of Zr, Nb, Y and Th, Hf, Ta presented in triangular diagrams after Meschede (1986) and Wood (1980) samples ES 10E–2, ES 10H and ES 20–2 show characteristics of E–MORB and within–plate tholeiites. Garnet–quartz–chlorite–

amphibole–albite schist is sampled in the quartz–sericite–chlorite schists unit. Its protolith rock is andesite. Geotectonic setting of garnet–quartz–chlorite–amphibole–albite schist is plotting between volcanic arc basalts and within plate tholeiites. garnet–quartz–chlorite–amphibole–albite schist in the field of calc–alkaline basalts.

- Barrovian regional metamorphism documented in this study is similar to observed regional metamorphism within the Tisza–Dacia Mega unit.

8. REFERENCES

Alderton, D. (2020): Mineralogy Non Silicates. In *Encyclopedia of Geology*, p. 382.

Antić, M. D.; Kounov, A.; Trivić, B.; Spikings, R.; Wetzel, A. (2017): Evidence of Variscan and Alpine tectonics in the structural and thermochronological record of the central Serbo–Macedonian Massif (south–eastern Serbia). In *International Journal of Earth Sciences* 106 (5), pp. 1665–1692.

Antonijević, I.; Veselinović, M.; Đorđević, M.; Kalenić, M.; Krstić, B.; Karajičić, Lj. (1970): Explanatory book for sheet Explanatory book for sheet Žagubica, Basic Geological Map 1:100.000.

Arkai, P.; Horvath, P.; Nagy, G. (1999): A clockwise PT path from the Variscan basement of the Tisza Unit, Pannonian Basin, Hungary. In *Geologia Croatica* 52 (2), pp. 109–117.

Árkai, P. (1984): Polymetamorphism of the crystalline basement of the somogy–dráva Basin (southwestern Transdanubia, Hungary). In *Acta Miner. Petr. Szeged* 26 (2), pp. 129–153.

Árkai, P.; Nagy, G.; Dobosi, G. (1985): Polymetamorphic evolution of the South Hungarian crystalline basement, Pannonian Basin: geothermometric and geobarometric data. In *Acta Geologica Hungarica* 28, pp. 165–190.

Balen, D.; Horváth, P.; Tomljenović, B.; Finger, F.; Humer, B.; Pamić, J.; Árkai, P. (2006): A record of pre–Variscan Barrovian regional metamorphism in the eastern part of the Slavonian Mountains (NE Croatia). In *Mineralogy and Petrology* 87 (1), pp. 143–162.

Balintoni, I.; Balica, C.; Ducea, M. N.; Hann, H.–P. (2014): Peri–Gondwanan terranes in the Romanian Carpathians: A review of their spatial distribution, origin, provenance, and evolution. In *Geoscience Frontiers* 5 (3), pp. 395–411.

Balintoni, I.; C. Balica; M.N. Ducea; H.P. Hann; Şabliovschi, V. (2010): The anatomy of a Gondwanan terrane: The Neoproterozoic–Ordovician basement of the pre–Alpine Sebeş–Lotru composite terrane (South Carpathians, Romania). In *Gondwana Research* 17 (2), pp. 561–572. DOI: 10.1016/j.gr.2009.08.003.

Balla, Z.; Bodrogi, I. (1993): The'Vékény Marl Formation'of Hungary. In *Cretaceous Research* 14 (4–5), pp. 431–448.

Barrow, G. (1893): On an Intrusion of Muscovite–biotite Gneiss in the South–eastern Highlands of Scotland, and its accompanying Metamorphism. In *Quarterly Journal of the Geological Society* 49 (1–4), pp. 330–358.

Bau, M. (1991): Rare–earth element mobility during hydrothermal and metamorphic fluid–rock interaction and the significance of the oxidation state of europium. In *Chemical geology* 93 (3), pp. 219–230. DOI: 10.1016/0009–2541(91)90115–8.

Berza, T.; Constantinescu, E.; Vlad, S.–N. (1998): Upper Cretaceous magmatic series and associated mineralisation in the Carpathian–Balkan Orogen. In *Resource Geology* 48 (4), pp. 291–306.

Berza, T.; Drăgănescu, A. (1988): The Cerna–Jiu fault system (South Carpathians, Romania), a major Tertiary transcurrent lineament. In *Dări de Seamă*, 72–73, 43–57.

Borojević Šoštarić, S.; Palinkaš, A. L.; Neubauer, F.; Cvetković, V.; Bernroider, M.; Genser, J. (2014): The origin and age of the metamorphic sole from the Rogozna Mts., Western Vardar Belt: New evidence for the one–ocean model for the Balkan ophiolites. In *Lithos* 192, pp. 39–55.

Boynton, W. V. (1984): Cosmochemistry of the rare earth elements: meteorite studies. In : Developments in geochemistry, vol. 2: Elsevier, pp. 63–114.

Butler, J. R. (1990): Facies of thermal metamorphism. In : Petrology. Boston, MA: Springer US, pp. 160–163.

Channell, J. E.T.; Horvath, F. (1976): The African/Adriatic promontory as a palaeogeographical premise for Alpine orogeny and plate movements in the Carpatho–Balkan region. In *Tectonophysics* 35 (1–3), pp. 71–101.

Csontos, L. (1995): Tertiary tectonic evolution of the Intra–Carpathian area: a review. In *Acta Vulcan* 7 (2), pp. 1–13.

Csontos, L.; Nagymarosy, A.; Horváth, F.; Kovac, M. (1992): Tertiary evolution of the Intra–Carpathian area: a model. In *Tectonophysics* 208 (1–3), pp. 221–241.

Csontos, L.; Vörös, A. (2004): Mesozoic plate tectonic reconstruction of the Carpathian region. In *Palaeogeography, Palaeoclimatology, Palaeoecology* 210 (1), pp. 1–56.

Cvetković, V.; Prelević, D.; Schmid, S. (2016): Geology of south–eastern Europe. In P. Papić (Ed.): Mineral and thermal waters of Southeastern Europe: Springer, pp. 1–29.

Dimitrijević, M. D. (1963): Sur l'âge du métamorphisme et des plissements dans la masse Serbo–macédonienne. In *Bulletin du VIe Congrès de l'Association géologique Carpatho–balkanique I, Stratigraphie, 3*.

Dorais, Michael J.; Tubrett, Michael (2008): Identification of a subduction zone component in the Higganum dike, Central Atlantic Magmatic Province: A LA-ICPMS study of clinopyroxene with implications for flood basalt petrogenesis. In *Geochemistry, Geophysics, Geosystems* 9 (10).

Dostal, J.; Durning, M. (1998): Geochemical constraints on the origin and evolution of early Mesozoic dikes in Atlantic Canada. In *European Journal of Mineralogy*, pp. 79–94.

Eskola, P. (1939): Die metamorphen Gesteine. In : Die Entstehung der Gesteine: Springer, pp. 263–407.

Floyd, P. A. (1965): Metasomatic Hornfelses of the Land's End Aureole at Tater–du, Cornwall. In *Journal of Petrology* 6 (2), pp. 223–245. DOI: 10.1093/petrology/6.2.223.

Fügenschuh, B.; Schmid, S. M. (2005): Age and significance of core complex formation in a very curved orogen: Evidence from fission track studies in the South Carpathians (Romania). In *Tectonophysics* 404 (1–2), pp. 33–53.

Fülöp, J. (1989): Introduction to geology of Hungary. Bevezetés Magyarország geológiájába (in Hungarian).

Gallhofer, D.; Quadt, A. von; Peytcheva, I.; Schmid, Stefan M.; Heinrich, C. A. (2015): Tectonic, magmatic, and metallogenic evolution of the Late Cretaceous arc in the Carpathian-Balkan orogen. In *Tectonics* 34 (9), pp. 1813–1836.

Gamal El Dien, H.; Li, Zheng–Xiang; K., Youngwoo; A.–A., Tamer (2019): Origin of arc magmatic signature: A temperature–dependent process for trace element (re)–mobilization in subduction zones. In *Scientific Reports* 9 (1), p. 7098. DOI: 10.1038/s41598–019–43605–9.

Geological Information System of Serbia: Geomorphological map of Serbia 1:300000. With assistance of Ministarstvo energetike, razvoja i zaštite životne sredine Republike Srbije. Available online at https://geoliss.mre.gov.rs/, checked on 1/18/2022.

Google Maps: Map of East Europe. Available online at https://www.google.com/maps/, checked on 1/18/2022.

Haas, J.; Császár, G.; Kovács, S.; Vörös, A. (1990): Evolution of the western part of the Tethys as reflected by the geological formations of Hungary: Acta Geodetica Geophysica et Montanistica Hungarica, v. 25: Akademiai Kiado, Budapest.

Haas, J.; Péró, C. (2004): Mesozoic evolution of the Tisza Mega–unit. In *International Journal of Earth Sciences* 93 (2), pp. 297–313. DOI: 10.1007/s00531–004–0384–9.

Haydoutov, I. (1989): Precambrian ophiolites, Cambrian island arc, and Variscan suture in the South Carpathian–Balkan region. In *Geology* 17 (10), pp. 905–908.

Hemley, J. J.; Jones, W. R. (1964): Chemical aspects of hydrothermal alteration with emphasis on hydrogen metasomatism. In *Economic Geology* 59 (4), pp. 538–569.

Hooper, P. R.; Hawkesworth, C. J. (1993): Isotopic and geochemical constraints on the origin and evolution of the Columbia River Basalt. In *Journal of Petrology* 34 (6), pp. 1203–1246.

Horváth, P.; Árkai, P. (2002): Pressure–temperature path of metapelites from the Algyő–Ferencszállás area, SE Hungary: thermobarometric constraints from coexisting mineral assemblages and garnet zoning. In *Acta Geologica Hungarica* 45 (1), pp. 1–27.

Iancu, V.; Berza, T.; Seghedi, A.; Marunţiu, M. (2005): Palaeozoic rock assemblages incorporated in the South Carpathian Alpine thrust belt (Romania and Serbia): a review. In *Geologica Belgica*.

Iancu, V.; Maruntiu, M.; Johan, V.; Ledru, P. (1998): High–grade metamorphic rocks in the pre–Alpine nappe stack of the Getic–Supragetic basement (Median Dacides, South Carpathians, Romania). In *Mineralogy and Petrology* 63 (3), pp. 173–198.

Ilinca, G. (2012): Upper Cretaceous contact metamorphism and related mineralization in Romania. In *Acta Mineralogica–Petrographica, Abstract Series, Szeged* 7, pp. 59–64.

Janković, S. (1997): The Carpatho–Balkanides and adjacent area: a sector of the Tethyan Eurasian metallogenic belt. In *Mineralium Deposita* 32 (5), pp. 426–433.

Janković S. (1990): The ore deposits of Serbia: Regional metallogen–ic settings, environments of deposition, and types.

Janoušek, V.; Farrow, C. M.; Erban, V. (2006): Interpretation of whole-rock geochemical data in igneous geochemistry: introducing Geochemical Data Toolkit (GCDkit). Journal of Petrology 47(6):1255-1259

Jelenković, R.; Kostić, A.; Životić, D.; Ercegovac, M. (2008): Mineral resources of Serbia. In *Geol. Carpath* 59 (4), pp. 345–361.

Jelenković, R.; Serafimovski, T.; Tasev, G. (2002): Metallic mineral resources of the Karpatho–Balkan metallogenic province: Eastern Serbian Sector (general review). In *RMZ–Materials and Geoenvironment* 49 (2), pp. 177–197.

Jovanović, D.; Cvetković, V.; Erić, S.; Kostić, B.; Peytcheva, I.; Šarić, K. (2019): Variscan granitoids of the East Serbian Carpatho–Balkanides: new insight inferred from U–Pb zircon ages and geochemical data. In *Swiss J Geosci* 112 (1), pp. 121–142.

Kalenić, M.; Đordević, M.; Krstić, B.; Bogdanović, P.; Milosaković, R.; Divljan, M. (1976): Explanatory book for sheet Bor, Basic Geological Map of SFRY 1:100.000.

Kalenić, M.; Hadži–Vuković, M. (1978): Basic Geologic Map of SFRY 1:100000, Sheet Kučevo. Veselinović, M. O.; Rakić, B.; Vujisić, Č.; Lončarević, M.; Navala, M.; Đorđević, M.; Vasiljev, N.; Banković, V.: Zavod za geološka, hidrogeološka, geofizička i geotehnička istraživanja, Beograd.

Kalenić, M.; Hadži–Vuković, M.; Dolić, D.; Lončarević, Č.; Rakić, M. O. (1980): Explanatory book for sheet Kučevo, Basic Geological Map of SFRY 1:100.000, p. 53.

Karamata, S. (2006): The geological development of the Balkan Peninsula related to the approach, collision and compression of Gondwanan and Eurasian units. In *Geological Society, London, Special Publications* 260 (1), pp. 155–178.

Karamata, S.; Ebner, F.; Krstić, B. (1996): Terranes—definition of the terrane, and importance for geologic interpretations. In *Terranes of Serbia. Belgrade, University of Belgrade*, pp. 23–24.

Kikuchi, Y. (1889): Cerasite in slate. In *Chigaku Zasshi* 1:36–38.

Kounov, A.; Seward, D.; Bernoulli, D.; Burg, J–P; Ivanov, Z. (2004): Thermotectonic evolution of an extensional dome: the Cenozoic Osogovo–Lisets core complex (Kraishte zone, western Bulgaria). In *International Journal of Earth Sciences* 93 (6), pp. 1008–1024.

Kovács, S. (1984): Tisia–probléma és lemeztektonika. In *Földt. Kut* 27 (1), pp. 55–72.

Kovács, S.; Császár, G.; Galácz, A.; Haas, J.; Nagy, E.; Vörös, A. (1989): The Tisza Superunit was originally part of the North Tethyan (European) margin. In *Evolution of the northern margin of Tethys. Mem. Soc. Geol. France* 154 (4), pp. 81–100.

Kräutner, H. G. (Ed.) (1996): Alpine rifting, subduction and collision in the Romanian Carpathians. 6th Symp. Tektonik–Strukturgeologie–Kristallingeologie, Salzburg, 10–15 April, 1996, Wien. Wien.

Kräutner, H. G.; Krstić, B. (Eds.) (2002): Alpine and Pre–Alpine structural units within the Southern Carpathians and the Eastern Balkanides. Proceedings of XVII. Congress of Carpathian–Balkan Geological Association Bratislava, September 1–4 2002: Geologica Carpathica 53 Special Issue. Available online at http://www.geologicacarpathica.sk/src/main.php.

Kräutner, H. G.; Krstić, B. P. (2003): Geological map of the Carpatho–Balkanides between Mehadia. In *Oravita, Niš and Sofia*.

Krstekanić, N.; Stojadinović, U.; Kostić, B.; Toljić, M. (2017): Internal structure of the Supragetic Unit basement in the Serbian Carpathians and its significance for the late Early Cretaceous nappe–stacking. In *Geoloski anali Balkanskoga poluostrva* (78), pp. 1–15.

Krstić, B.; Kalenić, M.; Rakić, B.; Rajčević, D.; Banković, V. (1974): Base geological map at 1: 100,000, sheet Belogradchik and textual explanation. In *Federal Geological Survey. Belgrade*.

Krstić, B.; Karamata, S. (1992): Terranes of the Serbian Carpatho–Balkanides. In *Comptes Rendus des Seances de la Soc. Serb. de Geol., livre jubilaire (1891—1991)*, pp. 57–74.

Krstić, B.; Maslarević, Lj. (1990): In the Herynid Kučaj zone, Eastern Serbia. In *Bulletin tomeCII: Classe des sciences mathematiques et naturelles*, p. 29.

Krstić, B.; Maslarević, Lj.; Ercegovac, M.; Sudar, M.; Đajić, S. (2004): Devonian in the Carpatho–Balkanides of Eastern Serbia. In *Bulletin T. CXXVIII de l'Académie serbe des sciences et des arts–Classe des sciences mathématiques et naturelles, Sciences Naturelles* 42, pp. 7–16.

Leake, B. E. (1964): The Chemical Distinction Between Ortho– and Para–amphibolites. In *Journal of Petrology* 5 (2), pp. 238–254. DOI: 10.1093/petrology/5.2.238.

Leeman, W. P. (1996): Boron and other fluid–mobile elements in volcanic arc lavas: Implications for subduction processes. In *Washington DC American Geophysical Union Geophysical Monograph Series* 96, pp. 269–276.

Lelkes–Felvári, G.; Arkai, P.; Sassi, F. P.; Balogh, K. (1996): Main features of the regional metamorphic events in Hungary: a review. In *Geologica Carpathica* 47 (4), pp. 257–270.

Lelkes–Felvári, G.; Sassi, F. P. (1981): Outlines of the pre–Alpine metamorphism in Hungary. In *IGCP project* (5), pp. 89–99.

McNamara, M. J. (1966): Chlorite–biotite equilibrium reactions in a carbonate–free system. In *Journal of Petrology* 7 (3), pp. 404–413.

Meschede, M. (1986): A method of discriminating between different types of mid–ocean ridge basalts and continental tholeiites with the Nb・1bZr・1bY diagram. In *Chemical geology* 56 (3–4), pp. 207–218.

Miyashiro, A. (1957): Cordierite–indialite relations. In *American Journal of Science* 255 (1), pp. 43–62.

Moazzen, M.; Oberhansli, R. (2008): Whole rock and relict igneous clinopyroxene geochemistry of ophiolite–related amphibolites from NW Iran–Implications for protolith nature. In *Neues Jahrbuch Fur Mineralogie–Abhandlungen* 185 (1), pp. 51–62.

Nance, R. D.; Murphy, J. B.; Strachan, R. A.; Keppie, J. D.; Gutiérrez–Alonso, G.; Fernández–Suárez, J. et al. (2008): Neoproterozoic–early Palaeozoic tectonostratigraphy and palaeogeography of the peri–Gondwanan terranes: Amazonian v. West African connections. In *Geological Society, London, Special Publications* 297 (1), pp. 345–383.

Năstăseanu, S.; Bercia, I.; Iancu, V.; Vlad, S.; Hartopanu, I. (Eds.) (1981): The Structure of the South Carpathians. Guide to Excursion B2 of the 12th Carpatho–Balkan Geological Association Congress, Bucharest, Romania.

Nicolescu, Ș.; Cornell, D. H. (1999): P–T conditions during skarn formation in the Ocna de Fier ore district, Romania. In *Mineralium Deposita* 34 (8), pp. 730–742.

Oczlon, M. S.; Seghedi, A.; Carrigan, C. W. (2007): Avalonian and Baltican terranes in the Moesian Platform (southern Europe, Romania, and Bulgaria) in the context of Caledonian terranes along the southwestern margin of the East European craton. In *SPECIAL PAPERS–GEOLOGICAL SOCIETY OF AMERICA* 423, p. 375.

Pamić, J.; Balen, D.; Herak, M. (2002): Origin and geodynamic evolution of Late Paleogene magmatic associations along the Periadriatic–Sava–Vardar magmatic belt. In *Geodinamica Acta* 15 (4), pp. 209–231. DOI: 10.1080/09853111.2002.10510755.

Pearce, J. A. (1982): Trace element characteristics of lavas from destructive plate boundaries. In *Andesites* 8, pp. 525–548.

Petrović, B. S. (1969): The structure of the Vlasina Crystalline Complex in the broad area of Crna Trava.

Prinz, G. (1926): Geography of Hungary. I. In *The origin, structure and form of the earth of Hungary (in Hungarian). Tud Gyujt* 15, pp. 1–200.

Rollinson, H. R. (2014): Using geochemical data. Evaluation, presentation, interpretation. London: Routledge.

Săndulescu, M. (1984): Geotectonica României (translated title: Geotectonics of Romania). In *Ed. Tehnică, Bucharest*.

Săndulescu, M. (1994): Overview on Romanian geology. In *Rom. Jour. of Tectonics and Regional Geology, Suppl. 2* 75, pp. 3–15.

Schmid, S. M.; Bernoulli, D.; Fügenschuh, B.; Matenco, l.; Schefer, S.; Schuster, R. et al. (2008): The Alpine–Carpathian–Dinaridic orogenic system: correlation and evolution of tectonic units. In *Swiss J Geosci* 101 (1), pp. 139–183.

Seghedi, A.; Berza, Tudor; I., Viorica; M., Marcel; OAIE, G. (2005): Neoproterozoic terranes in the Moesian basement and in the Alpine Danubian nappes of the South Carpathians. In *Geologica Belgica* 8 (4), pp. 4–19.

Shervais, J. W. (1982): Ti–V plots and the petrogenesis of modern and ophiolitic lavas. In *Earth and planetary science letters* 59 (1), pp. 101–118.

Spahić, D.; Gaudenyi, T.; Glavaš–Trbič, B. (2019): The Neoproterozoic–Paleozoic basement in the Alpidic Supragetic/Kučaj units of eastern Serbia: a continuation of the Rheic Ocean? In *Acta Geologica Polonica* 69 (4).

Spahić, D.; Bojić, Z.; Popović, D.; Gaudenyi, T. (2021): Vestiges of Cambro–Ordovician continental accretion in the Carpathian–Balkan orogen: First evidence of the 'Cenerian'event in the central Serbo–Macedonian Unit. In *Acta Geologica Polonica* 71 (2).

Sun, S.–S.; McDonough, William F. (1989): Chemical and isotopic systematics of oceanic basalts: implications for mantle composition and processes. In *Geological Society, London, Special Publications* 42 (1), pp. 313–345.

Thomas, J. B.; Bodnar, R. J.; Shimizu, N.; Chesner, C. A. (2003): Melt inclusions in zircon. In *Reviews in mineralogy and geochemistry* 53 (1), pp. 63–87.

Torres–Alvarado, I. S.; Pandarinath, K.; Verma, S. P.; Dulski, P. (2007): Mineralogical and geochemical effects due to hydrothermal alteration in the Los Azufres geothermal field, Mexico. In *Revista mexicana de ciencias geológicas* 24 (1), pp. 15–24.

Turner, F. J. (1981): Metamorphic petrology: Mineralogical, field, and tectonic aspects: McGraw–Hill Companies.

Vukmirović, D. (2011): Comparative overview of the number of population in 1948, 1953, 1961, 1971, 1981, 1991, 2002 and 2011in Republic of Serbia.

Weill, D. F.; Drake, M. J. (1973): Europium anomaly in plagioclase feldspar: experimental results and semiquantitative model. In *Science (New York, N.Y.)* 180 (4090), pp. 1059–1060. DOI: 10.1126/science.180.4090.1059.

Whitney, D. L.; Evans, B. W. (2010): Abbreviations for names of rock–forming minerals. In *American Mineralogist* 95 (1), pp. 185–187.

Winchester, J. A.; Floyd, P. A. (1977): Geochemical discrimination of different magma series and their differentiation products using immobile elements. In *Chemical geology* 20, pp. 325–343.

Winkler, H. G. F. (1965): Petrogenesis of Metamorphic Rocks.

Winkler, H. G.S. (1986): Petrogenesis of metamorphic rocks,(ed.) Springer: Berlin.

Wood, D. A. (1980): The application of a ThHfTa diagram to problems of tectonomagmatic classification and to establishing the nature of crustal contamination of basaltic lavas of the British Tertiary Volcanic Province. In *Earth and planetary science letters* 50 (1), pp. 11–30.

Yanev, S. (2000): Palaeozoic terranes of the Balkan Peninsula in the framework of Pangea assembly. In *Palaeogeography, Palaeoclimatology, Palaeoecology* 161 (1–2), pp. 151–177.

Yanev, S.; Lakova, I.; Boncheva, I.; Sackanski, V. (2005): The Moesian and Balkan terranes in Bulgaria: Palaeozoic basin development, palaeogeography and tectonic evolution. In *Geologica Belgica*.

Yardley, B. W.D. (1989): An introduction to metamorphic petrology: Longman Scientific and Technical. In *Essex, England*, pp. 61–90.

Ziegler, P. A. (1986): Geodynamic model for the Palaeozoic crustal consolidation of Western and Central Europe. In *Tectonophysics* 126 (2–4), pp. 303–328.